Additive manufacturing of biomaterials for bone tissue engineering – A critical review of the state of the art and new concepts

Marie-Michèle Germaini, Sofiane Belhabib, Sofiane Guessasma, Pierre Weiss, Pierre Corre, Rémi Deterre

Additive manufacturing of biomaterials for bone tissue engineering – a critical review of the state of the art and new concepts

Marie-Michèle Germaini, Sofiane Belhabib, Sofiane Guessasma, Rémi Deterre, Pierre Corre, Pierre Weiss

Keywords: (bone regeneration, biomaterial, additive manufacturing, modeling, design optimization, material and process selection, 3D imaging)

Additive manufacturing has attracted keen interest in the medical field in recent decades, especially for bone regeneration. Many additive manufacturing processes have been used to print medical devices such as implants, prostheses, and surgical guides, and for surgical planning in different medical fields, especially orthopedic, maxillofacial and dental surgery. Many materials can be manufactured by 3D printing with metal, ceramic, polymer or composite materials. Composite materials with organic and mineral components have been investigated to mimic bone functional and structural characteristics. In addition to the chemical composition, the modeling and optimization of the design can be optimized to enhance the biological and mechanical performance of the printed scaffolds.
This review presents a comparative evaluation of different material/additive manufacturing processes, and describes the best compromises for targeted clinical applications. The advantages and drawbacks of each additive manufacturing process are described in light of the biological results and essential properties expected by patients and clinicians.

Statement of significance:

3D (bio)printing appears to be an outstanding manufacturing route to revolutionize patient care with personalized medicine. Moreover, there are growing trends in the use of 3D printing in the medical education field and for surgical planning to alleviate surgeon practice and optimize esthetic results. Many reviews have described the growth of the different additive manufacturing techniques developed over time, their advantages and drawbacks and the work required to develop an accurate printable biomaterial fitting the 3D additive manufacturing process and the expectations of the final users and beneficiaries [1], [2], [3]. In this review, an emphasis is placed on the expectations of patients and clinicians regarding specific final clinical applications in craniomaxillofacial, orthopedic or dental fields for a specific biomaterial/additive material (AM) process couple. The primary focus of this review is a comparative analysis of the 4 main additive manufacturing processes used in bone tissue engineering: extrusion-based material, stereolithography, selective laser sintering and inkjet 3D printing. Qualitative and quantitative assessments using a performance index are calculated according to expected criteria for patient care, user-friendly handling, and the affordability of the process. We propose a guideline for users to choose the most appropriate material-process couple.

Highlights:

- The possibilities offered by additive manufacturing processes are examined with an emphasis on the required loop for developing biological implants
- The state of the art and evolution of the different classes of material have grown with the challenging needs of achieving bone regeneration

- Various AM processes are explored with an emphasis on the main methods used to design biological implants for bone repair, including a comparative and critical assessment of their advantages and drawbacks
- The critical analysis is summarized by establishing a performance index of the more promising biomaterial/AM process couples by considering the main requirements of a successful implantable 3D-printed device and accounting for patient and clinician points of view.

Content:

Abbreviation Index

AM: additive manufacturing
BJ: binder jetting
CAD: Computer-aided design
DIW: direct ink writing
DOP: drop-on powder
FDM: fused deposition modeling
LM: layered manufacturing
ME: material extrusion
MJ: material jetting
PBF: powder bed fusion
RP: rapid prototyping
SFFF: solid freeform fabrication
SLA: stereolithography
SLS: selective laser sintering
3DF: 3D extrusion of filament
3DP: inkjet 3D printing

1. Introduction

Additive manufacturing (AM), rapid prototyping (RP), solid freeform fabrication (SFFF), and layered manufacturing (LM) are all equivalent terms for 3D printing. In contrast to subtractive techniques, this manufacturing process is commonly defined as adding a feedstock material layer by layer according to predefined tool paths from a computer-aided design (CAD) [1]. This concept emerged in the 1980s thanks to several innovations, including the work of C.W. Hull on UV curable plastics that led to stereolithography technology as we know it today (US patent 4575330) [4]. In the late eighties, E.V. Fudim photosolidified an uncured

photopolymer by irradiation (US patent 4752498)[5] (US patent 4801477) [6]. Within the same time frame, F.G. Arcela et al. used another technique of additive manufacturing with a laser beam electron gun directed at a fusible for solidification of powder (US patent 4818562) [7]. In 1989, S.S. Crump used thermal solidification upon extrusion to produce 3D objects directly from computer instructions (512329) [8]. S. Yehoshua employed direct inkjet printing wherein the part is formed from a plurality of layers of ink dispensed from the printhead with a drying station that dries layers of the ink dispensed from the printhead on a per-layer basis. The additive manufacturing procedures listed above are further detailed in section 3.

The impacts of additive manufacturing processes on the manufacturing industry were broad, especially because designing complex technical parts can be achieved without modification of the production tool such as in molding and extrusion processes and well-known manufacturing processes that use molds or dies. In addition, additive manufacturing reduces material resource consumption and requires shorter manufacturing cycles to prepare technical parts. However, due to the relatively slower process, especially for processing large parts, AM processes are a perfect match for personalized, small-series products that can be costly using conventional processes. Moreover, since the process is fully automated, there is no need for constant monitoring, and remote production can be possible. Hence, in the medical field, additive manufacturing appears to be an outstanding technology for solving clinical problem. Surgical planning is often used in orthopedic and maxillofacial surgery, especially to augment patient education, improve surgical decision-making, and enhance preoperative planning. In orthopedic patients, the devices that are used to ensure optimal screw trajectory and implantation are called 3D graphs. 3D-printed orthopedic patient models and jigs have gone a step further by providing surgeons with a physical copy of the patient's affected part that can be seen as well as felt and moved around spatially [9]. While the use of 3D-printed models and jigs has now become routine, a similar revolution is happening in the field of designing and printing patient-specific implants. A customized implant for personalized medicine could

perfectly fill a bone defect thanks to clinical data from scans of patients. A tailored and control architecture with desired porosity could be designed to promote bone regeneration due to optimize fluid, cell and blood vessel integration and circulation to the core of the scaffolds when implanted. Examples of 3D-printed implants from CAD models from patient scans can be found in the scientific literature (Figure 1).

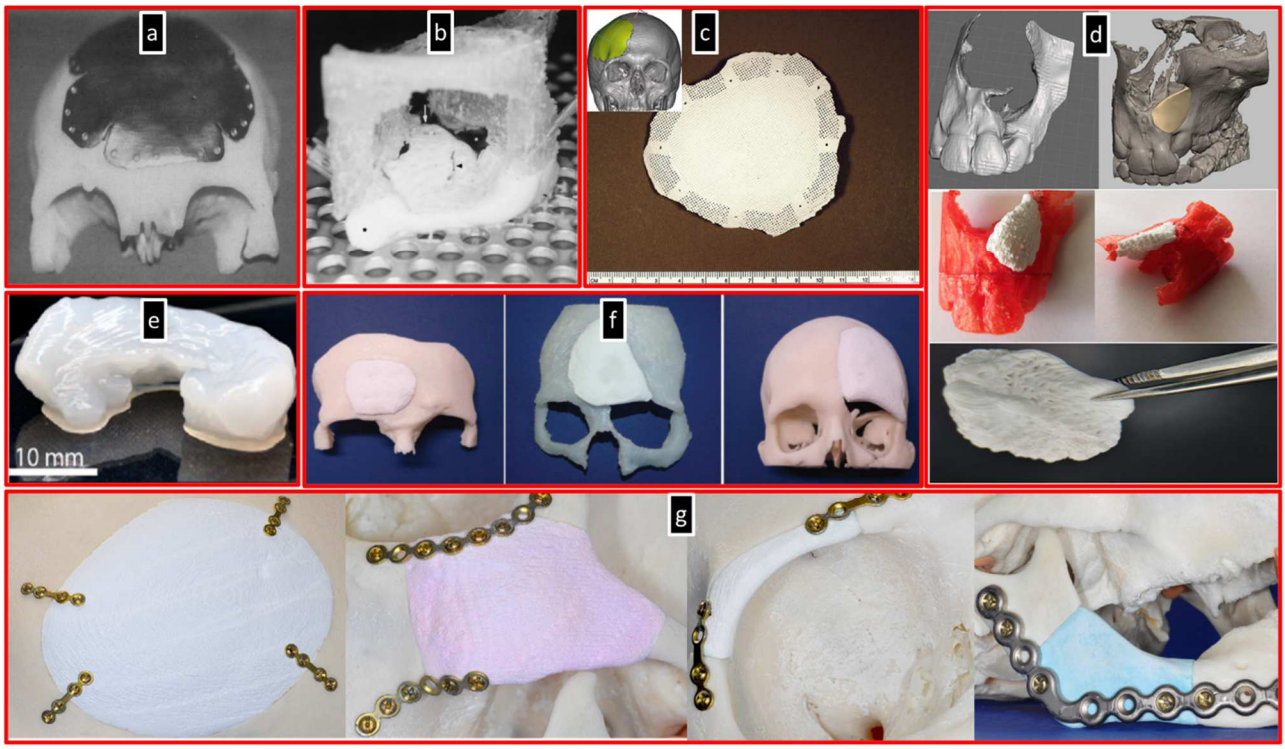

Figure 1: Various biomaterial/AM process couples found in the literature for printing personalized implants
a) titanium/SLS process
b) Hydroxyapatite/SLA process
c) Hydroxyapatite/SLA process
d) Calcium phosphate cement/extrusion-based process
e) Hydrogel of alginate/extrusion-based process
f) Calcium phosphate cement/powder bed process
g) Calcium phosphate cement/powder bed process

Bench research related to the development of 3D-printed implants has substantially increased in recent years. The number of publications found on the Web of Science search engine with the combination of the keywords “bone tissue engineering”, “additive manufacturing”, and “biomaterial” shows a tremendous rise in publications over the years. Interestingly, it took 20

years between the first AM-related patent before witnessing a significant increase in scientific publications related to this topic (Figure 2).

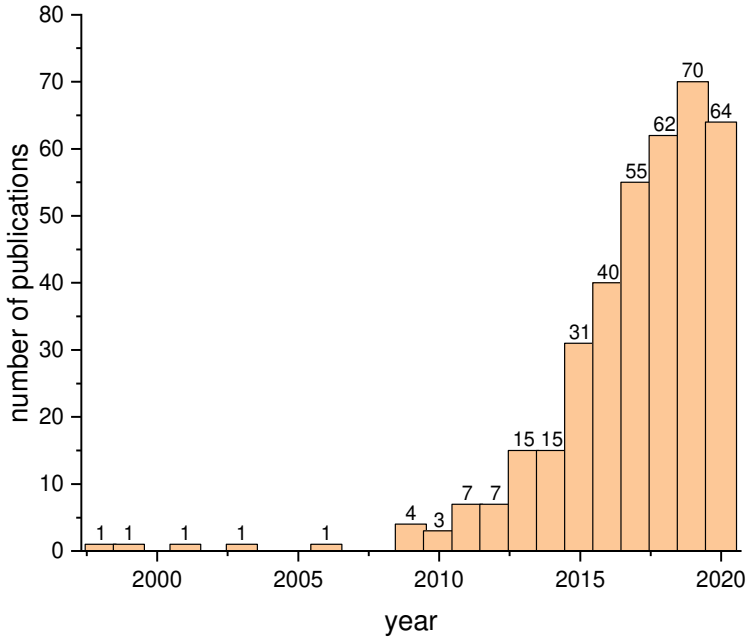

Figure 2: Dissemination metrics for additive manufacturing in bone tissue engineering from web of sciences

Nevertheless, the transfer of 3D-printed implants to clinical applications for bone repair/regeneration is still not common and widespread. The choice of biomaterial depends on the expected mechanical properties for replacement or regeneration according to the targeted tissue engineering application. This also depends on the bioresorption ability of the material. A material devoted to bone replacement must not be bioresorbable, contrary to one devoted to bone regeneration. In addition, the ability to be sterilizable and biocompatible is essential regardless of the considered clinical application.

For example, in the orthopedic field, a replacement of bone loss is often required. In the case of osteoarticular prosthesis, the biomaterial is not supposed to be resorbable. Indeed, it is quite challenging, when bone regeneration is expected, the biomaterial is not supposed to be

resorbable too quickly to avoid the loss of transient mechanical properties. In maxillofacial reconstruction, the biomaterial used in mandibular reconstruction is supposed to have high mechanical performance, as it is a load-bearing bone. In the case of filling the alveolar cleft, mechanical properties are not the expected essential characteristic, as this bone is non-bearing. Nevertheless, regeneration of this bone is expected to make tooth eruption possible. This clinical outcome underlies the bioresorbability of the chosen material. In some cases, when regeneration is expected, the biomaterial has to serve as a guide to promote bone renewal (osteoconduction); then, in a second step, it has to be bioresorbed to make space for the new bone.

The challenge in bone tissue engineering is to develop a biomaterial-based structure that is able to mimic the multiple physico-chemical properties of bone (physiology, morphology, architecture, and mechanical properties). Due to the layer-by-layer building strategy, additive manufacturing techniques are well suited to 3D reconstruction of complex tissue. Furthermore, the ability to integrate biological materials (cells, enzymes, growth factors) in the 3D construct enhances the functionality. This concept is often referred to as bioprinting and requires stricter regulation (e.g., cell therapy) if transferred in the clinic due to the use of biological materials.

This review lists the existing 3D printing technologies used for bone tissue engineering. A comparative analysis between the different pairs of material and additive manufacturing processes is presented. The comparison was conducted for a specification by considering the points of view of clinicians and patients, the need for long-term follow-up patient care, and crucial factors such as mechanical properties, biocompatibility and bioresorption.

2. Overview of the multiple possibilities offered by additive manufacturing

With the democratization of AM in the medical field, a wide range of printers and software are affordable for companies as well as personal use. Medical imaging data (scanner, MRI, or

ultrasonography of patients) are compatible with commercial 3D printer software. This cross-compatibility is made possible due to the integration of clinical patient data (DICOM file) into the digital chain of the 3D printer. One can easily obtain a CAD (computer-aided design) that represents the external shape of a bone defect in patient data from a scanner. The 3D-modeled bone defect is converted into STL format, representing the space tessellation of all internal and external surfaces. This format is not the final step as further processing is needed to achieve a layered representation from the slicing before converting the model to set of machine instructions through the G-code. Three-dimensional printer software handles most of these steps to obtain a 3D printed part of the piece from this layer by layer representation (Figure 3).

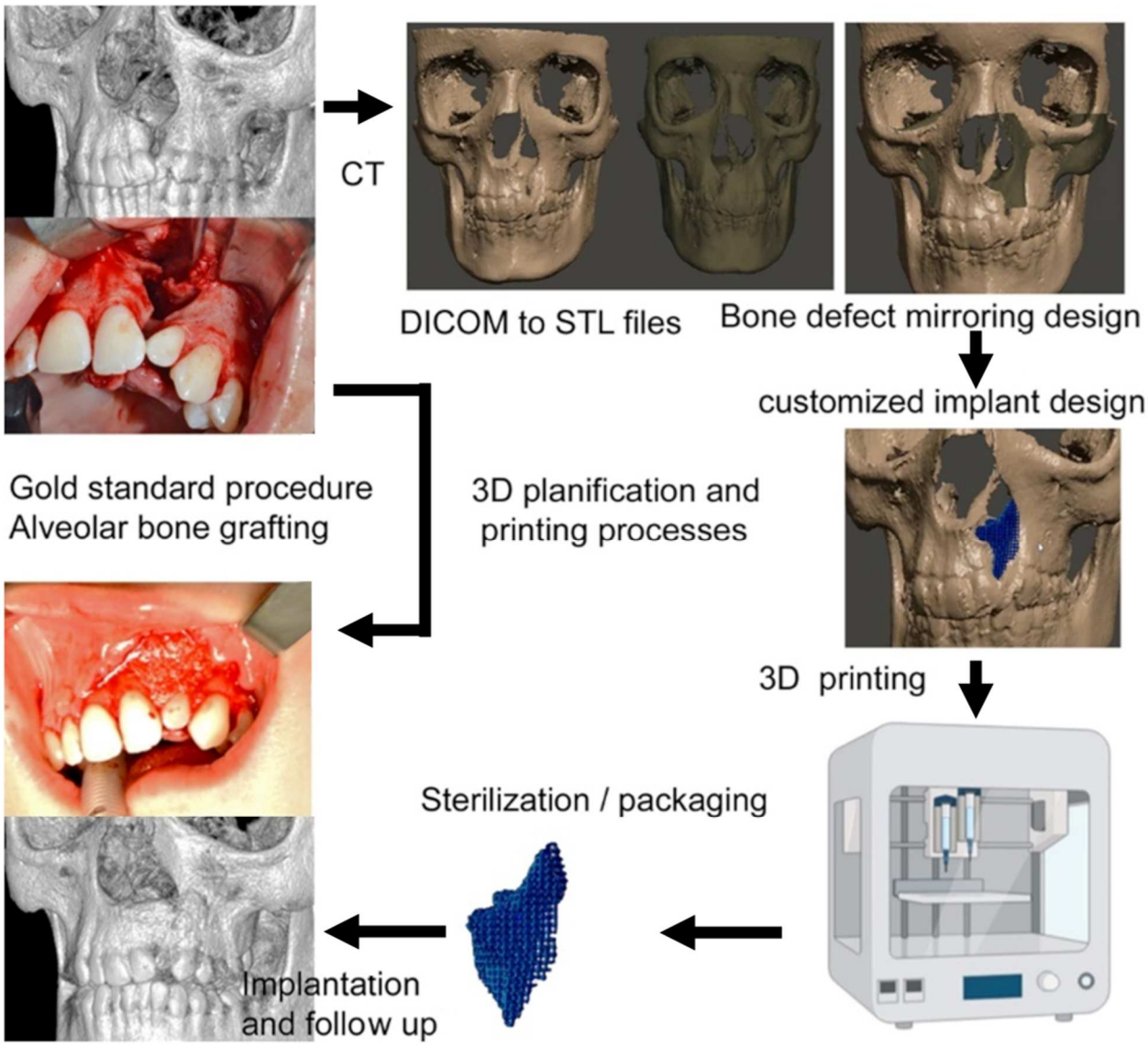

Figure 3: Flow chart of the 3D planning process for personalized patient care with 3D-printed implants. Example of a patient with left alveolar cleft. On the left, a bone grafting procedure (gold standard). On the right, the same patient DICOM files were used to design a personalized bone implant via mirroring planning on the healthy side.

Moreover, an increasing number of open-source software programs for 3D imaging are being developed (*3D slicer®, InVesalius 3®, Meshmixer®*, *Blue sky plan®, Blender®, Preform®*). This allows for the handling and mastering of 3D printing to be very affordable and more popular.

Nevertheless, it is not simple to transfer the bench 3D-printed implant toward clinical application, especially due to strict regulatory processes regarding medical devices.

This section is devoted to a detailed description of the chain that makes it possible to replace/to fill defective parts of a patient's body with parts obtained by additive manufacturing. A focus is placed on the rationale behind replacing defective human body tissue using additive manufacturing. The schematic in Figure 4 is divided into several blocks that illustrates the common steps in AM manufacturing applied to tissue engineering.

2.1 Design criteria

As noted above, it is necessary to obtain access to the data regarding the dimensions and exact geometry of the part to be replaced with a printing process. There are several measurement techniques that allow building a precise digital model of the body part, which is commonly referred to as a computer-aided design (CAD) model. The simplest method consists of making an approximate measurement of the target area and assigning it to a standard geometry such as a cylinder or plate or a combination of such geometries. More elaborate techniques call for acquiring a 3D model with a high resolution, which can take the form of 3D surface mapping or a 3D bulk structure. The first relies on 3D scanners, and the second is based on X-ray microtomography [10]. In particular, the last few years have witnessed increasing attention to X-ray microtomography, as it provides both surface and core information and helps determine what kind of inner microstructures are to be designed [11]. X-ray microtomography works by acquiring 2D radiographic images at different angular positions, and the resulting scans are exploited to build a 3D model using construction algorithms [12]. The gray level associated with each graphical unit in the three-dimensional space, i.e., the voxel, represents the transparency of the material point to X-rays and reflects its inner density. Thus, a reliable 3D CAD can be achieved from X-ray microtomography acquisitions, which show both the topography and the inner microstructure. With laboratory equipment such as X-ray microcomputer tomography (μCT), the resolution achieved is of the order of one micron and can decrease to 150 nm with nanotomography. Details as small as 50 nm can be viewed using

a particular setup with synchrotron radiation [13]. Postprocessing using image analysis software is needed to capture the main structural attributes, such as the surface roughness, density and porosity size distribution, porosity interconnectivity, and porosity wall thickness. Further exploitation of X-ray microtomography data is possible by converting binary images into 3D meshes and performing various computations using multiphysics finite element packages [14,15]. These computations can be used for the prediction of mechanical response under mechanical loading or to examine transfer phenomena. X-ray microtomography images can also be used as a starting point for slicing, which results in a realistic model for 3D printing. However, the approach of building a slicing object for printing based on X-ray microtomography data is less frequently used because of several issues such as the size and large details of the resulting slicing files.

2.2 Material selection

Second, microstructural, physical and chemical analyses are carried out on the defective or missing human tissue to be replaced. The objective is to obtain material selection criteria that reproduce the functionality of the part to be replaced or allow for further development and formulation of an ad hoc material with satisfying performance. In this regard, several research efforts have been dedicated to formulating biocompatible materials [16]. The recently widespread additive manufacturing techniques provide great flexibility to process a variety of materials, for which intrinsic properties prior to and after 3D printing need to be determined. Among these properties is the rheology of the material, which plays an important role in successful printing, especially when using deposition techniques such as fused filaments (FDM) or liquids (LDM) for 3D printing. In the case of the FDM process, for instance, low viscosity is needed to ensure the flow of the material through the nozzle, and the stiffness of the material needs to be high enough to prevent the printed object from collapsing. The thermal behavior of the feedstock material may also be important for additive manufacturing

processes that use heating sources. The laying down kinematics, printing and base temperatures, and other printing parameters should be adapted to the thermal properties of the feedstock material reflected by its thermal expansion thermal conductivity and heat capacity [17,18]. An important design constraint is the creation of an environment capable of ensuring cell viability (cell nourishment, biocompatibility, resorption, adapted stiffness) [19]. The design of supposedly living tissue/bone-like pieces reduces the material selection to those that are biocompatible and exhibit a low inflammatory response. There is a huge amount of research that is currently being undertaken to identify new materials that meet the targeted specifications, especially biomass such as **zinc**. These materials have to meet the AM processability criteria mentioned above to be considered reliable feedstock materials for 3D printing [20].

2.3 Virtual design

From the material testing results (second stage), material performance criteria are available to evaluate the fitness of the virtual design. This is done in the third stage. Numerical modeling is used to predict the design performance by relying on both the intrinsic properties of the feedstock materials and the design specifications. The predicted response can be a pure mechanical response or a complex multiphysical response that translates the ability of the design to sustain mass and heat transfer together with the mechanical stability. A numerical prediction based on finite element calculations generally follows five dependent steps: defining the geometry based on CAD models or 3D imaging acquisition. The meshing of the design is the second step, which consists of a continuous mapping of the design body with structural elements with a set of defined variables such as the displacement, temperature, and concentration. The material model needs to be defined for each phase composing the design. This is the third step, where presupposed knowledge about the physical and chemical properties of the intrinsic material should be used. The fourth step consists of defining the

computation conditions, which take the form of surface or body loads according to realistic criteria. The final step is solving the set of equations of the studied physics by iterative or direct schemes and retrieving the solutions. These solutions comprise two types: global results such as the overall reaction force and mechanical stress or detailed spatial distributions representing the counterplots of quantities of interest such as the deformation of each material point. The predicted results can be compared in a direct scheme to the design characteristics, such as the amount of porosity and density, to derive direct correlations between the design variables and the predicted performance.

2.4 Design optimization

Within this stage, the final design that meets all expectations in terms of mechanical stability, cell growth potential and mass transfer capabilities is further processed from the CAD to the sliced feature. The slicing step is generally performed in the software that controls the printing process by importing the digitalized model of the body part to be printed as an STL file. The main role of the slicer consists of breaking down the 3D part into a series of 2D layers and adopting a filling strategy for these layers. The filling pattern is defined according to the type of AM and can take several forms, such as the trajectory of the printing head or laser in-plane coordinates. The criterion used for pattern filling is generally purely geometric, and the number of allowed printing parameters that can be modified in the slicer depends significantly on the degrees of freedom allowed for by the printer manufacturer (closed or open-source software). The selection of adequate printing parameters is classically performed via trial-and-error, and process optimization is not yet fully available for most commercial solutions. The large number of printing parameters that need to be appropriately set can be confusing, and for most preliminary trials, can compromise the quality or feasibility of the printing. This is particularly true if the feedstock material is a newly developed filament, as in the case of the FDM process. A simple parameter such as the part orientation can lead to a variety of

renderings because the slicing of the part according to different orientations results in differences in support amounts and mechanical anisotropy [21–23]. Once the slicing parameters are set, the slicer generates an instructions file (commonly known as G Code format). These instructions dictate the behavior of the printer (heating and cooling operations, control of the kinematics of the material laying down) for each building layer. For an FDM-type process, the filament is simply laid down along its length after reducing its diameter, typically from 1.75 mm to 100–400 μm. For SLS, SLM or stereolithography processes, local melting or polymerization are more involved via the action of a light source. The use of biocompatible material adds more challenges beyond those of the printing process because the physiological properties of the printed part are intimately related to the capabilities of predicting cell growth and differentiation. These additional capabilities should be determined from the set of printing parameters and the material design. This is referred to as the 4D printing process, where the postprinting transformation through time represents a new dimension. Parts that are printed using this strategy are named adaptive structures.

Once the part is printed according to an optimized design and identified set of printing parameters, additional steps may be needed. Postprocessing, such as annealing, can be applied to achieve a more cohesive structure and better mechanical stability. An optimization loop can also be developed to handle the process-induced defects that are inherent in the printing process. If the result is acceptable, in vivo tests can be planned according to established protocols.

2.5 Biological assessment

In vitro tests are used to check the biocompatibility of a medical device: ISO 10993. In vivo tests are mandatory to evaluate the fitness of printed prototypes to sets of criteria such as the mechanical strength, cell proliferation, cell differentiation, and inflammatory response. Depending on the score obtained during these tests, improvement of the material may be

needed by circling back to stage II. Attempts to reformulate the material with better intrinsic properties can be a costly option because of the need to go through the same printing optimization procedures. However, reconsidering the design criteria by adjusting geometrical variables such as the porosity, wall thickness, and size may be a cheaper option that can be fully conducted in stage III.

A successful in vivo result requires evaluation of the implant at different time frames, which renders the exploration of design modification slightly difficult because the design optimization needs to consider short-, medium- and long-term behavior.

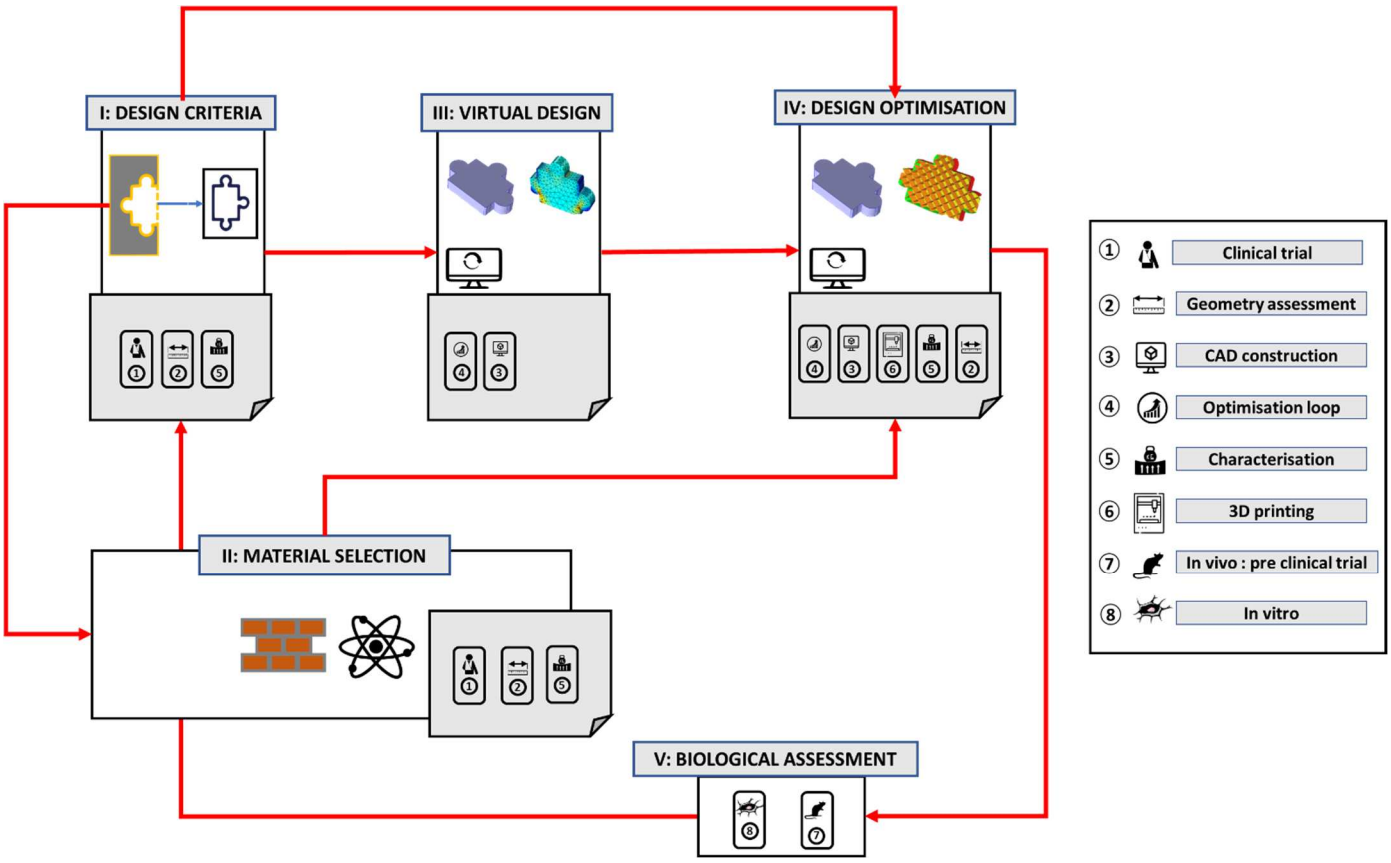

Figure 4: Schematic representation of the common steps in bioprinting procedures to design implants intended for medical uses.

2.6 Concluding remarks

Analysis of the AM literature shows that most AM solutions follow a direct loop procedure in which the outcome of a particular technology is not fully mastered. Optimizing the design based on trial and error helps to understand the flaws of the process and how to eliminate them. While this is traditionally done in many applications, there is much room for improvement if topology optimization is included in the loop. Bridging additive manufacturing with topology optimization is natural since CAD models of the designs that are used as a basis for 3D printing are the same models that are exploited to determine the design performance through numerical predictions. Within the context of bioengineering, constraints related to the evolution of implants add challenges to the optimization process, but this linking is still not out of reach. By using proper optimization algorithms and time-dependent predictions, designs that anticipate the response of the printed structure under physiological conditions can be made according to the material test procedures and requirements.

3. AM process: a promising tool for mimicking the multifunctional and architectural aspects of bone tissue

3.1 description of the bone tissue and its functions

Deep knowledge of bone tissue is critical to consider its regeneration.

The simplest approach consists of mimicking the structure and chemical composition of bone. To mimic natural bone, it is crucial to know its main characteristics. Nevertheless, it is not so minimalist; bone is multifunctional and structural and has many different aspects including anatomical location, sex, age, and physiopathology. Most adult skeletal diseases are caused by excessive osteoclastic activity, which leads to an imbalance in bone turnover and increased resorption at the expense of bone synthesis. This imbalance can cause diseases such as osteoporosis (related to aging, especially in the female population) and periodontal disease or can be the consequence of autoimmune or tumor pathology such as rheumatoid arthritis, multiple myelomas and cancers at a metastatic stage [24]. Bone diseases can also be due to

growth disturbances resulting from genetic or dysfunctional origins. Bone fractures are also frequent. Thus, maintaining the integrity of the skeleton and its functional appearance essentially relies on the balance of the stages of bone remodeling described above [25] (Figure 5).

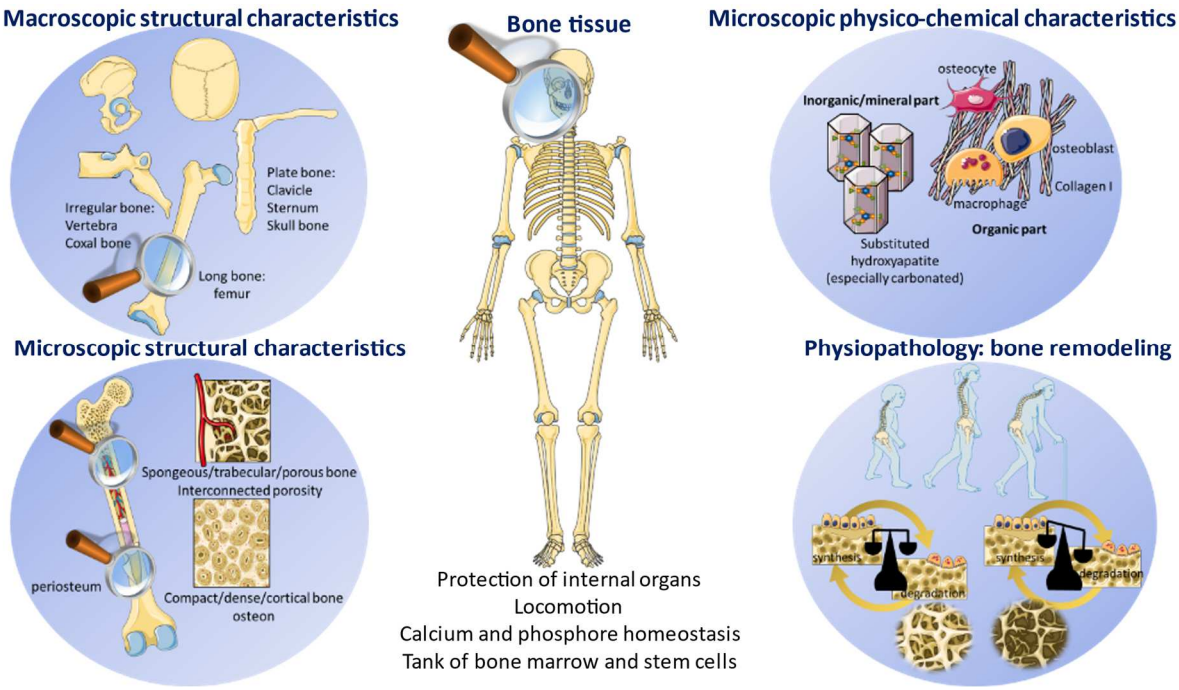

Figure 5: Bone: a multifunctional and multistructural tissue.

3.2 composition of the bone tissue

Bone tissue is a living connective tissue made of two parts: a mineral and an organic **part** [26],[27]. The organic membrane is composed of 90% collagen proteins, mainly type I, and 10% noncollagen proteins, such as bone sialoprotein (BSP), osteocalcin (OSC), osteopontin (OSP), osteonectin (ONN) and fibronectin (FN). A small amount of lipids also makes up the extracellular matrix (ECM). The inorganic or mineral phase consists mainly of apatite crystals, sized on the order of a hundred nanometers [28]. These crystals are similar to the hydroxyapatite crystals of formula $Ca_{10}(PO_4)_6(OH)_2$, but natural bone apatite is not pure stoichiometric hydroxyapatite and contains traces of other elements, such as carbonate (CO_3)

and magnesium (Mg), sodium (Na), and chlorine (Cl) [29], [30], [31], [32]. Silicon (Si) can also be found in small quantities in mature bones in the calcification phase. The amount of silicon in the bone varies with the age and sex of an individual. It also varies depending on the type of bone [33]. Except for the ossicles of the ear, bones are vascularized and made up of a double layer that varies in thickness according to their role. A smooth, dense, continuous outer layer covers the bone named cortical or compact bone. The inside of cancellous or trabecular bone comprises many spaces, or pores, which contain the bone marrow and blood vessels (Figure 6).

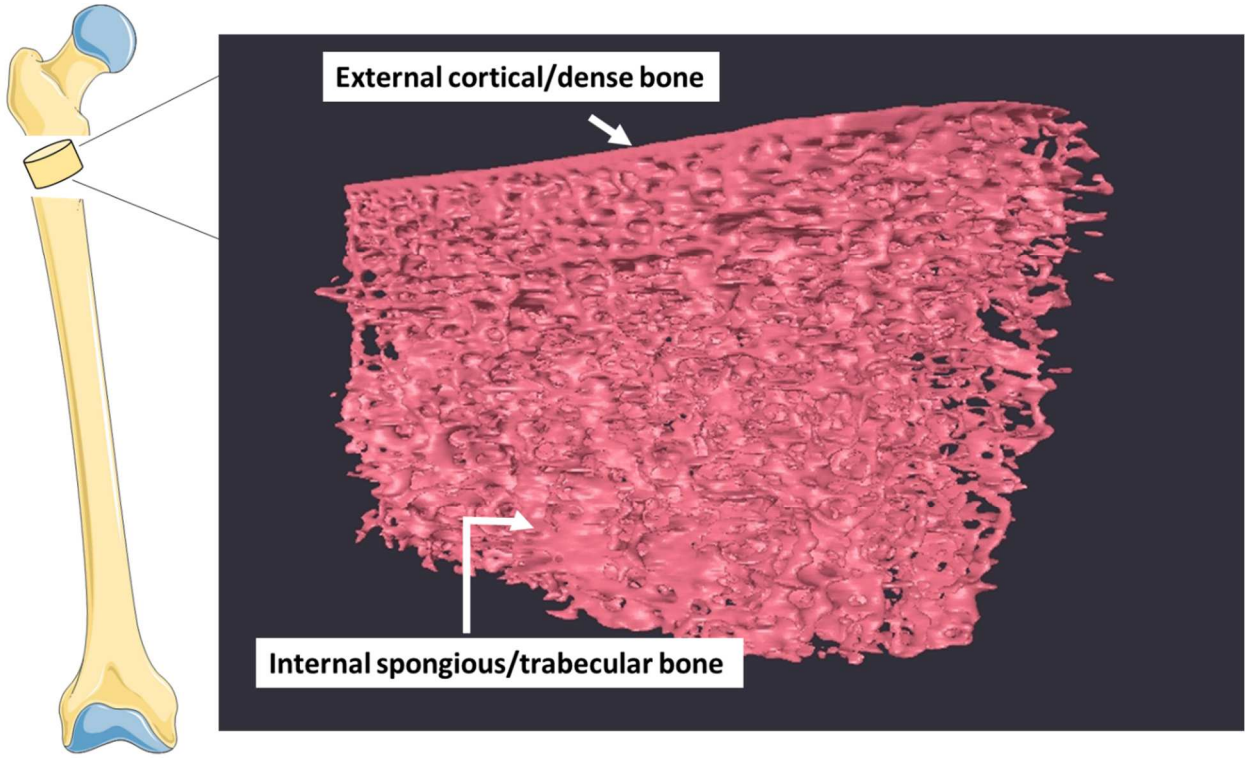

Figure 6: Micro-CT of a sample of femur showing external cortical/dense bone and internal spongious/trabecular bone.

Compact bone contains several subunits that are made up of concentric bony lamellae called osteons. At the heart of these osteons, there are cavities named the Haversian canals that contain blood vessels [34], [35].

The internal spongious bone is composed of bone cells:

- Osteoblasts, which synthesize the tissue,

- Osteoclasts, which resorb it,

- Osteocytes housed in bone cavities (osteoplasts), which contain mechanoreceptors that regulate osteoblast and osteoclast activity.

- Cells bordering the surface of the tissue that are less active than the osteoblasts from which they are derived but participate in the maintenance of the tissue, as they have a mechanical sensor function.

3.3 The bone remodeling

As a dynamic tissue, bone undergoes perpetual renewal [36],[37]. Once the skeleton has reached maturity, regeneration occurs periodically to replace the old bone with new bone, avoiding old bone accumulation. This process is called remodeling or renewal and is responsible for the complete regeneration of the adult skeleton every 10 years. Bone remodeling is ensured by the coupled action of two distinct types of cells: osteoblasts, which synthesize bone tissue, and osteoclasts, which absorb it. The initial phase begins with the activation of osteoclasts, whose main role is the degradation of the organic part by the action of enzymes such as cathepsin and collagenases as well as the dissolution of the mineral part by the formation of an acidic environment by the action of proton pumps. This step is activated in response to different stimuli (bone crack, loss of mechanical stress, low blood calcium, altered levels of hormones and cytokines in fluids). The osteocytes interconnected in the extracellular bone matrix on a network extending 130–390 nm in diameter experience the loss of mechanical stresses due to cracks. Bone cracks then cause osteocyte apoptosis, inducing the secretion of chemoattractant factors such as M-CSF (macrophage-colony stimulating factor) and RANK-L by osteocytes and osteoblasts. These factors stimulate the differentiation of osteoclasts by interacting with the RANK receiver expressed on them and recruiting them. These multinucleated cells have the capacity to dissolve the bone mineral

phase by the action of carbonic anhydrase. This enzyme catalyzes the conversion of carbon dioxide and water to carbonic acid: $CO_2 + H_2O = H_2CO_3$.

An H+/ATPase (adenosine triphosphatase) proton pump also creates an acid compartment in the area of interest to be dissolved by releasing H+ protons into the medium [38]. Osteoclasts also carry out the enzymatic degradation of the organic bone matrix via the action of collagenase and cathepsin K [39], [40].

When bone resorption gaps have been created, the action is finished, and the cells die by apoptosis. The dead osteoclasts are then replaced by macrophages, which are responsible for cleaning the bottom of the resorption gap. This phase of remodeling is called the inversion phase. During the second phase of bone turnover, macrophages are replaced by mesenchymal stem cells (MSCs), which reside in the bone marrow and differentiate into osteoblasts. Once osteoblasts are formed, they can synthesize the bone matrix and mineralize it. After synthesis of the organic matrix by osteoblasts, there is gradual mineralization by deposition of biological hydroxyapatite between collagen fibrils[38], [39], [41].

This action takes place within a site called the basic multicell unit (BMU), which is 1–2 mm long and 0.2–0.4 mm wide and comprised of osteoclasts, osteoblasts, a central vascular capillary and nerves associated with connective tissue. Each BMU is active in a particular place and period of time. In a healthy adult, 3–4 million BMUs are initiated per year, and approximately 1 million functions at any given time. The life of a BMU is 6–9 months, and its speed of action is approximately 25 µm per day. The lifespan of osteoclasts is 2 weeks, while that of active osteoblasts is 3 months. The interval between successive remodeling events at the same location is 2–5 years. The bone volume replaced by a single BMU is approximately 0.025 mm^3. The skeleton renewal rate is equal to 100% per year in the first years of life and then decreases to approximately 10% per year [27], [36]. This allows for bone to ensure its multiple functions: body protection (the heart, lungs, and other organs and structures in the chest are protected by the rib cage); support of structural and mechanical action of soft

tissues, such as the contraction of muscles, expansion of lungs [42], and motion; and a reservoir of endocrine systems that regulate the level of calcium and phosphate ions in the circulating body fluids. Bone is also a production site for the blood-forming system, i.e., bone marrow. In some pathological cases such as osteoporosis, the balance between bone resorption and bone neosynthesis is disrupted (Figure 4).

3.4 Human bone characteristics and AM

The health state of the bone tissue depends on the integrity of each length scale of the structure: nanostructural, microstructural and macrostructural. The mechanical properties of bone depend on the integrity of the macroarchitecture (global shape) and microarchitecture (especially porosity), which in turn depend on the nano and microphysicochemical components encompassing biological materials (cells and their secretomes). Disturbances in skeletal structure and function are caused by an imbalance in bone turnover (osteoclast bioresorption and osteoblast bone neosynthesis) that leads to morbidity and shortened lifespan. Hence, biomaterials for bone repair must ideally mimic autologous bone and encompass several properties, including mechanical and structural properties such as the porosity and chemical properties (phosphorus, calcium, hydroxyapatite). Due to the potential for designing optimized biomaterial architectures, additive manufacturing processes are very promising to enhance bone repair, especially in personalized patient care (Figure 7).

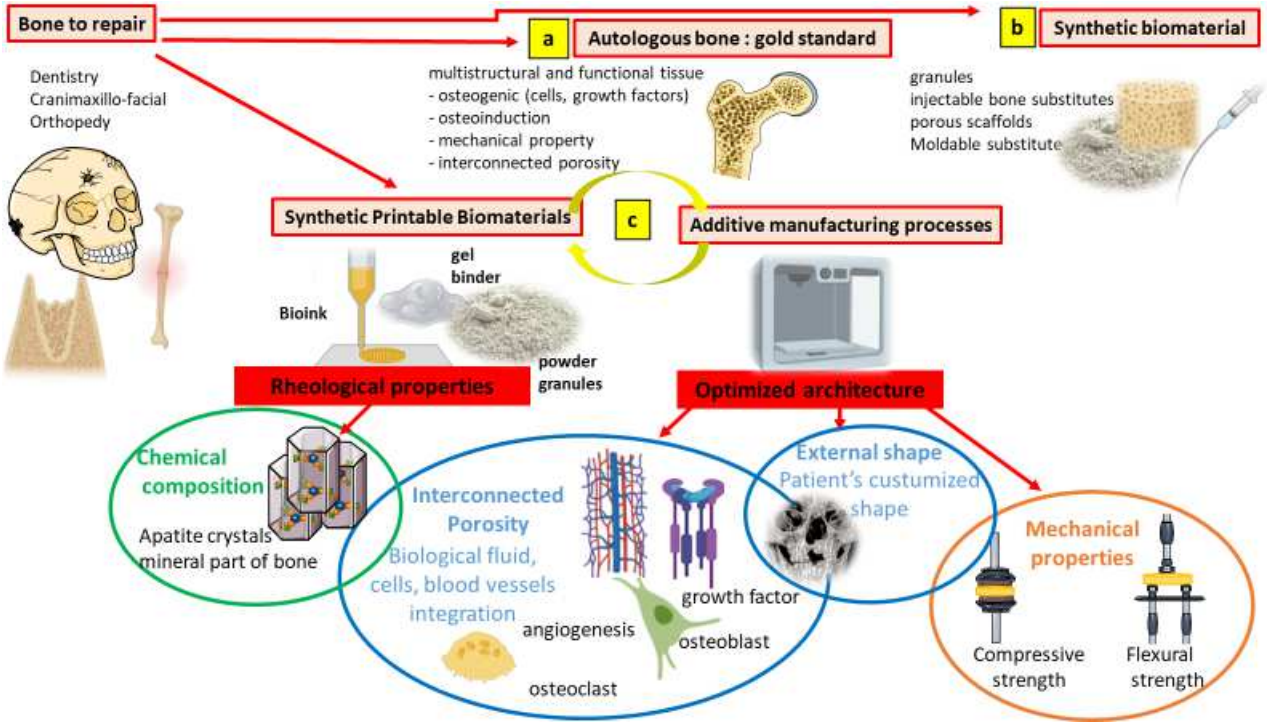

Figure 7: Alternative processes for bone regeneration
a) autologous bone graft, the gold standard
b) synthetic biomaterial
c) Biomaterial/additive manufacturing pair for customized personalized implants

3.5. Bone regeneration and AM processes

The desire to overcome the well-known cons of using autografts, such as comorbidity and short supply, gave rise to a keen interest in biomaterials. A growing trend in the 1990s made scientists and clinicians more acquainted with the use of synthetic or natural biocompatible, bioactive, bioresorbable materials to improve bone repair, especially in the orthopedic craniomaxillofacial and dental surgery fields [43].

The specifications of a biomaterial for bone repair depend on the location of the bone to repair and its load-bearing or low/non-bearing function (Figure 8). They also depend on the surgeon's point of view and preference when several possibilities can be envisaged. For example, some cranio-maxillo-facial surgeons still prefer using titanium due to its greater impact protection. In addition, some consider that resorbable plates are not as effective as titanium plates for facial fracture repair [44].

Efforts have been made to initiate bone regeneration instead of only bone replacement, leading to research to design accurate biomaterials and conduct efficient bone tissue engineering (Figure 8). The challenge consists in regenerating bone instead of merely replacing it. Design of a 3D implant based on the selection of the material and the architecture is crucial for reaching this goal.

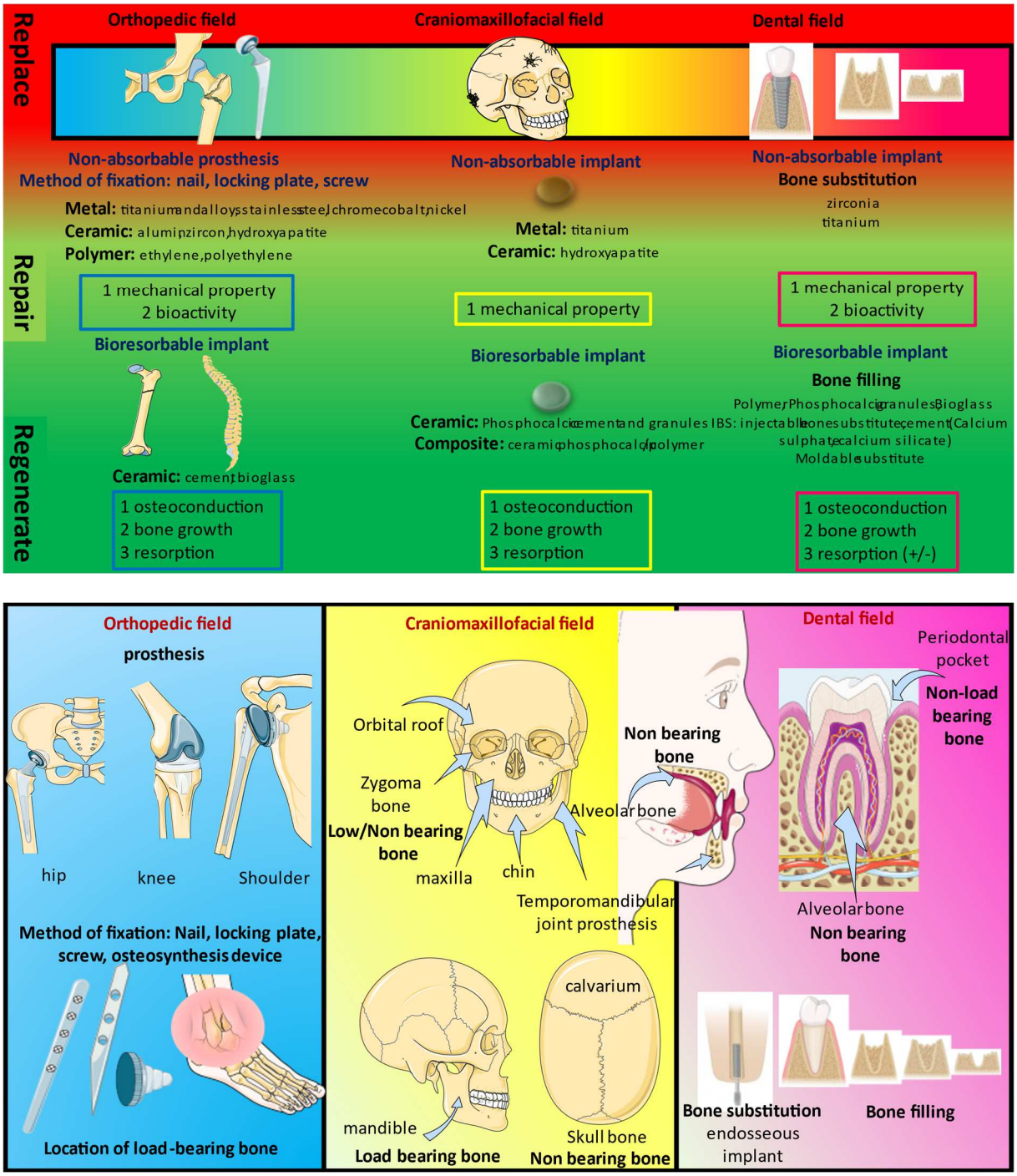

Figure 8: Fields of surgical medicine that deal with bone repair and bone regeneration.

The first intended applications include fracture repair, deformity correction, and arthrodesis using the nail, locking plate, and screw methods of fixation [45], [46], [47].

In orthopedic surgery, replacing bone can be the second targeted therapeutic application, especially following limb amputation. The large size of the defect encompasses bone and soft tissue losses such as muscle and articulation loss, necessitating a replacement to repair functions of locomotion and gripping. The term prosthesis is used for an implanted medical device instead of implant. In recent decades, several successful low-price prostheses have been designed, such as hip and knee prostheses. These prostheses permit the reliable restoration of mobility while reducing pain within hours. The biomaterials used are nonresorbable and bioinert, and do not show any biological reactions. Alumina (Al_2O_3), titanium oxide (TiO_2), and **zirconium** are used in orthopedic surgery as endosseous implants to improve bone integration. Polyether-ether-ketone (PEEK) is a widely used orthopedic material with an elastic modulus that is more similar to bone than metals and ceramics, especially for spine fusion. It is radiolucent, and its mechanical properties are closer to bone compared to titanium decrease stress shielding [48]. In addition, bioactive materials display bone-bonding ability and stimulate positive biological reactions at the material/tissue interface. Different kinds of surface modifications can extend the tissue repair and osseointegration ability of materials.

The material surface of orthopedic prostheses plays a crucial role in biological interactions. Modification of the surface topography, surface roughness or surface chemistry can lead to the best performance in osseointegration, biocompatibility, and mechanical resistance [49].

Surface modifications can be divided into two categories: physical and chemical. Chemical modification encompasses different techniques of coating or chemical grafting. Physical modifications result in a change in the topography, roughness and morphology of the surface. Sandblasting followed by acid etching may currently be regarded as the gold standard technique to create microrough surfaces [50]. However, advanced technical processes to

modify the physical properties of materials can also be used to alter the surface chemical properties (Figure 9).

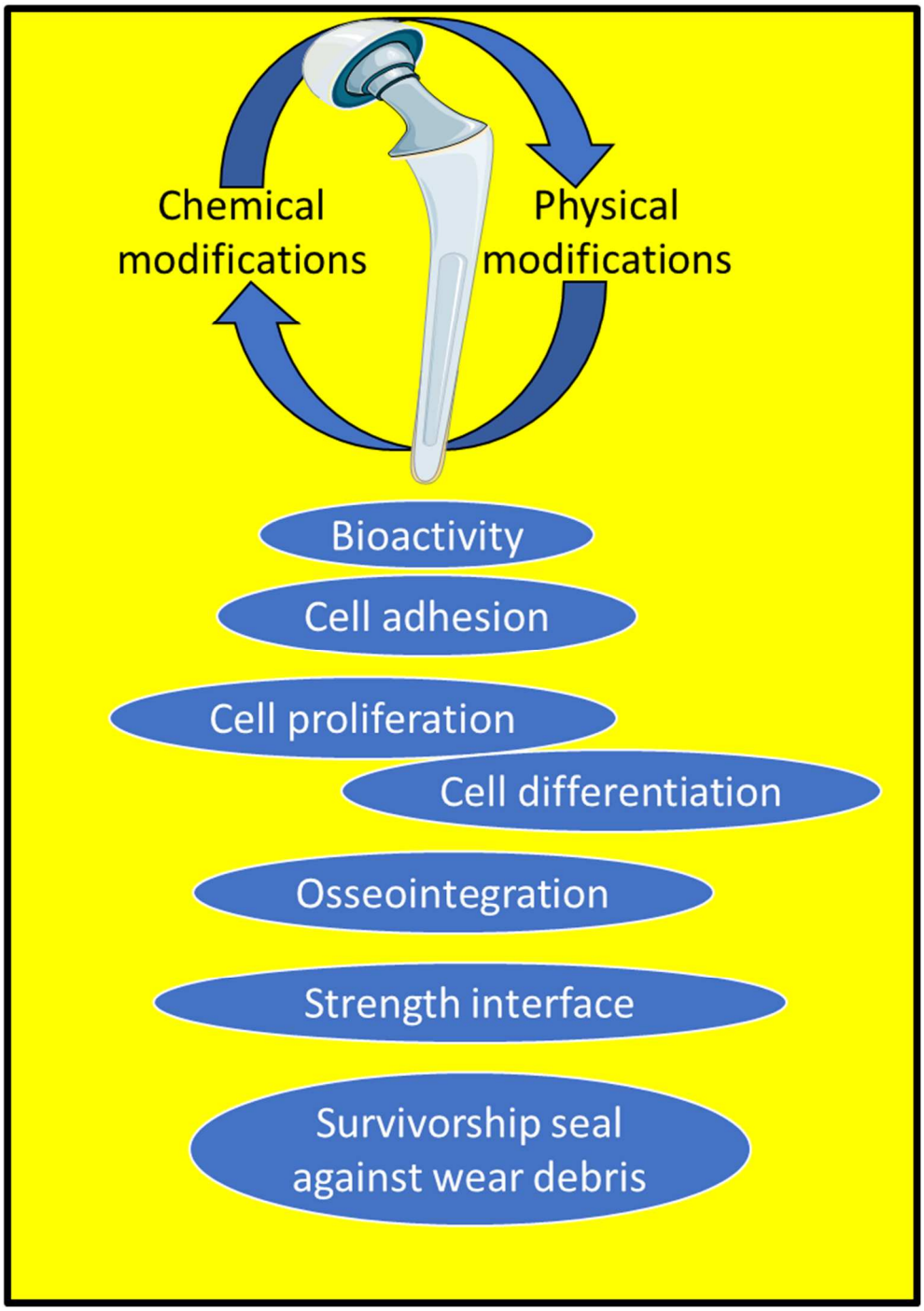

Figure 9: The synergistic effects of chemical and physical surface modifications involved in the biological reactions and interactions of biomaterial surfaces with the host environment.

More challenging orthopedic surgeons seek bone regeneration in the case of spinal fusion and fracture of long bones.

Cranio-maxillo facial surgery is a complex field of bone reconstruction, as it deals with bones in tight contact with organs and nerves implied in different senses: hearing, sight, taste, and smell.

Depending on the location, bone has a load-bearing function, i.e., the mandible and maxilla are load-bearing bones. Zygomatic bone and calvaria are nonbearing bone (Figure 10). The development of a wide range of materials used in reconstructive surgery, such as titanium, polymethylmethacrylate (PMMA) and polyetheretherketone (PEEK), has been especially useful in cranio-maxillofacial surgery. In 1999, an AM titanium implant was created by Winder et al. **[51]**. Then, a 3D-printed personalized titanium cranial plate implant (BioArchitects, the United States) was approved by the FDA [3]. PEEK was first reported to be used in cranioplasty in 2007 **[52]**. In 2013, the world's first personalized 3D-printed PEEK skull implant (Oxford Performance Materials, the United States) was approved by the FDA [3]. Cranio-maxillofacial and dental fields have some commonalities, as they require the repair and regeneration of bone in the oral mucosa. Extra precaution should be taken to avoid infections. Regeneration is required and underlies the use of a bioresorbable material that serves as a support for new bone formation initially and then disappears to provide space for the new bone and permit facial growth and dental eruption, especially in children. In the dental field, bone augmentation is the most common clinical application, especially before implantation. These materials are called IBS (injectable bone substitute) or moldable substitutes and are expected to be bioresorbable. This is the intrinsic characteristic of cement. Cements are manufactured by mixing a solid part (powder of calcium sulfate or silicate) with a liquid part (phosphate buffer, acidic solution) to result in an easy-to-handle formable paste. In dental surgery, calcium silicate and calcium sulfate have been used for a long time [53],

[54],[55] [56], [57]. Nevertheless, nonabsorbable materials are also used in dentistry to serve as a barrier to prevent wound space colonization by gingival cells, for example [58].

4 The limits of AM: the barriers to clinical translation of AM implants

As explained in Section 2, the typical AM part manufacturing follows a direct path, i.e., a measurement of tissue to be repaired at the scale of the individual, leading to a reconstruction of the 3D CAD model before considering the part printing structure and printing of the part. This resulted in a rather rapid prototyping reasoning, often done with materials that are not yet compatible for integration and replacement of the defective part of the human body. Thus, to achieve structures capable of replacing bone, for example, there are challenges on several levels. It is first necessary to formulate a biocompatible base material and properly characterize its rheology, which must be AM-friendly. Modeling work is also necessary, taking the process into account in the optimization.

Even with some advantages such as a gain of time in certain cases and the precision of the pattern, some conditions can be incompatible with the AM process. For example, the AM process may not be adapted to a specific desired application because it does not meet the tolerance and surface finish specifications. For example, in orthopedics the femoral head part must be smooth to facilitate joint movement and avoid erosion. The part can be completed by postprocessing to achieve the desired tolerances and surface finish. Other clinical challenges are related to the complexity of the shape, as accurate filling of the defect can be hampered due to bone residue or possible conic shapes with the narrow side accessible and an inaccessible wide part (Figure 10).

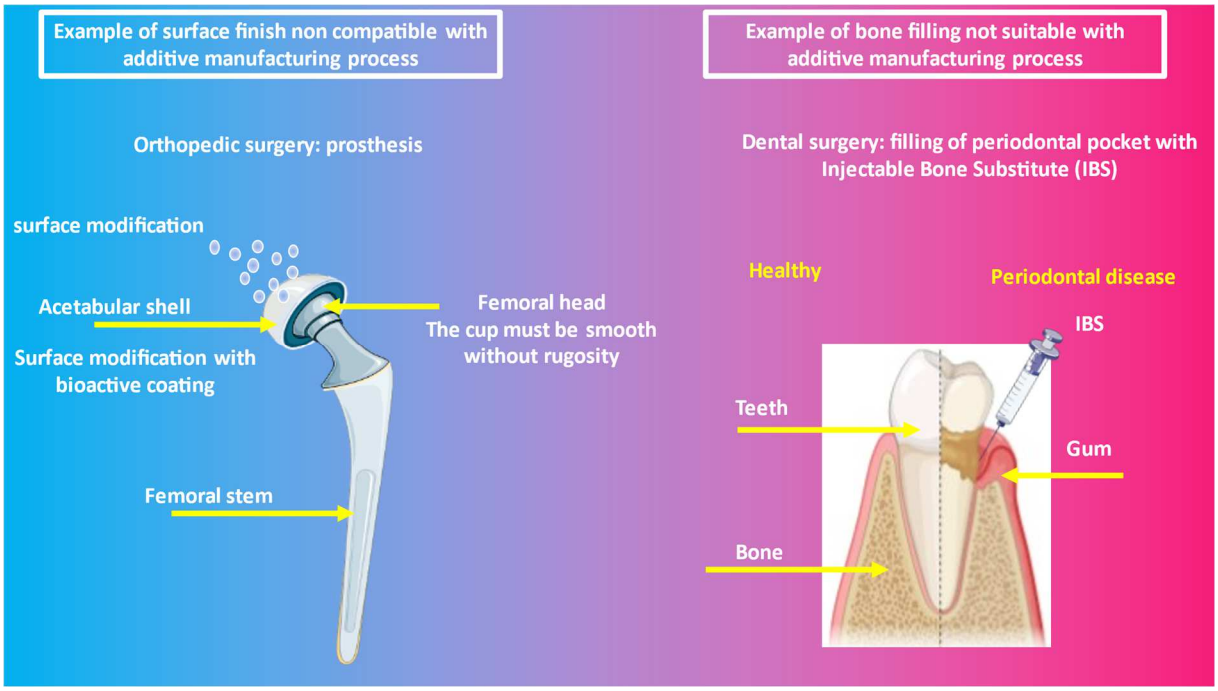

Figure 10: Examples of clinical applications where AM is not the most suitable manufacturing process

In some cases, an injectable material is more suitable. For example, the filling of a defective periodontal pocket, which is a small bone defect between the gum and teeth, can be accurately performed with IBS (injectable bone substitute), and is a noninvasive surgery that allows for filling through a small entrance.

Moreover, the fabrication of 3D-printed scaffolds has several requirements to ensure success and widespread application. An important factor is the collaboration between medical and engineering experts and familiarization with 3D bioengineering abilities. The 3D printer should print quickly with high resolution and be compatible with biocompatible materials/living cells with an affordable cost. Biomaterial selection consists of determining optimal combinations to obtain the desired functional, mechanical and supportive properties. Evaluation of different criteria of additive manufacturing technologies should consider the technical feasibility to reach the expected outcome for clinicians and patients.

Autologous bone grafts continue to represent the gold standard treatment for critical-sized bone defects. Several factors have contributed to the slow translation of research from the bench side to the bedside, including technical, collaborative and regulatory issues. The use of 3D printing in the clinic requires expertise in several multidisciplinary fields. The clinician must provide the patient scan, design the implant with the engineer/prosthesist and master the 3D printing process. The pharmacy must package and sterilize the implant.

Although AM is promising, the clinical applications where it is mature and used routinely for bone tissue engineering remain limited. AM has started to be very useful for surgical planning because it allows for an accurate surgical gesture. This application is encountered more frequently in craniomaxillofacial and orthopedic patients [9], [59]. For example, orthognatic surgery that aims to correct the jaw position is a very demanding field. 3D-printed cutting guides and resin prostheses to be inserted at the level of the jaw osteotomy to start the programmed displacement upstream are applicable in cases of increased jaw height and have been shown to lead to better outcomes than the traditional artisanal method [60]. Five orthopedic patients with acetabular fractures underwent successful surgery using specific plate templates from virtual surgical planning and 3D printing. These plate templates were matched with the acetabular plate design and used intraoperatively to avoid intraoperative contouring, decrease the morbidity of patients and prevent wastage of resources in preoperative planning and computer design [45]. Another clinical study performed in orthopedic surgery between December 2014 and December 2015 on ten patients who underwent posterior cervical fusion surgery with cervical pedicle screws, laminar screws or lateral mass screws proved the efficiency of 3D surgical planning for the accurate positioning of screws. Individualized 3D printing templates were made with photosensitive resin by a 3D printing system to ensure that the screw shafts entered the vertebral body without breaking the pedicle or lamina cortex [61].

A study that investigated clinicaltrial.gov (https://clinicaltrials.gov/) proved that AM for printing 3D implants for bone repair and regeneration is less common than 3D surgical planning for education, guidance or plates (Table 1).

Title of the clinical trial	Conditions	Interventions	Location
Jaw Reconstruction With Printed Titanium and Free Tissue Transfer	Neoplasm, Oral Osteoradionecrosis of Jaw Mandibular Diseases (and 3 more...)	Procedure: Mandibular reconstruction with free tissue transfer.	United Kingdom
Clinical Application of Personal Designed 3D Printing Implants in Bone Defect Restoration	Defect; Internal Prosthetic Device, Implants and Grafts, Orthopedic, Bone Graft	Procedure: 3D printing implant Procedure: autogenous bone grafting	China
3D-Printed Personalized Metal Implant in Surgical Treatment of Ankle Bone Defects	Bone Diseases	Device: 3D printed personalized metal implant	China
Efficiency of 3D-printed Implant Versus Autograft for Orbital Reconstruction (TOR-3D)	Significant Bone Defect in the Orbit	Procedure: Bone autograft Procedure: Orbital reconstruction by 3D-printed porous titanium implant	Not specified
Assessment of Maximal Incisal Opening Using Patient Specific Titanium Eminoplasty Versus Inlay Autogenous Bone Graft for Treatment of Chronic Mandibular Condylar Dislocation	Chronic Mandibular Condylar Dislocation	Device: Patient-Specific Titanium Eminoplasty Procedure: Inlay Autogenous Bone Graft	Not specified
The Use of 3D Printing in Orbital Fractures	Orbital Fractures	Device: office-based 3-dimensional printers (OB3DP) Device: standard stock orbital plate	United States
Lumbar Fusion With Next Spine 3D-Printed Titanium Interbody Cages	Lumbar Degenerative Disc Disease	Device: Interbody cage (titanium)	United States
	Lumbar Spinal Stenosis Lumbar Spondylolisthesis (and 2 more...)	Device: Interbody cage (PEEK)	United States
Talus Replacement Registry	Avascular Necrosis of the Talus	Device: 3D talar augmentation	United States
Clinical Application of Personal Designed 3D Printing Implants in Bone Defect Restoration	Defect; Internal Prosthetic Device, Implants and Grafts, Orthopedic, Bone Graft	Procedure: 3D printing implant Procedure: autogenous bone grafting	China

Table 1: A summary of clinical trials using the AM process for education, guidance, plate or implantation for bone repair/regeneration (clinicaltrials.gov consultation on 20 November 2020).

5. A historical overview of the concept of biomaterials for bone regeneration

In the medical field, biocompatibility is undoubtedly the most essential expected property for a medical device [62], [63], [64], [65]. Nevertheless, to improve bone repair and achieve bone regeneration, several other biological properties such as bioresorption [25], [27], [36], [40],[66], [67], bioactivity [38], [39], [41], mechanical performance [68], [69], [70], and adapted architecture with desired porosity [71], [72], [73], [74] have been investigated for the development of different materials (Table 2).

Microporosities in 3D-printed tri-calcium-phosphate-based bone substitutes enhance osteoconduction and affect osteoclastic resorption [75].

Optimal pore dimension influences osteoconduction (osteoconduction is defined as a three-dimensional process observed when porous structures are implanted in or adjacent to bone and when the porous structure becomes filled with newly formed bone). The long-held belief

that optimal osteoconduction is achieved using bone substitutes with pore diameters of 0.3–0.5 mm needs to be reconsidered in light of the study of Ghayor et al. [76], who determined an upper limit of the pore diameter for optimal bone ingrowth. They found that osteoconduction was significantly improved in bone substitutes with a pore diameter of 0.7–1.2 mm and that a pore size of 1.5 mm or greater had a detrimental effect on the bone bridging capabilities, which are an indirect measure of osteoconduction [76].

Optimal pore shape has the ability to influence osteoinduction (osteoinduction is defined as a three-dimensional process observed when porous structures are implanted in an ectopic site and the porous structure nonetheless becomes filled with new bone). This has been attributed to the ability of concavity to entrap osteoinductive molecule, [31], [49].

Implant characteristics	Expected outcomes
Biocompatibility [62],[63],[64],[65]	- Nontoxic end products (inert biomaterials): in vitro - Non-fibrotic biomaterials: in vivo - No foreign body reaction to materials: in vivo
Bioresorption [66],[67],[27],[25],[40],[36]	- Controlled degradation: enzymatic degradation (biological process) and dissolution - Promotion of new bone ingrowth and substitution - Transient mechanical properties sustained
Bioactivity [39],[41],[38]	- Osseointegration: Interaction and binding to the host tissue via possible chemical surface modification.
Mechanical properties [68], [69],[70]	- Stiffness, deformation at elastic limit, compressive strength and traction close to the bone to replace - Adaptation of Young's modulus considering the type of bone to replace and its function (no/low or load bearing)
Architectures (Porosity) [71], [72], [73], [74], [76], [49]	- Interconnected porosity for vascularization and fluid circulation (oxygen, nutrients) - Pore sizes: - 300–500 µm **allows** new bone ingrowth **- 0.7–1.2 mm optimal osteoconduction** **->1.5 mm: detrimental for osteoconduction (hampers bone bridging)** - > 300 µm **promotes** vascular ingrowth - ~100 µm to promote cell migration **- concavity: optimal osteoinduction**

Table 2: Summary of desirable properties for efficient biomaterials with bone healing performance

Historical development of biomaterials with new properties evolving with clinical need has been realized by Hench [77].

For bone tissue engineering, the history of biomaterials has proceeded from the first-generation concept to the third generation [77] (Figure 10).

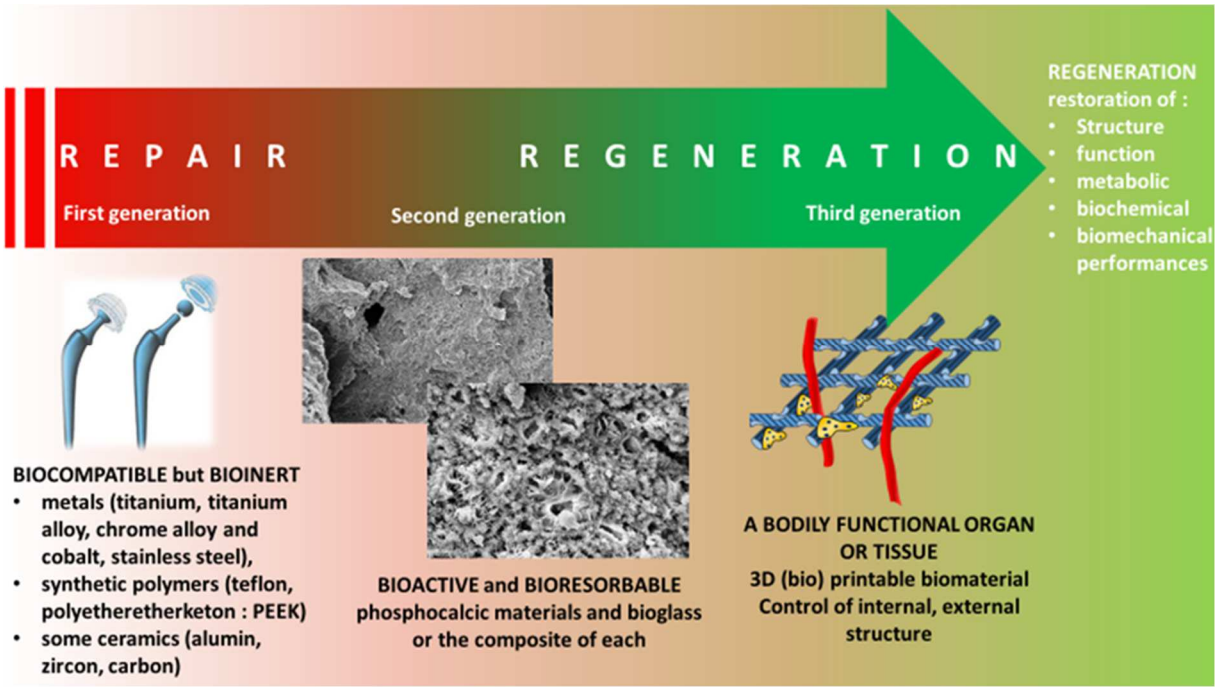

Figure 10: An overview of the concepts of biomaterials for bone tissue engineering.

5.1. First generation of materials

The first generation of materials were mainly used in the 1960s-1970s and were named bioinert materials. The initial goal was bone repair to deal with mechanical deficits and replace damaged bone instead of regenerating it.

Bioinert materials are well tolerated by organisms and encompass metals (titanium, titanium alloy, chrome alloy and cobalt, stainless steel), synthetic polymers (polytetrafluoroethylene (PTFE: Teflon®), polyetheretherketone (PEEK)) and some ceramics (alumina, zirconia, carbon). Titanium and **zirconium**, which have osseointegration properties, are used in orthopedic, craniomaxillofacial or dental implants [78]. Bioinert metal is defined as a metal that does not release toxic byproducts when implanted, but the formation of fibrous tissue impairs positive interactions with the surrounding live tissue [31], [79].

5.2. Second generation of materials

In the second generation, the biomaterials were named bioactives and bioresorbables. These properties are directly linked to the chemical composition and structure of materials that allow

for modification at the surface of the materials over time. A bioactive material is characterized by its ability to form a layer of apatite when dissolved. This layer promotes interaction with the tissue interface via chemical links. Among the materials studied to understand this interaction are calcium phosphate materials, bioglass and their composites [78]. A recent review by Kokubo showed that different types of links are involved between bone and bioactive materials. P_2O_5 and CaO appeared to not be essential for a material to form surface apatite. The required condition for a material to form surface apatite is the presence of functional groups that permit apatite nucleation. Functional groups such as Si–OH, Ti–OH, Zr–OH, Nb–OH, and Ta–OH are effective for apatite nucleation. This mechanism can be applied for all types of materials even if no calcium or phosphate is included in the chemical composition. This indicates that when one of these functional groups is formed on the surface of a metal, even a metal without any calcium phosphate, apatite formation on its surface can be induced. For example, it was hypothesized that if sodium ions were incorporated into the thin surface of a titanium oxide layer of Ti metal, sodium ions would be released from the surface via exchange with H_3O^+ ions in the surrounding fluid to form Ti–OH^- groups on the Ti metal surface [38].

In 1991, Kokubo proposed that the bone-bonding capacity of a material could be evaluated by examining apatite formation on its surface in an acellular simulated body fluid (SBF) without the need to perform any animal experiments [39]. In 2007, SBF was standardized as a solution for the in vitro evaluation of the apatite-forming ability of implant materials with the ISO 23317 standard [80].

Hence, tissue regeneration is facilitated due to better interaction between the implant and the surrounding tissue as well as the release of ions in the medium that activate cell signaling [77], [81]. For example, calcium ions and carbonate ions are involved in the activation or inhibition of osteoclasts [82], [83], [84].

5.3. Third generation of materials

The development of third-generation biomaterials is challenging for the scientific community, as these materials are intended to achieve tissue regeneration, with the aim of developing materials that will help the body heal itself once implanted [43]. Hench defined the regeneration of tissues as follows:

- restoration of structure,
- restoration of function,
- restoration of metabolic and biochemical behavior,
- restoration of biomechanical performance [77].

Peter V. Giannoudis proposed the concept of the diamond, which describes the critical characteristics of an ideal bone graft substitute for bone regeneration of large bone defects in nonunion fractures [85].

Regarding the biological mechanism of bone repair that involves different kinds of cells and growth factors, an ideal material should behave as natural living bone tissue; they should be biomimetic implants because they have all the properties of bone. Therefore, an ideal implant would be a three-dimensional macroporous scaffold imbedding growth factors and cells. The most commonly used growth factors in clinical applications are bone morphogenic protein (BMP), especially BMP2 and BMP7. The osteogenic cells should be mesenchymal stem cells. Stem cells are multipotent, which means that they are able to differentiate into osteogenic cells. However, some crucial aspects remain unanswered, such as the type of mesenchymal cells to be used, the kind of growth factor and the optimal concentration to be used. Is it possible to use a cocktail of growth factors? How should they be mixed? To the knowledge of the authors, no definitive answer has been described at present [85], [86], [87], [88].

Other researchers claim that instead of cells, use of their secretome is enough and safe to regenerate tissue. No results concluded that mesenchymal stem cells are more efficient to

generate bone ingrowth than the addition of total bone marrow [89], [90]. Extracellular vesicles have attracted keen interest due to their regenerative potential [91], [92], [93].

It is worth noting that every medical field has its own prioritization of expected mechanical, physicochemical, structural, and biological properties from a biomaterial and medical device (Figure 8).

Furthermore, there is a clear need to develop standardized protocols to control the release of biological molecules and their clearance at the application site. For example, clinical studies support that, despite some encouraging results, the available evidence does not generally support the use of bioactive factors as a routine alternative to the currently used bone regenerative interventions in the craniomaxillofacial area [94].

These expectations stimulated the scientific community by opening the research field on new advanced manufacturing processes. 3D (bio)printing of materials is at the forefront to improve the regenerative properties of biomaterials. The procedures of tissue engineering that consist of adding cells and/or growth factors in a tridimensional scaffold to recreate bodily functional tissue or organs are still experimental and very costly. While more complex tissues like skin and organs such as the heart, lung, and liver have been successfully recreated in the lab, they are a long way from being fully reproducible and ready to implant into a typical patient. Printing biological molecules or cells remains challenging for two main reasons: feasibility and regulatory requirements for clinical transfer. One of the strategies consists of pretreating biomaterials by immersion and impregnation extemporaneously after printing with biological molecules and/or cells. This suggests an advanced design of biomaterials to potentiate loading and drug release. This is controlled by the design of the porosity, which increases the specific surface area and the surface properties [95]. The absorbed biological factors could be released to induce biological pathways that promote tissue regeneration. Another strategy to overcome the regulatory limits of using cells and growth factors in the human body is to design an internal structure of implants to create interconnecting porosity as well as a specific

topography of the surface of implants to increase bone repair. This optimized architecture and surface design will enable the implants to directly interact with the surrounding fluid and adsorb host biological factors to release them in a controlled way.

6. Overview and assessment of different 3D manufacturing processes

Three dimensional printing is commonly used in the aeronautic, jewelry, automotive, building, industrial accessory design and medical fields. AM technologies can be divided into various categories. Commercially available AM technologies are classified into three major categories based on the material deposition method, working principles and energy sources: (1) laser-based machines, (2) direct printing technologies, and (3) nozzle-based systems [68], [204]. According to the standards established by the International Organization for Standardization (ISO) and American Society for Testing and Materials (ASTM), AM technologies can be divided into seven categories: (1) binder jetting (BJ), (2) direct energy deposition, (3) material extrusion (ME), (4) material jetting (MJ), (5) powder bed fusion (PBF), (6) sheet lamination, and (7) vat photopolymerization (Table 4) [69]. Each manufacturing process works best with a specific material, and has particular cons and pros (Table 3).

AM process Category	AM process	Work principle and definition	Materials processed
1) Binder jetting	Inkjet head Particle binding Powder bed BJ (binder jetting) Drop-on powder (DOP)	Binding agent is dispensed as droplets onto powder particles, causing their consolidation due to the 3D space movement layer by layer	Polymers, ceramics, metals and composites (powder)
2) Direct energy	Laser Metal Deposition (LMD) Electron Beam Free-Form Fabrication (EBF3) Electron Beam Melting (EBM)	Metal powder is carried by gas into the focal point of a laser, creating a melt, or an electron beam within a vacuum chamber is used to melt	Metals (only conductive materials)
3) Material extrusion	Fused Deposition Modeling/melting (FDM)	Heated thermopolymer is extruded through a print nozzle	Polymers and polymer matrix composites containing a small amount of ceramics
	Fused Deposition of Ceramics (FDC)	Thermopolymer is loaded with ceramic material and extruded; polymer burnout leaves the ceramic part behind	Ceramics, polymers and composites, colloidal gels, or polyelectrolytes
	Low-temperature deposition manufacturing (LDM) Direct ink writing (DIW) or plotting	Similar to the above technology, except that nonheating liquid materials are deposited in a low-temperature environment. The colloidal inks are directly extruded from an orifice or a nozzle to fabricate the architecture	
4) Material jetting	Drop on Demand (DOD)	Material is deposited onto substrate or build plate as droplets from piezoelectric or thermal actuators within a print head.	Liquid photopolymers
	Multi-Jet Modeling (MJM)	Similar to DOD, multiple materials can be dispensed from the same printhead.	
	Laser-Induced Forward Transfer (LIFT)	Material on a quartz ribbon is ejected by selective laser heating on the ribbon backside.	
5) Powder bed fusion	Selective Laser Sintering (SLS)	A focused laser beam is used to sinter powder particles	Polymers, ceramics, metals and composites
	Selective Laser Melting (SLM)		Metals (such as titanium alloys), polymers, ceramics
6) Sheet lamination	Ultrasonic additive manufacturing (UAM) laminated object manufacturing (LOM)	Sheet lamination forms 3D objects by stacking material such as paper, plastic or metal foil and laminating them using welding, adhesive, heat or pressure.	Plastic, sheet or ribbons of metal
7) Vat photopolymerization	Stereolithography (SLA)	A laser initiates polymerization within a bath of photopolymer,	Photopolymer resin and its composites
	Digital Light Processing (DLP) Continuous Liquid Interface Production (CLIP)	Similar to SLA, but a projected mask is used to cure each layer. A mask from the bottom of the vat polymerizes the photopolymer beyond a barrier region where no polymerization occurs. The build plate continuously raises from the barrier upwards.	

Table 3: Classification of AM processes according to the ASTM [96]

Four main processes are used in biomedical applications for bone tissue engineering [70]:

1-Stereolithography (SLA),

2-Selective laser sintering (SLS),

3-Material extrusion (direct ink writing, plotting, or low-temperature deposition manufacturing or extrusion-based 3D printing (EB))

4-Inkjet 3D printing (3DP) or powder bed or drop-on powder (DOP).

This review focuses on these four AM processes.

The SLA and SLS are light-based techniques. In selective laser sintering (SLS) and stereolithography (SLA), light is used to sinter powder materials or photopolymerize liquid material into designed 3D structures [4],[97]. The plotting process encompasses fused deposition modeling (FDM)[98] and 3D bioplotting (3D extrusion of filament (3DF) or direct ink writing (DIW)). In fused deposition modeling (FDM) and 3D extrusion techniques, the material is thermally or chemically processed as it passes through a nozzle. Inkjet 3D printing/powder bed processes consist of the binding of powders on a Z axial moving bed, enabling the creation of a 3D model. As an indirect manufacturing technology, inkjet head 3DP is also referred to as 3DP, 3DPP, particle binding or powder bed and BJ (binder jetting) [99]. The main materials for specific AM processes in bone tissue engineering are displayed in Table 4.

Work principle	AM process	Main advantages	Main drawbacks	Material processed
Light-based technique (light is used for polymerization or sintering)	Stereolithography (SLA)	- high resolution - highest fabrication accuracy - an increasing number of available materials can be processed	- expensive - smelly and toxic reagent - time-consuming postprocessing (debinding and sintering) - shrinkage of the printed part - slow printing - limited materials	Hydroxyapatite [100] Polypropylene fumarate [101] Poly lactide PDLLA [102] Polycaprolactone [103] Polyethylene glycol [104]
	Selective laser sintering (SLS)	Compatible with metal (especially titanium for cranial implant providing high impact protection)	- expensive - slow printing - not compatible with hydrogel	Polycaprolactone[[105]] Hydroxyapatite [106],[[107]] Bioactive glass Composite: bioactive magnesium–calcium silicate/poly-ε-caprolactone (Mg–CS/PCL) [108] Metal: Inconel 625 superalloy, Ti-6AI-4 V and Monel [109]
Plotting (material passes through a nozzle and is shaped by melt or low-temperature extrusion deposition)	Fused deposition modeling (FDM)	- a large variety of materials available (including bioresorbable material) - melt processing yields dense and tough polymer structures ideal for load-bearing tissue - low cost - high speed - simplicity	- lower resolution than SLA - incompatible with printing of cells - limited to material thermoplastic - weak mechanical properties - needle clogging	PCL [110]
	3DFilament extrusion (3DF) Direct Ink Writing ink (DIW) or Low-temperature deposition manufacturing (LDM) or plotting or robocasting		- can require a debinding step - weak mechanical properties - needle clogging - postprocessing: post hardening - higher requirements for the physicochemical properties of materials than those for 3DP and SLS (high printability of materials, including high fluidity, fast formability)	Calcium phosphate granule + hydrogel [111] Cement putty[112], [113], [114], [115], [116] Bioglass putty [117]
Powder + binder deposition	3D printing (3DP)	- powder-based material (especially calcium phosphate cement close to the mineral part of bone) - rapid printing of large structures	- debinding step - sintering step - low mechanical properties - lack of adhesion between layers - postprocessing: drying/sintering	Brushite [118] Monetite [118] Tetra calcium phosphate:TTCP [119] dicalcium phosphate dihydrate: DCPD [119] Calcium phosphate cement [120] Composite bioglass/βTCP[121]

Table 4: Assessment of additive manufacturing processes used for 3D printing of biomaterials for bone repair

7. Expected essential properties of the final AM product for patient bone repair

7.1 Biocompatibility

Biocompatibility is an essential expected property for 3D-printed pieces for all clinical applications.

By definition, biocompatibility is a measurement of how compatible a device is with a biological system. A battery of tests and protocols have been validated by organizations such as the International Organization for Standardization (ISO) for testing such aspects of biomaterials. Together, these characteristics have formed the basis for ‘‘biocompatibility’’, a difficult-to-define term that could be equated with biological safety. The ISO 10993–1: 2018 standard defines biocompatibility as the “ability of a medical device or material to perform with an appropriate host response in a specific application”. The characteristics of an ideal implantable biomaterial have invariably included the concept of ‘‘inertness’’, with the expected host response being one of fibrous connective tissue encapsulation. A material that caused no harm to the recipient was considered to be acceptable and desirable. That is, materials shown to be nontoxic, nonimmunogenic, nonthrombogenic, noncarcinogenic and nonirritant were preferred. Many studies provide an update and expansion of the current understanding of the concept of biocompatibility [64], [65], [122]. Although in esthetic surgery the application of filling wrinkles with fibrous tissue is expected, in the case of bone regeneration, nontoxicity to cells, nonfibrous encapsulation and a noninflammatory response are expected. The foreign body reaction composed of macrophages and foreign body giant cells at the end-stage response of the inflammatory and wound healing responses following implantation of a medical device, prosthesis, or biomaterial is a subject of study. Biomaterials can cause inflammation in the first step of implantation. This can be caused, for example, by the exothermic reaction during self-setting hardening of cement [123] and acidic setting

reaction [124]. The most important criteria depend on the duration of the inflammatory process, which should not last too long to avoid unresolved chronic inflammation.

7.2 Sterilization

Sterilization is an operation that eliminates or kills microorganisms carried by inert contaminated media. The ability to sterilize materials is an essential property that enables their use in the clinic.

ISO 11737 defines different processes for sterilization [125]. Medical devices are sterilized in a variety of ways, including using moist heat (steam), dry heat, radiation, ethylene oxide gas, vaporized hydrogen peroxide chlorine dioxide gas, vaporized peracetic acid, and nitrogen dioxide. The sterilization method must preserve the integrity of the mechanical, chemical, and biological properties of the material. For instance, gamma radiation at 25 G is a standard authorized by NF/EN 556 and NF/EN ISO 11137 for inorganic materials but hydrogel/organic material cannot be sterilized by gamma irradiation, illustrating the problem of sterilization of composite inorganic/organic materials [126,127] .

Preparation in an aseptic way could be a tolerable alternative for composite materials.

7.3 Mechanical properties

The mechanical properties of the printed part depend on the biomaterial used and can be optimized via the design of the 3D modeling [128]. The mechanical properties can be divided into three types. Young's modulus is related to the stiffness of the implants. Cells are able to feel the stiffness of biomaterials, which determines their differentiation fate. This stiffness is a crucial cue for cells to engage fate differentiation [129]. Stiffness is essential, as it can be felt as a clue for stem cell differentiation [68]. Young's modulus of 20 kPa has been found to allow for stem cell differentiation in osteogenic cells with a hydrogel [68]. The flexural and compressive strength is defined as the capability of the material to support maximal stress until it breaks. These values characterize the material resistance. The material

must withstand deformations during impact as well as stresses during its use by the surgeon and during its implantation. These stresses must not exceed the yield point (the stress beyond which the strain becomes irreversible). The yielding of materials can be measured from compression, bending, or tensile testing.

7.4 Bioresorption

Bioresorption followed by bone substitution is expected for an implant devoted to regenerating bone. The rate and speed of degradation must be in accordance with the bone growth rate to allow for suitable mechanical performance in the defective bone location.

Inorganic materials can be degraded by one or both of the following mechanisms: (1) Dissolution by physicochemical processes or (2) bioresorption by biological processes [130], [131]. Dissolution occurs in biological fluid and depends on factors such as the solubility constant of the implant matrix, the surface area to volume ratio of the implant, local acidity, fluid convection and temperature [132], [133], [134]. Bioresorption is mediated by biological processes due to enzymatic and acidification reactions occurring in bone cells, especially osteoclasts, and, to a lesser extent, macrophages [135], [136].

The end-product must be eliminated from the organism by renal filtration, for example, to avoid the toxicity of too many concentrated ions in the systemic circulation or organs [137].

7.5 Resolution of the AM process and accuracy of the final part

In the medical field, the accuracy of the part to be used is essential for perfectly filling complex-shaped bone defects. This dimensional accuracy depends on the resolution of the AM process.

The smaller the part printed with a fine porosity is, the higher the resolution of the AM process. The score used for the assessment is proportional to the precision of the geometry achieved by the process. The score may look like a performance index [138].

The resolution of the printed part will determine the quality of the final piece, especially if it is a small part with the desired micro- and nanoporous architecture.

The resolution of the final piece, which is especially dependent on the resolution of the AM process, is sought for 3D-printed implants from patient scans for surgical planning because it mimics the surgical gesture as accurately as possible. For a small part with a fine microarchitecture, the highest resolution is preferred to a concordance between the 3D modeling expected results and the printed results. Table 5 gives an overview of the different resolutions of the AM processes in the literature.

AM process	Resolution	Ref.	Min-Max Marge
SLA	10 µm Generally 1.2-200 µm (can reach 100 nm) 10-100 µm	[86], [87] [88] [64]	100 nm-200 µm
FDM	50-200 µm 250-370 µm 50-200 µm 127 µm	[86], [87] [88] [64] [50]	50-370 µm
SLS	80 µm 80-250 250-700 µm 45-100 µm	[86] [87] [88] [64]	45-700 µm
3DF	5-200 µm <200 µm 200-800 µm	[86], [87] [88] [64]	5-800 µm
3DP	100-250 µm 80-250 µm 40-500 µm 350-500 µm	[86] [87] [88] [64]	80-500 µm

Table 5: Accuracy of different AM processes
SLA: stereolithography
FDM: fused deposition modeling
SLS: selective laser sintering
3DF: 3D extrusion of filament
3DP: inkjet 3D printing

8 Expected properties of the AM-based final product for follow-up patient care

The essential properties depend on the nature of the biomaterial used for printing the implant. Metals are not compatible with medical imaging, which is required for follow-up patient care to control repair. For certain indications, it is necessary to be able to follow the evolution of bone substitutes radiographically. Therefore, controlling the radiopacity of the implant compared to the calcification of new bone is necessary.

Metal is not compatible with imaging for following such as MRI. For MRI, the metal must be nonmagnetic; otherwise, it is dangerous for the patient. Metals interfere with the radio projections of the scanners and produce artifacts. Metal implants are devoted to replacing bone instead of regenerating it. Titanium and **zirconium**, the most frequently used metals can be osseointegrated in the bone host when implanted but cannot be degraded to be replaced by new bone [50]. Nevertheless, advanced iron-based and magnesium-based alloys have been investigated for their potential as biodegradable metals [143]. Degradable metallic materials could potentially replace corrosion-resistant metals currently used for applications requiring good mechanical properties but non-permanent replacement, such as cardiovascular stents as well as pediatric and orthopedic applications. Biodegradable metallic materials represent a breakthrough technology. Implants made from biodegradable metals are significantly stronger than their polymer counterparts and fully biodegradable in vivo, thereby avoiding long-term complications and the need for secondary surgery [144], [145], [146]. 3D printing of degradable magnesium metal has also been investigated and has yielded successful results [147], [148].

9 Expected properties of the AM final product for clinician-friendly use

This aspect is related to the affordability of the equipment, the cost of the printer as well as its size. AM technology is becoming more accessible due to the expiration of earlier patents,

which has given manufacturers the ability to develop new 3D printing devices. Recent developments have reduced the cost of 3D printers [139]. A comparison of prices can be estimated based on the complexity of the technology. A printer using an electron beam, laser or UV light will be more expensive than the simplest technology requiring a system based on pressurized air to extrude the material from a print head nozzle. Hence, classifications from the more expensive to the cheapest printer can be achieved according Wang et al. [140] and Chen et al. [3] (Table 6).

SLA	SLS	FDM	3DF	3DP	Reference
++	+++	+	+	+	[140]
++	+++	+	+	++	[3]

Table 6: Classifications of the price of AM processes: +++ highest price; ++ intermediate price, + lowest price.

The size of the printer is another practical aspect to account for. Several commercial printers have a desktop compatible size. Interestingly, 3D printers that allow for printing in a sterilizable atmosphere can be found on the market.

In addition, there are limitations due to regulations concerning medical devices that make the integration of supply production in hospitals complex. For example, the service may be subcontracted or centralized by an accredited company.

10. Assessment of material/AM process pairs

10.1 Stereolithography

Stereolithography (SLA) was developed by Chuck Hull of 3D Systems® in 1986. SLA is the most developed rapid prototyping (RP) method and offers the highest accuracy and precision [97]. The device production is compatible with CAD files from clinical data. Implants can be designed from scanning data and imaging technologies such as magnetic resonance imaging (MRI) or tomography techniques (CT). Calcium phosphate materials are the biomaterials commonly used by SLA to print bone implants for bone tissue engineering. Calcium phosphate material with a chemical composition close to the mineral part of bone can be

used with SLA, such as calcium phosphate ceramic slurry, hydroxyapatite [102] or beta tricalcium phosphate [103]. Hydroxyapatite bioceramics were used for the manufacture of an orbital floor prosthesis from spiral CT data, which were converted to vector file format for subsequent prosthesis manufacture [100]. Brie et al. used the stereolithography technique to produce hydroxyapatite implants with three-dimensional shapes derived directly from the scan file of the patient's skull without molding or machining. These new implants are well suited for the reconstruction of large craniofacial bone defects (greater than 25 cm^2) [141].

The SLA technique relies on a photosensitive monomer resin that forms a polymer and solidifies when exposed to ultraviolet (UV) light. The main advantage of stereolithography is its capacity to produce a high-quality surface finish. The disadvantages are related to the fact that some materials are expensive, smelly and toxic and must be shielded from light to avoid premature polymerization. The parts may be brittle and translucent, and they need supports that may adversely affect the surface finish when removed. The choice of resins was limited, but presently, a considerable amount of material can be used. A variety of photopolymers are available for SLA, including epoxy-based systems and acrylates, but only a few are biodegradable. Several nondegradable poly(ethylene glycol)–dimethacrylate hydrogels have been built using SLA [104], [142], [143]. Biodegradable resins proposed for the SLA process have been based on polypropylene fumarate [101] and trimethylene carbonate copolymers, a biodegradable resin based on fumaric acid monoethyl ester functionalized poly(d,l-lactide) (PDLLA) oligomers. Porous polylactide constructs were prepared by stereolithography for the first time without the use of reactive diluents [102]. *N*-Vinyl-2-pyrrolidone (NVP) was used as a reactive diluent. Polycaprolactone has also been used in SLA. PCL-based photocrosslinkable and biodegradable resins were formulated and used without solvents to accurately prepare designed porous 3-D scaffolds using stereolithography [103].

The main advantage of SLA is its high resolution [103], [144].

Stereolithography requires a photoinitiator to crosslink the slurry using a computer-controlled laser beam or a digital light projector that requires removal. Hence, debinding and sintering of the 3D piece make the route time-consuming [141], [145], [146]. Shrinkage of the piece occurs but can be anticipated. Ceramic and calcium phosphate parts made with the SLA technique have low mechanical properties. Sintering can modify the pore volume as well as the crystallinity, leading to changes in the mechanical properties [147], [148]. Moreover, the control of microporosity that can be created during the sintering step specific to the SLA technique makes it possible to design materials with optimal osteoconduction thanks to a synergistic architecture. In addition to the macroporosity and microporosity created by the AM process, the nano- and microporosity created by the sintering enhance osteoconduction and affect osteoclastic resorption. The higher 1,200°C of the sintering temperature of the calcium phosphate item 3D printed using the SLA technique results in the lowest microporosity and inhibits osteoclastic degradation of the material. Nano- and microporosity are crucial for osteoconduction (the formation of newly formed bone that will fill the degraded biomaterial). A low sintering temperature makes it possible to create nano- and microporosity in the final 3D printed item [75].

In conclusion, the published studies indicate that the SLA process with calcium phosphate material requires meticulous work to develop a printable formulation composed of a binder resin and a photopolymerizable reagent. As it is an older additive manufacturing method, SLA has the advantage of several commercially available 3D printers that do not require customization of parameters. The process is time-consuming, as manufacturing requires two additional steps before recovering the final printed piece: debinding and sintering. Moreover, sintering causes shrinkage of the final piece that must be considered. The final part can reach a modulus in the range of the lower value of the trabecular bone. Nevertheless, the elasticity is low. The printed part can be brittle and deformable. The SLA process is compatible with different polymers but requires optimization of the formulation, i.e., the photoiniatiator to

make them UV curable. Sometimes, the commercially available machines require optimization of the parameters (laser) to print this kind of developed polymer biomaterial. SLA machines for medical applications can also require optimization of commercially available 3D printers to enable printing in a sterile atmosphere (Table 7).

Material	Biological assessment	Mechanical Properties	Implant characteristics	Bioresorption	Specificity of the process	Sterilization/disinfection/ decontamination	Conclusions/ summarization
SLA/Calcium phosphate materials							
Suspension of hydroxyapatite ceramic in resin [100]	Not tested	Not tested	- spiral CT data from a pediatric skull phantom - Cross-hatched pattern pore: 2.18 mm	Not tested	-commercially available 3D printer (3-D Systems 250 Model stereolithography machine (Valencia, Calif) - debinding step	Not specified	- SLA with calcium phosphate material required the development of a printable formulation: binder resin, photopolymerizable. - Most of commercially available 3D printers do not require customization of parameters. - SLA requires two additional steps before recovering the final printed piece: debinding and sintering - the sintering causes shrinkage of the final piece - the final piece can reach a modulus in the range of the lower value of the trabecular bone. The elasticity is low; the piece can be brittle and deformable.
Mixture of resin and powder HA [141]	- No signs of inflammation - no movement observed - 18–43% of the porous zones colonized by bone tissue	Not tested	- implants from the scan file of the patient's skull (5–11 cm) - no molding or machining. - dense structure - macroporous areas only at the edges for better biointegration. - manufacturing deformation during the sintering stage: small overhang. - pore size 300–550 µm - pore density: 50–70%. - cost of the implants: 8,000 and 10,000 euros.	Not tested	- Debinding step and sintering for consolidation of the implant	gamma irradiation	
Calcium polyphosphate (CPP)+ polymer binder [149]	Not tested	- Toughness values over time in tris buffer (aging test): D0: 1.64 MPa.mm D1: 1.44MPa.mm D10: 0.40MPa.mm -Maximum bending stress D0 : 31.59MPa D1 : 24.19MPa D10 : 11.19MPa	- average porosity: 27.7 ± 2.0%. - shrinkage	- hydrolytic degradation of CPP in tris-buffer (phosphorus ions release)	- debinding: 525 °C - Sintering at 600 °C	Not tested	

Table 7: A critical assessment of material/SLA additive manufacturing process pairs.

Material	Biological assessment	Mechanical Properties	Implant characteristics	Bioresorption	Specificity of the process	Sterilization/disinfection/ decontamination	Conclusions/ summarization
SLA/polymers							
poly(ε-caprolactone) (PCL)-functionalized with methacrylic anhydride + Irgacure 369 photoinitiator [103]	cytotoxic test with NIH3T3 fibroblast validated by MTS assay	specimens: 100 × 7 × 0.5 mm^3 Stiffness (Young's modulus) - 15.4 ± 0.7 MPa maximal tensile strength: - 2.55 ± 0.12 MPa Elongation at break: - 19.3 ± 0.5%	- cylindrical structures - gyroid pore network - interconnected porosity of 70.5 ± 0.8% volume - pore size: 400–500 µm	Low degradation kinetic (lower than PLA) [97] However, PCL has a long degradation due to its semicrystallinity and hydrophobicity [105]	- commercially available SLA printer	immersion in 70% ethanol.	
- Biomaterial: Poly(propylene fumarate) (PPF) - Solvent: diethyl fumarate (DEF) - photoinitiator: bisacrylphosphrine oxide (BAPO) [101]	Not tested	compressive modulus: 19±7.8 to 140 ±6.1 MPa	- orthogonal cubic-lattice disks: 1 cm long, 1 cm wide, and 0.3 cm thick, - square or hexagonal pores - strut thickness: 300 µm. - pore sizes: 400 µm to 1 mm,	Not tested	optimization of the UV curable polymer solution composition and the laser parameters of the machine	Not determined	- material choice restricted to photopolymer. - optimization of parameters (laser) can be required - optimization of the commercially available 3D printer is necessary to allow for printing in a sterile atmosphere.
Polylactide [102]	MC3T3 cell line adhesion and proliferation	- Flexural modulus: 2.5±0.5GPa- 3.4±0.1GPa. - Flexural Strength: 80±8MPa -94±1MPa. - Strain at failure: 4.2±0.8% -6.1±0.2%	- Tensile test specimens (ISO 37–2), films measuring 70*24*0.5 mm^3 for the mechanical tests - 3D scaffold with a gyroid architecture	Not tested	Commercial printer equipped with a digital micromirror device	disinfection in 70% isopropanol	
Poly(ethylene glycol) dimethacrylate (PEGDMA) +photoinitiator ((Irgacure 2959) [143]	Murine OP-9 MSC attachment	Not tested	- pore size: 175–425 µm - Wall thickness: 9–200 µm	Not tested	Fabrication with the third harmonic wave of an Nd:YAG laser (355 nm), which generated nanosecond pulses	filter sterilized (0.22 µm)	
Poly(ethylene oxide) (PEO; and poly(ethylene glycol) dimethacrylate + photoinitiator Irguagure [143]	Determination of the number of live and dead cells (Chinese hamster ovary, CHO) by a hemocytometer and Live/Dead assay	-average value of the modulus of elasticity: 1.116±0.21 kPa.	- cylindrical molds (diameter, 17.2 mm; height, 3.3 mm) for the compressive tests. - resolution of the technique was found to be approximately 150±10 µm per layer and 250 µm in the x–y plane. The dimensions of the scaffold were found to match those of the CAD drawings within a 0.5% range.	Not tested	- Commercially available stereolithography machine with minimal modifications, including cleaning and emptying the vat of resins to avoid contamination of cells.	UV sterilization	

Table 7 (continuation): A critical assessment of material/SLA additive manufacturing process pairs.

10.2 Material-based extrusion

10.2.1 Fused deposition modeling

A FDM machine consists of a movable head that deposits a thread of molten material onto a substrate. The build material is heated above its melting point, solidifies immediately after extrusion and cold welds to the previous layers. An advantage of this system is that it may be viewed as a desktop prototyping facility in a design office. The most commonly used materials are cheap, nontoxic, nonsmelly and environmentally safe. There are also a large range of colors and materials available, such as investment casting wax, ABS (acrylonitrile butadiene styrene), various plastics, medical grade ABS (MABS) and elastomers. Parts made using this technique have a high stability since they are not hygroscopic. A system that costs approximately 100,000 dollars (the cheapest can cost 300 dollars) deposits approximately 380 mm of material a second, produces layer thicknesses of 50–762 mm and has an accuracy of ± 127 μm [94].

Various materials can be designed in filaments to be used with the FDM technique.

Fused deposition modeling was used to produce novel scaffolds with honeycomb-like patterns, fully interconnected channel networks, and controllable porosity and channel size with a bioresorbable polymer PCL (poly(epsilon-caprolactone)) [110]. A one-shot extruder was first used to fabricate PCL monofilaments. The implant was modeled by the deposit of filaments to produce porous scaffolds made of layers of directionally aligned microfilaments using this computer-controlled extrusion and deposition process [110]. Polycaprolactone exists in a rubbery state at room temperature and has a low melting temperature of 60 °C.

Another unusual property of PCL is its high thermal stability. Whereas other tested aliphatic polyesters had decomposition temperatures between 235 °C and 255 °C, PCL has a decomposition temperature of 350 °C [150]. Over a period of 3–4 weeks in culture, the fully interconnected scaffold architecture was completely 3D-filled by cellular tissue. Fibroblasts

and osteoblast-like cells proliferated, differentiated, and produced cellular tissue in an entirely interconnected 3D polycaprolactone matrix [151]. The true benefit of FDM is the ability of this process to enable the fabrication of multidirectional physical gradients within scaffolds [152]. The controllable parameters of the FDM technique, especially the printing temperature, influence the thermal cycling during the laying process, which influences the crystallinity of the material as well as the porosity, giving rise to a tuned mechanical performance of the printed part [128]. FDM can be considered the most prevalent AM technique because it constitutes almost half of the AM machines in the current global market. However, the thermal behavior of the polymer and the amount of retained heat can cause unwanted deformations. Currently commercialized products manufactured by FDM include Osteoplug™ and Osteomesh™ (Osteopore), which are thin interwoven meshes and three-dimensional implants, respectively [153].

Polycaprolactone (PCL) is mainly used to fabricate scaffolds by employing FDM [154], [155]. Probst et al. used a composite PCL comprised of medical grade PCL and tricalcium phosphate [156]. PCL scaffolds manufactured by FDM have favorable biocompatibility and a low cost of manufacturing, leading to approval by the US Food and Drug Administration for use in human bone tissue.

10.2.3 Direct Ink Writing

This 3D solid free form fabrication method is based on extrusion of the material, necessitating that the material possesses rheological properties allowing for it to pass through a nozzle. Different types of materials can be used, including polymers, suspensions of ceramics and composites.

10.2.3.1 Rheological properties of printable materials by extrusion

Shear thinning is one of the requirements that allows for passage through a needle. The viscosity decreases when pressure is applied by a mechanical or pneumatic process (Figure 11 a).

To avoid spreading of the printed filament after applying pressure, the self-healing characteristics (Figure 11 b) allow for the fast recovery of the initial properties of the formulation [157].

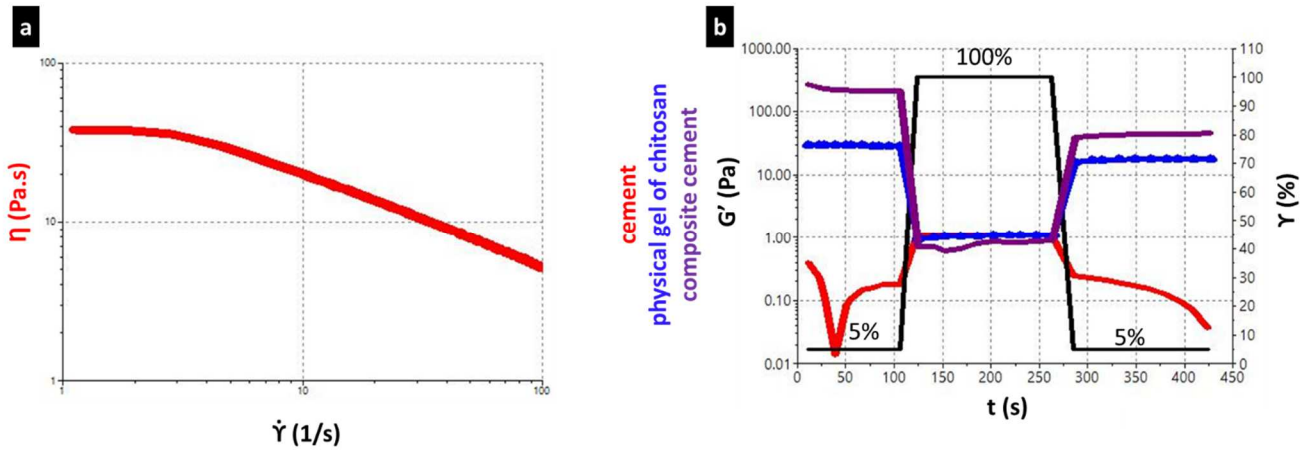

Figure 11: a) Example of a pseudoplastic physical gel of chitosan: when the shear rate increased, the viscosity (Ƞ) decreased, which allowed for the gel to pass through a needle. b) Cyclic deformation of a composite cement before setting (blending of hydrogel and cement powder: purple), cement alone (red) and the physical gel (blue). The cement alone does not self-heal, in contrast to the mixture.

When cyclic deformations of 5%, 100% and 5% are applied, the elastic/solid/conservation modulus (G') decreases when the deformation increases, which allows for the gel to pass through the needle. After deformation, the gel returns to the elastic/solid/conservation modulus of the origin. Developing an ink with accurate rheological properties is critical to gain accuracy and have a more precise reproduction of the CAD file.

Ketal et al. proposed quantitative metrics to assess the geometrical attributes of printed components vis-à-vis their 3D-CAD (computer-aided design) inputs. They presented an original method to assess the external geometrical attributes of 3D-printed components using laser triangulation-based 3D scanning. A printability index was created to compare the overall geometric fidelity of the printed specimen to its CAD input [158].

Structures containing cell-laden hydrogels, called bioinks, are compatible with SFF fabrication and are presently of high interest but very challenging.

The rheological properties of the formulation must meet requirements that make it possible to be extrudable with cells. The pressure applied must be compatible with the survival of the cells in the gel [159], [160]. This challenge has been met by a research team in Texas in the United States. A NICE (nanoengineered ionic covalent entanglement) bioink formulation with multiple desirable characteristics for 3D bioprinting bone tissue, including high print performance, enzymatic degradability, and osteoinductivity, was developed for printing with the 3DF technique. The printable proof of concept was validated by printing customized implants of mandibular bone defects from patient CT scans, allowing for us to envision this formulation and process as an alternative to the use of autografts [161]. The NICE bioinks were composed of methacrylate gelatin (GelMA), κ-carrageenan, nanosilicates, and photoinitiator (Irgacure 2959) dissolved in purified water. The covalently crosslinked GelMA network of NICE bioinks is susceptible to enzymatic (collagenase) degradation. The addition of nanosilicates to polymeric networks such as GelMA has been shown to preserve the osteoinductive ability of nanosilicates in the absence of osteoinductive agents, as noted

by De Godoy et al. [162]. The optimized NICE bioink can induce osteogenic differentiation of encapsulated stem cells in the absence of osteoinductive agents and tissue remodeling, even in the absence of osteoinductive factors.

10.2.3.2 Composite formulation for 3D printing by extrusion

For rigid materials such as inorganic materials (calcium phosphate cement, granules or ceramic), the addition of an organic part (polymer) can improve the mechanical and rheological properties. Such formulations, called composite formulations, can be injectable and display rheological properties that allow for printing [163], [164] (Figure 10).

Compared with hydrogels, the mechanical properties such as the Young's modulus, compressive strength and flexural strength of the composite formulation with the addition of the mineral part are closer to those of the bone, making it more adapted for bone repair [165], [166]. Most of the time, the mechanical properties of trabecular bones are closer than those of compact bone. It is still challenging to obtain a biomaterial with a value as high as that of cortical bone. Different polymers can be added to the mineral part.

The concentration of PLA can give rise to acidification of the formulation. Nonionic surfactants such as pluronik can be added to the mineral part to improve the rheological properties of the formulation but are very easily dissolvable and can cause toxicity. A step of debinding is required after the printing. A mixture of calcium-deficient hydroxyapatite cement and pluronik as a surfactant was printed by robocasting (3DF: 3D printing of filament) with a 250 µm resolution and displayed in vitro and in vivo biocompatibility [112]. The physicochemical properties of such cement are close to the mineral phase and low crystallinity of bone.

The self-hardening of the cement makes it possible to avoid the time-consuming step of sintering. Nevertheless, a setting time compatible with the time of printing remains challenging.

Using a suspension of phosphate calcium such as granules could avoid the limitation of self-hardening cement that is too fast. The drawback of this process is the size of granules, which can require the use of a larger needle size, affecting the resolution of the deposited material. The crystallinity of the suspension is higher than the crystallinity of bone, decreasing the resorption property [167]. A sintering step would also be required for the consolidation of the printed part. Such a composite suspension of chitosan and calcium phosphate granules has been printed by an extrusion process with a resolution of 400 µm [111]. The 3DF: 3D printing of filament process has also been used to print calcium silicate cement Ca_3SiO_5 and C_3S were prepared by the sol−gel method, and hydroxypropylmethylcellulose (HPMC) was selected as the binder because it is a biocompatible, biodegradable, hydrophilic polymer with desirable mechanical properties. This formulation appeared very bioactive and self-hardened in water. Implanted in rabbits, bone regeneration has been noted [116]. Strontium-containing bioglass (Sr-MBG: mesoporous strontium-containing bioglass) scaffolds with mesopores and regular macropores have been successfully fabricated using an extrusion 3D printing technique [117]. 3D printing of Sr-MBG scaffolds provided interconnected macropores and high porosity and enhanced the compressive strength by 170 times compared to the MBG scaffolds produced by polyurethane foam templating [168]. Some of the studies listed above are summarized in Table 7, with an assessment of the advantages and drawbacks of each material considering the material-based extrusion AM process. In conclusion, for the use of calcium phosphate material in extrusion-based AM processes, rigorous work is needed to develop printable ink for extrusion.

Binder is sometimes required to make a printable paste or putty. Hence, an additional debinding step can be required. Support is sometimes needed for complex 3D shapes, requiring a step to remove the sacrificial ink.

The debinding and removal of the sacrificial ink can cause shrinkage of the piece. This can be especially observed during the setting time of cement (although a lesser extent than what can be observed after sintering of ceramic).

Direct ink writing enables printing of scaffolds made of different materials due to the possibility of using several printer heads. Composite bioink made of calcium phosphate material and hydrogel has higher mechanical properties than pristine calcium phosphate paste (Table 8). Regarding FDM, the most thermosensible polymer used in bone tissue engineering is polycaprolactone, which is a resorbable polymer that generally requires preliminary shaping in filaments.

Material	Biological assessment	Mechanical Properties	Implant characteristics	Bioresorption	Specificity of the process	Sterilization/disinfection/decontamination	Conclusions/Summarization
Direct Ink Writing							
Calcium phosphate material							
Calcium phosphate cement [169]	Implantation in femur of dog - new bone formation - a rich widespread blood vessel network in the macropores.	Not tested	- cylindrical CAD model (5 mm diameter and 10 mm height) - 3D mesh with a rectilinear pattern - infill of 45%	- multinucleated osteoclast-like cells eroded the materials	- use of pluronik as binder - debinding step	gamma irradiation (25 kG)	- development to set up the printable ink - Binder can be required, necessitating a debinding step. - A support is sometimes required for complex 3D shapes, requiring a step to remove the sacrificial ink. - The debinding and removal of the sacrificial ink can cause slight shrinkage of the piece.
Calcium phosphate cement + oil-based carrier liquid [115]	- MSC adhesion - bone ingrowth in a small animal model of cleft alveolar osteoplasty	Not tested	- diameter: 3.0 mm - height: 3.2 mm - thickness: 0.48 mm (four layers) for biological evaluation - CAD file of alveolar cleft	no sign of degradation	- commercially available printer - 230 µm needle - plotting speed:10 $mm \cdot s^{-1}$ - air pressure:150 kPa. - strand widths: 199.8 ± 9 µm and 195.6 ± 9 µm) - use of a sacrificial ink of 10% methylcellulose - postprocessing to wash away the sacrificial ink in the fridge overnight. - hardened in an aqueous environment. - washing steps in acetone to remove residual oil of the CPC paste.	Not determined	

Table 8: A critical assessment of material/extrusion-based material additive manufacturing process pairs.

Material	Biological assessment	Mechanical Properties	Implant characteristics	Bioresorption	Specificity of the process	Sterilization/disinfection/decontamination	Conclusions/Summarization
Direct Ink Writing							
Composite biomaterial							
pasty calcium phosphate cement + (triglyceride+Polysorbate 80); [170]	cytotoxicity assay on hMSCs cultivated in the presence of cell culture medium preincubated with cement samples	-Young's modulus: 191±38 MPa - stress of 2.6±1.0 MPa without irreversible deformation under compression - compressive strain of 1.6±0.6% - strength: 6.1±1.8 MPa	cube of 34 layers: an alternative x-y layer with a 0/45/90 °C lay-down pattern and a strand distance of 850 mm.	Not tested	- plotting with compressed air - A commercially available 3D plotting system developed by Fraunhofer IWS (Dresden) - needle diameter: 838 mm -Setting in water	Y-irradiation	- the composite formulations have deformation ability. - accuracy less than that of SLA. - A bigger needle diameter can be required to avoid clogging. - Different formulations can be printed with commercially available 3D printers with several printer heads without optimization of parameters. - The ability to control the temperature inside the syringe can help control the viscosity and rheological property of the composite slurry.
Calcium phosphate cement + chitosan [111]	Not tested	Not tested	130 – 140 µm of distance between layers	Not tested	- commercially available 3D printer: robocasting system (3DInks, USA) - Conical nozzle with 400µm internal diameter -9–10 mm·s^{-1}for speed ink deposition	Not tested	
sulfoaluminate cement + HPMC Hydroxypropyl methyl cellulose, water reducing agent + tartaric acid + water [113]	Not tested	compressive strength: more than 30MPa flexural strength: less than 5MPa	For compressive strength: cubic samples (20 mm * 20 mm * 20 mm) For three-points bending test: prism specimens (20 mm * 20 mm * 60 mm)	Not tested	- commercially available 3D printer. - extrusion through screw mixing under an air pump pressure of 0.3 MPa - loading speed: 15 mm/s - printing speed:10 mm/s.	Not tested	
Ternary composites containing mesoporous bioglass fibers of magnesium, (mMCS), gliadin (GA), calcium silicate and polycaprolactone [117]	- MC3T3-E1 viability, adhesion - in vivo implantation in femoral defect of rabbit: new bone formation	- compressive strength: 10.5 MPa-12.1 MPa	- Scaffold dimensions: (Φ 12×2 mm, Φ 5×5 mm) - line width: 500 µm, - pore size: 500 µm - line height: 500 µm	- weight loss and surface modification in acidic solution	- Commercially available printer: 3D Bioprinter (Qingdao Unique Co., Ltd., Qingdao, China) - printing temperature: 130 °C (the composite powders were heated to 130 °C for 30 minutes, and screw-extruded through a metal nozzle of	gamma rays from a cobalt 60 source	

					gage 2 (inner diameter of 0.33 mm). - feeding rate: 100 mm/min.		
bioactive silicate cement: tricalcium silicate (Ca_3SiO_5 and C_3S) + Hydroxypropylmethylcellulose (HPMC)[116]	- attachment and proliferation of rat bone marrow stem cells (rBMSCs) - in vivo implantation in rabbit femur: osseointegration and new bone formation	compressive strength and modulus increased with time, which reached 12.9 MPa and 680.9 MPa, respectively, for a scaffold with porosity of 61% after setting for 7 days	- for compressive strength test: 10 × 10 × 10 mm, -different shape with interconnected porosity (6 × 10 mm)	- weight loss after soaking in Tris−HCl solution - in vivo bioresorption	- self-setting in deionized water at 37 °C - commercially available 3D printer equipped with three-axis positioning system - pressure: 200−400 kPa - dispensing speed: 10 mm s−1.	Not determined	

Table 8 (continuation): A critical assessment of material/extrusion-based material additive manufacturing process pairs.

Material	Biological assessment	Mechanical Properties	Implant characteristics	Bioresorption	Specificity of the process	Sterilization/disinfection/decontamination	Conclusions/Summarization
Fused deposition modeling							
Polymer							
Polycaprolactone PCL[171]	Not tested	Depending on the porosity - compressive stiffness: 4–77 MPa - yield strength: 0.4–3.6 MPa - yield strain: 4% - 28%	- rectangular prisms (32.0 mm long by 25.5 mm wide by 13.5 mm high - honeycomb-like pattern, - fully interconnected channel network. - channel size 160–700 μm, - filament diameter 260–370 μm - porosity 48–77%	Not tested	A one-shot extruder (Alex James & Associates Inc., Greensville, SC) was first used to fabricate PCL monofilaments with a diameter of 1.70+0.08 mm from PCL pellets	Not determined	Requires manufacturing the polymer in the correct shape to be printed

Table 8 (continuation): A critical assessment of material/extrusion-based material additive manufacturing process pairs.

10.3 Selective laser sintering

SLS uses a fine powder that is heated with a CO_2 laser with power in the range of 25–50 W such that the surface tension of the grains is overcome and they fuse together. Without powder thermal preprocessing, the powder may flow poorly and may "ball" or form molten clumps during laser exposure rather than wetting into the present and previous layers [172]. Before starting the printing, the entire bed is heated to just below the melting point of the material to minimize thermal distortion and facilitate fusion to the previous layer. Each layer is drawn on the powder bed using the laser to sinter the material. Then, the bed is lowered, and a powder-feed chamber is raised. A new covering of powder is spread by a counterrotating roller. The sintered material forms the part while the unsintered powder remains in place to support the structure and may be cleaned away and recycled once the build is complete.

The feasibility of using SLS to produce parts from glass-ceramic materials for bone replacement applications has been investigated. A formulation made of SiO_2 Al_2O_3 P_2O_5 CaO CaF_2 that crystallizes to a glass ceramic with apatite and mullite phases was produced, blended with an acrylic binder, and processed by SLS [173].

SLS was applied with ultrahigh molecular weight polyethylene (UHMWPE) without a successful outcome. The drawback is the uncontrolled shrinkage of the manufactured part. Moreover, the material exposed to the laser beam was shown to have undergone degradation in terms of chain scission, cross-linking, and oxidation. It has been concluded that the development of improved starting powders, particularly with increased density, is required to apply this technology to the fabrication of UHMWPEs [174]. Polycaprolactone is also compatible with this technique [175]. A porous scaffold with sufficient mechanical properties (compressive modulus and yield strength of 52 to 67 MPa) was implanted in vivo

with good bone regenerative results. The printable proof of concept of an anatomy-specific exterior architecture derived from pig CT scans has been used to design condyl defects in pigs [63].

Metal implants were modeled with the SLS method for cranioplasty. Nevertheless, the use of metals that are nonbioresorbable limits bone regeneration, as mentioned above. Metal or nylon medical devices printed using the selective laser sintering technique can act as life-like nylon models that have proven to be very useful in preoperative planning. The nylon models are extremely accurate (to within 0.1 mm) and could also be used for preoperative planning of complicated skull base and spinal cases. Nevertheless, pieces can deform during production, reducing their accuracy. Materials other than titanium (such as acrylic) could be used to produce cranioplasty plates from computer-generated models. Some surgeons prefer titanium due to its greater impact protection, while others consider that resorbable plates are not as effective as titanium plates for facial fracture repair. Casting the titanium plates has the added potential advantage of providing greater protection by increasing the plate thickness when necessary. The main disadvantage of these computer-assisted techniques is their cost, which remains too high. It is necessary to have access to a computer workstation with a large memory capacity and run appropriate software that will render the CT data. The final cost of the implant includes the cost of running the work station, royalties for software use, production of the model by a computer modeling technique and fabrication of the prosthesis. On average, the cost per titanium plate would be approximately $2,500 [176].

Hydroxyapatite powder can be used with selective laser melting. However, a binder is required. This decreases the component strength and bioactivity, so research has been conducted to find new formulations. Direct selective laser melting of HAP (hydroxyapatite powder) has been conducted to avoid the use of binder [177]. The blending of HA with polyetheretherketone has also been investigated to avoid using a binder [178]. Porous polycaprolactone (PCL) scaffolds were computationally designed and fabricated via

selective laser sintering. Polycaprolactone (PCL) is a bioresorbable polymer with potential applications for bone and cartilage repair [175]. Metal (Inconel 625 superalloy, Ti-6AI-4 V and Monel) can be shaped by the combination of SLS and hot isostatic pressing (HIP). A net shape manufacturing method known as SLSIHIP combines the strengths of selective laser sintering (SLS) and hot isostatic pressing (HIP) to provide metal implants with high mechanical performance [109].

The studies listed above are summarized in Table 9, with a description of the outcome displayed in the literature to assess the advantages and drawbacks of each material for the SLS AM process. In conclusion, SLS can be used with various powder materials. The use of calcium phosphate powder in the SLS technique may require optimization of the printer. SLS is very versatile in terms of using a wide range of materials. It has been shown that both the mechanical properties and the geometry of bone scaffolds manufactured by SLS are directly dependent on infused sequential layers and process factors such as the particle size, temperature of the powder bed, intensity of the beam, scan speed and hatch distance [153]. The process remains time-consuming, as a binder is required to link grain powder, leading to a debinding step as well as the sintering for the consolidation of the part. Composite powder can also be used; nevertheless, the sterilization of the composite can be complex due to the different behaviors of the organic and the inorganic phases. Except for a standardized process used in the pharmacopoeia: ethylene oxide, disinfection has only been realized in ethanol. Metal powder required a preliminary heating treatment to make the powder more malleable for melting under the laser. It is also worth noting that the metal powder is expensive.

Material	Biological assessment	Mechanical Properties	Implant characteristics	Bioresorption	Specificity of the process	Sterilization/disinfection/ decontamination/	Conclusions/Summarization
Calcium phosphate powder							
Calcium phosphate powder + poly(methymethacrylate-con-butylmethacrylate) latex polymer [101]	- implantation in rabbit calvaria and dog oral cavity - bone ingrowth were observed	- Strength range in compression: 2,000 psi - Strength range in 4-points bending: 2,200 psi	- tiny rectangles, 0.12x 0.16x 0.05 - open interconnected macroporosity: > 100 µm - printing of a human anatomical facsimile from CT images	Not tested	-3D printer prototype: equipped with modulated 25 W CO_2 laser - debinding step - sintering step	Not determined	- optimization of the printer to enhance the laser parameters. - time-consuming process: debinding and sintering
Polymer powder							
ε-polycaprolactone powder [102]	Bone ingrowth	Compressive modulus: 52–67 MPa yield strength: 2.0–3.2 MPa	- printing of scaffold from CAD based on an actual pig condyle - orthogonal pores 1.75–2.5 mm - porosity: 63–79% for mechanical tests: porous scaffolds (5.0 mm by 4.5 mm by 1.5 mm)	Not tested	- layer thickness 100 µm. - preheating of the powder to 49.51 °C canning - laser parameter (450 mm focused beam diameter) at 4.5 W power and 1.257 m/s (49.5 in/s) scan speed.	Not determined	- High resolution of the printed filament:100 µm. - Several parameters of the laser must be optimized.
Polylactic acid PLA[103]	human adipose-derived stem cell viability	Not tested	Cylindrical scaffolds: 12 mm diameter and 5 mm long	Not tested	- layer thickness: 0.2 mm - porosity 1 mm	-soaking in 75% ethanol and exposure to UV light for 1 h.	

Table 9: A critical assessment of material/SLS additive manufacturing process pairs.

Material	Biological assessment	Mechanical Properties	Implant characteristics	Bioresorption	Specificity of the process	Sterilization/disinfection/decontamination	Conclusions/Summarization
composite powder							
Mg–CS (Magnesium calcium silicate) powder+PCL powder [79]	Adhesion and proliferation of human MSC	Not tested	- pore size: 450µm, - scaffold of 16 layers (8 mm height, 10 mm diameter) - layer distance: 500 µm	degradation in SBF	- Special design of the 3D printing: system built in the lab, equipped with CO_2 laser fiber (2 W).	immersion in 75% ethanol and exposure to UV light	- Sterilization is complex - disinfection should avoid degradation of the composite.
Polycaprolactone+nanoparticules of hydroxyapatite [104]	- Attachment and proliferation of human bone marrow stromal cells. -in vivo implantation in rabbit femur defects for 3, 6, and 9 weeks: new bone formation	compressive strength: 1.38–3.17 MPa	porosity: 70.31%-78.54%	Not determined	Not determined	Ethylene oxide fumigation	
Poly-epsilon-caprolactone/hydroxyapatite [78]	Saos-2 cell viability Bioactivity: apatite crystal formation at the surface	Not determined	Not determined	Not determined	Not determined	70% ethanol	
Metal powder							
Titanium[176]	Not tested	Not tested	CT scan data of a skull; Titanium sheet 0.5–0.75 mm thick	Not tested	-A fine layer of nylon powder is heated by the laser beam. - computer guide allows for melting the powder in appropriate locations in that layer.	Not tested	- An indirect method can be used to cast a mold and print the final piece. - Thermal pretreatment of metal powder is required

Table 9 (continuation): A critical assessment of material/SLS additive manufacturing process pairs.

10.4 Inkjet 3D Printing or powder bed

Inkjet 3D printing or the powder bed technique is based on the direct binding of a powder bed by inkjet of a binder solution. 3D powder printing was developed by Michal J. Cima and coworkers in 1993. The model is printed in layers composed of a starch-based powder bed and glued together with a liquid binder [179]. In some cases, to reach a suitable strength, the scaffolds are sintered after printing. This postprocessing exposes the final part to failure due to the burn out due to the binder that is present or because of a high binder concentration. Therefore, the binder concentration must be minimized while providing sufficient mechanical stability to the printed structure. Moreover, sintering causes a dimensional change in the final part.

This technique has been used at McGill University to print brushite, monetite and hydroxyapatite cement with a low-temperature process. This technology used a printer head of ink jet phosphoric acid solution that hardened the cement at the site to print. The internal porosity of such a printed material and the resolution are in the range of millimeters [118], [119], [180], [181].

This technology was applied to print dense implants without porosity for skull bone repair from patient CT-scans [182]. The drawbacks of this process concern the brittleness of the obtained implant, which makes them hard to handle by surgeons. Nevertheless, increasing the acid phosphoric concentration and immersing the part in acid phosphoric during the self-hardening increased its mechanical properties, which may reach 22 MPa of compressive strength [181]. Some of the studies listed above are summarized in Table 10, with a description of outcomes displayed in the literature to assess the advantages and drawbacks of each material for the powder bed AM process. In conclusion, this process uses powder. For the cement, self-hardening at room temperature makes it possible to avoid the sintering step.

Moreover, the room temperature process makes it possible to load the scaffold with biological molecules in situ.

Biomaterial	Biological assessment	Mechanical Properties	Implant characteristics	Bioresorption	Specificity of the process	Sterilization/disinfection/ decontamination/	Conclusions/Summarization
Calcium phosphate material							
Calcium phosphate cement [119]	Not tested	compressive strength: 4.0–6.4 MPa	- printing of scaffold from patient's tomographic data. - for mechanical test: cylindrical specimens 12 mm (diameter) x 24 mm (length) - layer thickness: 88 mm	Not tested	- commercial 3D powder printing system - fabrication at room temperature - liquid binder phase: 2.5% Na_2HPO_4,	Not tested	-Using cement makes it possible to avoid the sintering step. - possibility of in situ loading with accurate location of biological molecules is possible. - 3D printer is commercially available - the comparison of mechanical properties is complex as different sample dimensions were used. The values are in the range of the lower value of trabecular bone.
Dicalcium phosphate dihydrate (brushite) [180]	Intramuscular implantation in rat	compressive strengths:0.9–8.7 MPa - phosphoric acid post treatment: 22 MPa	- dimensional accuracy ± 200 µm cylindrical samples for axial compression 20 mm height and 10 mm diameter - Samples for diametral tensile strength: (h = 5 mm, d = 10 mm) - 4-point bending strength: cuboids 10 mm x 5 mm {x 80 mm)	dissolution	- commercially available 3D-powder printing system (Z-Corporation, USA) - binder: phosphoric acid (H3PO4)	Soaking in 75% ethanol	
Dicalcium phosphate dihydrate (DCPD) or tetracalcium phosphate (TTCP) powders [118]		strengths of DCPD: 0.3 ± 0.6–22.3 ± 1.5 MPa-strengths of HA: 1.9 ± 0.2–5.8 ± 0.3 MPa	- cuboid: 8 mm× 8 mm× 3 mm - pore: 1.31 ± 0.11) mm	Not tested	- loaded with 200 ng VEGF or 56 ng of copper sulfate -commercially available 3D-powder printing system (Z-Corporation, USA -binder: 10% phosphoric acid and 1 M NaH2PO4 for TTCP and 20% phosphoric acid for TCP powder	soaking in 70% ethanol	
Composite							
Bioglass+βTCP [121]	MG-63 viability and proliferation	compression strength:7.4–11 MPa	Diameter: 10.6±0.02 mm, mean height: 2.94 ± 0.26 mm	Dissolution in SBF	- Commercially available 3D printer: Inkjet 3D Printer (ZPrinter 310 Plus, Z Corporation, Rock Hill, SC, USA) - binder water soluble: 10–15 wt % dextrin - sintering of BG 350◦C and kept at this temperature for 60 min	Not specified	In contrast to cement that is self-hardening, using calcium phosphate ceramic powder requires a debinding and sintering step

Table 10: A critical assessment of material/powder bed additive manufacturing process pair.

10.5 Conclusion: assessment of the performance and classification of different biomaterial/AM process couples based on the scientific results presented in the literature (a methodological approach to the calculation of a performance index).

A qualitative assessment of each biomaterial/AM pair was performed based on the following criteria: expected properties for bone repair patient-care efficiency (1) which is evaluated with the Performance Index PI (1), user-friendly AM processing (2) which is evaluated with the Performance Index PI (2) and the efficiency of the process (3) which is evaluated with the Performance Index PI (3) (Table 11). A system of comparison with three levels (high, medium, and low performance) has been used. “High performance” is the highest ranking of biomaterial/AM processes regarding the specification. “Medium performance” relates to an intermediate ranking of the biomaterial/AM processes. “Low performance” has been attributed to the lowest ranking of biomaterial/AM processes.

This review aims to provide a framework that validates the technical feasibility of using a biomaterial/AM process couple for a specific clinical application, thereby assisting the user with deciding on the most appropriate biomaterial/AM process couple. The framework comprises three levels of ranking that are crucial for the expected clinical outcome for clinicians and patients and also for compliance with the expectations of industrial production and engineering of biomaterials. Each global level has been subdivided into different parts that may cover a global expectation:

1) Expected properties for bone repair patient-care efficiency

- mechanical performance of the printed item
- osseointegration of the implant
- bioresorption of the implant
- compatibility of the implant with medical imaging

2) User-friendly AM processing

- compatibility of the process with the printing of biological items (cells, growth factors)
- price of the 3D printer
- complexity of the development of the printable formulation
- time involved in the printing process
- complexity of the parameters to be set

3) Efficiency of the process

- shrinkage of the printed item
- accuracy of the process

- matching of the CAD file with the printed implant.

Depending on the area of expertise of the engineer, the financial support, the already available equipment, individual manufacturers of 3D printed items can have different requirements and priorities. Therefore, a coefficient can be attributed to different levels or sublevels of the framework to emphasize the most important characteristics to be fulfilled by the biomaterial/AM process couple. The same can be done for the levels and sublevels that relate to the expectations of clinicians and patients. Hence, biomaterial/AM process couples are not either good or bad. A compromise has to be reached. Indeed, thanks to the example of ranking that we have performed below, it is possible to note that several biomaterial /AM process couples received the same sublevel ranking in the framework. It can also be seen that for a given level of the framework, a biomaterial/AM process couple can receive a lower ranking than another couple whereas this same couple receives a higher ranking than the other couple for another level.

For example, the calcium phosphate material + photopolymerizable resin/SLA couple received the lowest ranking for the mechanical property but received the highest ranking for the osseointegration and the accuracy of the process, whereas the PCL/FDM couple received the highest mechanical performance ranking but the lowest osseointegration and an intermediate ranking for the accuracy of the process (Tables 11 and 12).

Each procedure has advantages and disadvantages that should be weighed individually from case to case. Regarding the more important characteristic to consider for the specific application to be achieved, the readers will be able to choose the couple of interest that best matches their expectations.

Moreover, this assessment will allow the industrial production and the engineering of the material to be focused on the properties that need to be prioritized. An upgrade of the different processes could be readily highlighted thanks to this methodology that makes it possible to have an overview of the pros and cons of different biomaterial/ AM process couples.

Following are the explanations of how the ranking and the performance index have been attributed based on scientific publications. It is worth noting that only commonly used techniques and formulations have been taken into account in the ranking. Every innovative formulation and technique aimed at upgrading the process has been highlighted without being specifically involved in this latter assessment. For example, specific formulation for SLA without the requirement of a binder, SLS technique coupled with the isostatic technique to improve the mechanical performance of the printed item, and metal combined with an organic component to develop a composite item printed by SLS are examples of such breakthrough

technologies for which proof of concept has been validated without yet being commonly used in the clinic. The mechanical properties of the different biomaterial/AM process couples have been mainly attributed to the characteristic of the biomaterial used, even if the AM process is a breakthrough technique that has been successfully used to design architectures with enhanced mechanical properties due to for example the orientation of the printed filament and the layout of the printed layers [21], [22], [128].

The category "low performance" has been attributed to the cement/powder bed couple because cement has a poor mechanical performance, close to that of trabecular bone, and is not suitable for load-bearing bone replacement [183]. The compressive strength of such an implant 3D printed with this process is 0.9 MPa–8.5 MPa [118]. Gbureck et al. have shown that sodium citrate solution treatment of the 3D printed item can improve the compressive strength, thereby allowing compressive strengths of up to 22–156 MPa to be obtained [181], [184].

"High performance" has been attributed to the PCL/FDM couple: stiffness of the polymer is increased with the possibility of designing a 3D structure that enhances the mechanical properties [22], [21], [128].

"Medium performance" has been attributed to the composite material (organic part and inorganic part)/extrusion-based biomaterial (direct ink writing) couple because the brittleness of the inorganic component is balanced by the stiffness of the organic part [185], [186].

"Low performance" has been attributed to the calcium phosphate material + photopolymerizable resin/SLA and the calcium phosphate powder/SLS couples because calcium phosphate is a brittle material. Even after the sintering for consolidation of the grain and cohesion of the boundary grain, the material remains brittle, [141], [146], [148].

"High performance" has been attributed to the metal (titan, zirconium)/SLS couple because metals have very high mechanical performance and are used especially in orthopedics for load-bearing bone replacement [43]. The combination of SLS and hot isostatic pressing (HIP) make it possible to upgrade the mechanical performance of the printed item [109]. The osseointegration property was mainly attributed to the bioactivity of the biomaterial used, such as its ability to form a carbonated apatite layer on its surface. "High performance" has been attributed to the cement/powder bed couple because of good osseointegration thanks to the bioactive layer that can be formed at the surface of cement [187], [188], [189], [190].

"High performance" has been attributed to the calcium phosphate material + photopolymerizable resin/SLA and to the calcium phosphate powder/SLS couples because calcium phosphate material is also bioactive [78].

“Low performance” has been attributed to the PCL/FDM couple because polycaprolactone is not a bioactive material when used alone. The addition of calcium phosphate makes it possible to develop a composite bioactive material [191].

“Intermediate performance” can be attributed to the composite material (organic part and inorganic part)/extrusion-based biomaterial (direct ink writing) couple because the calcium phosphate material provides the bioactivity property to the composite formulation. The optimum ratio of the organic and inorganic parts to develop a formulation with accurate bioactivity while also being extruded thanks to optimal rheological properties is challenging [111], [186], [191], [192].

“Low performance” has been attributed to the metal (titan, zirconium)/SLS couple because metals are bioinert, although depending on the chemical group that can form at the surface of the biomaterial when implanted in the host, a bioactive layer can be formed at the surface. The required condition for a material to form surface apatite is the presence of functional groups that permit apatite nucleation. Functional groups such as Si–OH, Ti–OH, Zr–OH, Nb–OH, and Ta–OH are effective for apatite nucleation. This mechanism can be applied for all types of materials even when no calcium or phosphate is included in the chemical composition [38].

Regarding the price of the 3D printer, a more precise ranking can be performed by the reader after the prospecting of different commercial providers. In this review, the assessment was focused on the complexity to manufacture the printer and the required maintenance of the device, which correlate directly with the price. 3D printers capable of extrusion, which is used by the composite material (organic part and inorganic part)/extrusion-based biomaterial (direct ink writing) couple received a “high performance” ranking. This is the best ranking for the price parameter. FDM/PCL also received a “high performance” ranking because a heating platform is associated with the extrusion process that does not require significant complexity in the manufacturing or maintenance. A pressurized air entrance or a mechanical pressure system is required.

The 3D printers that require a laser have been classified among the most expensive printers. and 1 star has been attributed to the three couples: calcium phosphate material + photopolymerizable resin/SLA, calcium phosphate powder/SLS, and metal (titan, zirconium)/SLS. It is also worth noting that the metal powder is expensive.

The intermediate ranking has been attributed to the cement/powder bed couple because this technology is more complex than an extrusion technique, although it does not require the use

of a laser. The powder is solidified thanks to a system of droplets of binder liquid circulating continuously in the system.

Regarding the complexity of the development of the printable formulation, the lowest ranking (low performance) has been attributed to the composite material (organic part and inorganic part)/extrusion-based biomaterial (direct ink writing) couple because finding the good rheological characteristics and/or the crosslinking of the organic part of the material is challenging and requires a formulation encompassing all of these properties [160], [193], [194], [195]. “Low performance” has also been attributed to the calcium phosphate material + photopolymerizable resin/SLA and the calcium phosphate powder/SLS couples because the use of an accurate binder is required. For the SLA, the use of a photoinitiator is required. A post-processing step, the debinding step, is required, which introduces a degree of complexity in the formulation of the material. Nevertheless, some breakthrough formulations that do not require binder have been devised [177], [178].

“Medium performance” has been attributed to the PCL/FDM couple because there is a more complex additional step to manufacture the polymer as the rubber form before being used by the FDM technique.

“High performance” has been attributed to the metal (titan, zirconium)/SLS and the cement/powder bed couples. For these couples, the setup is essentially based on the parameters of the device and the process. For the powder bed, the raw powder is glued thanks to the binder liquid droplets circulating in the system, [118], [119], [181], [180], [187]. Metal powder required a preliminary heating treatment to render the powder more malleable for melting under the laser and binder jetting, although no complex formulation is required [113], [180]. It is worth noting that more breakthrough formulations such as composite metal have been devised. Nevertheless, sterilization of the composite can be complex due to the different behaviors of the organic and inorganic phases. Except for a standardized process involving ethylene oxide used in the pharmacopoeia, disinfection has only been carried out with ethanol.

Regarding the time of the printing process, the assessment depended on whether there are several steps in the process, such as a debinding step and a sintering step. Hence, calcium phosphate material + photopolymerizable resin/SLA and calcium phosphate powder/SLS couples received a “low performance” and have been classified in the lowest rank compared to the other couples. Stereolithography requires a photoinitiator to crosslink the slurry using a computer-controlled laser beam or a digital light projector that requires removal. Hence, debinding and sintering of the 3D item make the process time-consuming, [141], [145], [146].

The metal (titan, zirconium)/SLS couple received a “medium performance” ranking because there is a pretreatment step of the metal to make it more malleable [113], [180]. Moreover, the items have a grainy surface without any post-processing. Post-processing of the surface can be required.

The composite material (organic part and inorganic part)/extrusion-based biomaterial (direct ink writing) couple also received an “intermediate performance” ranking because it can take a long time to print the item, depending on its size. The speed of the printing cannot be very high so as to allow a balance between the accuracy of the filament and the force required for the extrusion. Clogging is another limiting factor.

The cement/powder bed and the PCL/FDM couples received “high performance” rankings, i.e., the highest rank, as there is no need for additional debinding or sintering steps.

The complexity of the parameters to be set has relied on the complexity of the printer. Providers try to design printers that are increasingly user-friendly. Cement/powder bed, PCL/FDM, metal (titan, zirconium)/SLS, and calcium phosphate powder/SLS received the “intermediate performance” ranking.

The particle size, temperature of the powder bed, intensity of the beam, scan speed, and hatch distance are the parameters that need to be set [153]. The composite material (organic component and inorganic component)/extrusion-based biomaterial (direct ink writing) received the “low performance” ranking, which is the lowest rank because the setup of the printer depends on the setup of the formulation that determines the success of the extrusion. The accuracy of the printed filament also depends on the setup. The speed of the printing will influence the thickness of the filament. The calcium phosphate material + photopolymerizable resin/SLA couple received the “low performance” ranking, which is the lowest rank because the SLA process with calcium phosphate material requires meticulous preparation to develop a printable formulation composed of a binder resin and a photopolymerizable reagent. Moreover, sintering causes substantial shrinkage of the final item compared to other processes. It is worth noting that this is not problematic because this can be compensated for. Nevertheless, this remains a setup that needs to be taken into account. The main advantage of SLA is its high resolution [103], [144]. The calcium phosphate material + photopolymerizable resin/SLA couple received the highest rank (“high performance”) for the accuracy of the process.

The cement/powder bed couple received the lowest rank (1 star) because only a dense item with macroporosity can be designed. Microporosity and nanoporosity cannot be designed with

this technique. The internal porosity of such printed materials and the resolution are on the order of millimeters, [118], [119], [180], [181].

All the other couples received an intermediate performance ranking because by modulating the formulation setup and the parameters of the printer it is possible to achieve a very good level of accuracy.

Regarding the match between the CAD file and the printed implant, the development of increasingly sophisticated software allows for very good control of this parameter possible. This will depend on the expertise of the developer. All the couples received the intermediate performance ranking. Nevertheless, the metal (titan, zirconium)/SLS couple received the highest level, because selective laser sintering (SLS) is a rapid manufacturing process that allows the items to be produced directly from the CAD model without item-specific tooling. This technique has the big advantage of being the only one capable of manufacturing metal structures (such as titanium and cobalt chrome).

A nuance has been highlighted regarding the bioresorption of two biomaterial/AM process couples (calcium phosphate material + photopolymerizable resin/SLA and metal (titan, zirconium)/SLS) that depend especially on the nature of the material used. In biological as well as synthetic systems, calcium phosphates can transform from one form to another, depending on the pH and the composition of the synthetic solution or the biological microenvironment. The vast majority of calcium phosphate bioceramics are based on HA, β-TCP, and α-TCP. To improve bioresorption of HA, blending with β-TCP has been performed, which gave rise to biphasic calcium phosphates (BCPs) in the 1990s [196]. The formation of different types of calcium phosphates in both synthetic and biological systems depends on the solution pH, temperature, and composition. The concept of BCP has been extended by preparation and characterization of biphasic TCP (BTCP), consisting of both α-TCP and β-TCP phases [197]. Bioresorbable metals are presently undergoing extensive investigation [198], [199],[200], [201].

The global Performance Index represents the product of the three PIs:

Global PI=PI(1).PI(2).PI(3)

The qualitative assessment of the Performance Index (Figure 12 and Table 11) is translated into a quantitative assessment (Table 12) to obtain a better complementary representation.

	expected properties for the bone repair patient-care efficiency (1)				user-friendly AM processing (2)					efficiency of the process (3)		
Properties	mechanical performance of the printed piece	osseointegration of the implant	bioresorption of the implant	compatibility of the implant with medical imaging	compatibility of the process with the printing of biological part (cells, growth factors)	price of the 3D printer	complexity of the development of the printable formulation	time of the printing process	complexity of the parameters to be set	shrinkage of the printed piece	accuracy of the process	loyalty between the CAD file and the printed implant
cement/powder bed	low	high	yes	yes	yes	intermediate	high	high	intermediate	no	low	intermediate
PCL/FDM	high	low	yes	yes	no	high	intermediate	high	intermediate	no	intermediate	intermediate
composite material (organic part and inorganic part)/extrusion-based biomaterial (direct ink writing)	intermediate	intermediate	yes	yes	yes	high	low	intermediate	low	no	intermediate	intermediate
calcium phosphate material+photopolymerizable resin/SLA	low	high	possible	yes	no	low	low	low	low	yes	high	intermediate
metal (titan, zirconium)/SLS	high	intermediate	In general No (Iron and Magnesium metal are bioresorbable)	no	no	low	high	intermediate	intermediate	no	intermediate	high
calcium phosphate powder/SLS	low	high	yes	yes	no	low	low	low	intermediate	yes	intermediate	intermediate

Table 11: Qualitative assessment of different biomaterial/AM process pairs
High: the best performance of the biomaterial/AM process pairs for the user;
best biological and mechanical properties with the cheapest price
Intermediate: intermediate performance of the biomaterial/AM process pair for the user
Low: lower performance of the biomaterial/AM process pair for the user;
lowest biological and mechanical properties with a more expensive price

The assessment of different criteria may highly vary regarding a specific application. In the case of orthopedics or dentistry, when bone regeneration is not the expected clinical outcome, nonabsorbable metals with osseointegration ability will be prioritized; for example, the SLS/titan couple will be prioritized. In the case of education, a less precise AM process with a material that is not necessarily biocompatible will be prioritized; for example, FDM can be a good candidate. For surgical planning, when accurate precision between the CAD file and the printed piece is expected, a more precise AM process is needed; for example, the SLA process would be prioritized and the printed material is not expected to be biocompatible or resorbable so polymer should be privileged.

For bone tissue engineering, when the combination of biological parts such as growth factors and cells is expected in the printing process, an AM process that maintains the viability of cells and functionality of peptide growth factors will be prioritized. The direct-ink process will be selected with material that does not require postprocessing treatment such as debinding and sintering.

Moreover, the assessment of the quality of the final part properties varies based on several criteria. The mechanical properties of the printed implant are the most illustrative case. Depending on the dimensions of the part to be printed, the method used to realize the testing and design of the porosity, the mechanical properties measured can differ for the same biomaterial. The type of device used for the characterization such as a compression machine or ultrasound, the type of measurement (longitudinal or transverse) and the sample size can influence the results obtained and make comparison difficult. After testing bone samples of different sizes for mechanical tests, Linde et al. concluded that a cube with a side length of 6.5 mm or a cylindrical specimen with a 7.5 mm diameter and 6.5 mm length are suggested standard specimens for comparative studies on trabecular bone mechanics [202].

Hence, a system of stars has been created to generalize the evaluation because some general trends may emerge. Hence, three levels of graduation have been used.

Three stars were attributed to the best biomaterial/AM process for a specific criterion: two stars for intermediate performance and one star for lower performance. Matching the stars with an encrypted value makes it possible to create a performance index (Table 12).

Criteria / biomaterial/ AM process	Expected properties for the bone regeneration patient-care efficiency		PI of the expected properties for bone repair PI (1)	classification	User-friendly AM processing				PI of the user-friendly AM processing PI (2)	classification	Efficiency of the process		PI of the efficiency of the biomaterial/ AM process PI (3)	Classification
	mechanical performance of the printed piece	osseointegration of the implant			price of the 3D printer	complexity of the development of the printable formulation	Time of the printing process	complexity of the setting parameters			accuracy of the process	loyalty between the CAD file and the printed implant		
cement/powder bed	66%	100%	66%	1	66%	100%	100%	66%	44%	1	33%	66%	22%	3
PCL/FDM	100%	66%	66%	2	100%	66%	100%	66%	44%	1	66%	66%	44%	2
composite material (organic part and inorganic part)/extrusion-based biomaterial (direct ink writing)	66%	66%	44%	2	100%	33%	66%	33%	7%	3	66%	66%	44%	2
calcium phosphate material+ photopolymerizable resin/SLA	33%	100%	33%	1	33%	33%	33%	33%	1%	5	100%	66%	66%	1
metal (titan, zirconia)/SLS	100%	66%	66%	2	33%	100%	66%	66%	14%	2	66%	100%	66%	1
calcium phosphate powder/SLS	33%	100%	33%	1	33%	33%	33%	66%	2%	4	66%	66%	44%	2

Table 12: Quantitative assessment of different biomaterial/AM process pairs: the performance index
"High" indicates the best performance of biomaterial/AM process pairs (3/3=1=100%)
"intermediate" indicates intermediate performance of biomaterial/AM process pairs (2/3=0.66=66%)
"low" indicates the lowest performance of biomaterial/AM process pairs (1/3=0.33=33%)

The global PI for one level of graduation is calculated by multiplying all the performance percentages : Global PI=PI(1).PI(2).PI(3).

The pairs with three stars obtained the best mark of 3; two stars indicates intermediate performance; and one star indicated a lower evaluation (Table 12). To quantify the global performance of the process, we defined a performance index (PI). The PI is a concept used by Ashby [138] to classify material and process performance. The PI was calculated as follows: related to one property (I): PI is proportional to the ratio of this property versus the property of the best material (Equation 1):

$$(1): \mathrm{PI} = \frac{\text{Material Property}_i}{\text{Best Material Property}}$$

The global performance index PI of the material according to its n properties, P_i, is defined as follows (Equation 2):

$$(2): \mathrm{PI} = \mathrm{P_1\,P_2P_3\,...\,P_n}$$

$$\mathrm{PI} = \prod_{i=1}^{n} \mathrm{P_i}$$

A global performance index for each biomaterial and AM process was calculated taking into account three main expected properties: (1) properties for bone repair (mechanical properties and osseointegration); (2) user-friendly process properties (the price of the 3D printer and complexity of the preparation of the formulation, time of the total process to obtain the final 3D piece, complexity of setting up the printing parameters); and (3) efficiency of the process (accuracy of the process and loyalty between the CAD model and final 3D-printed piece).

The results are summarized in Table 13, which is shown as a graphical figure to better visualize the classification (Figure 12).

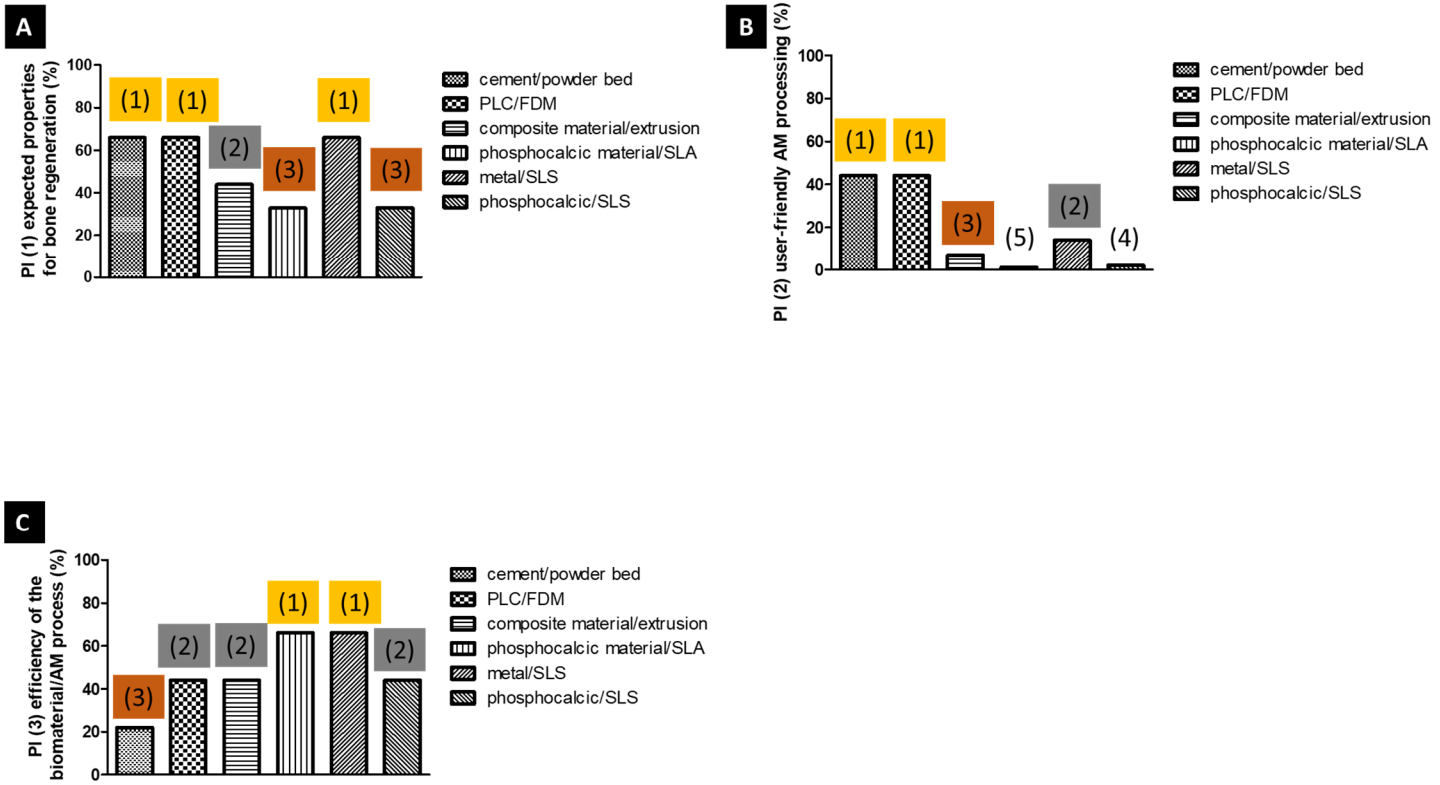

Figure 12: Classification of different biomaterial/AM process pairs
(1): first ranked performance
(2): second ranked performance
(3): third ranked performance
(4): fourth ranked performance
(5): fifth ranked performance

This matching was performed with nonbinary criteria such as the bioresorption property of the biomaterial, compatibility of the implant with medical imaging, compatibility of the process with the printing of biological parts (cells, growth factors), and shrinkage of the printed piece (Table 11).

- The time of processing takes into account the debinding and/or sintering steps, which are associated with the calcium phosphate material+photopolymerizable resin/SLA process and calcium phosphate powder/SLS processes. A thermal pretreatment of metal powder is also required for the SLS AM process.

- The complexity of the formulation development was evaluated considering the requirement of developing a noncommercial ink to make it printable with accurate rheological properties. This is especially the case for the direct ink writing process. For the FDM process, the available commercial filament PCL makes it an increasingly democratized AM process. The photopolymerizable resin/binders used in SLA and SLS, which sometimes have to be developed and require a good ratio for blending, result in the intermediate performance of this process.

- The complexity of the parameters to be set up comprises the number of parameters to adjust as well as their difficulty. This concern especially affects the SLA and SLS techniques because, in addition to the common parameters to adjust such as the speed of printing of layers, the speed of the laser path, or the z height setting, the laser performance has to be set up. Some commercial printing requires a specific optimization.

- The accuracy of the process concerns how fine the products that can be achieved using the printed filament are.

- The matching between the CAD file and the printed implant comprises the accuracy between the expected size of the final piece and the obtained printed size. All the processes are estimated to have intermediate performance because of shrinkage of the sintered piece for

SLA or SLS affects the dimensions. The printing of cement by powder bed or direct ink writing can cause a slight retraction of the printed piece. The extrusion of PCL can cause slight extension of the filament. Nevertheless, these phenomena can be considered and anticipated during the design of the piece. A summary of the assessment by classification allows for us to note that extrusion-based biomaterials ranked fourth but remained tied to the powder bed to make it possible to print biological material. In contrast, FDM/PCL got the first ranking but is not compatible for printing biological parts. The calcium phosphate+resin/SLA pair is last in the ranking although it received the top place for the efficiency of the biomaterial/process. This technique remains the most accurate (Figure 11)

According to the ranking, the metal/SLS process shows the best mechanical properties, although it is worth noting that this biomaterial/AM process is not compatible with printing of biological parts or patient follow up by medical imaging techniques such as MRI or scanners (Table 7).

Hence, it is worth noting that it is also possible to improve the biological performance of 3D-printed parts in situ with biological parts by soaking techniques or immersion in biological fluids such as total bone marrow before implantation.

To optimize the adsorption and absorption in the core of the implant, an accurate porosity design can be achieved. Designing a specific porosity makes it possible to enhance the mechanical performance. This is reviewed in the next section.

11. AM-based scaffold design to enhance bone regeneration performance

An advantage of using AM instead of a simple injectable biomaterial, for example, is that it is possible to control the design of the material, which is only limited by imagination. AM appears to be an outstanding process to create synthetic multifunctional and multistructural bone tissue. Dense cortical and interconnected porous bone can be reproduced. Nevertheless, it is not easy to mimic the structure and good functional performance of nature. The material

for printing is chosen according to a viscosity that sometimes does not match Young's modulus of bone. The accuracy of the process sometimes makes it complicated to obtain a fine layer compared to the natural bone. Once implanted, the biomaterial will be subject to various external physiological stimuli that have not necessarily been taken into account in the AM process.

For all these reasons, investigations have been carried out on the effects of different aspects of the structure of a scaffold. The volume of porosity has been considered and the size, shape and organization of pores have been studied. A decrease in the mechanical properties is related to the volume of the porosity. Some computational technology designs allow for good compliance between the biological performance obtained with the porosity and the underlying mechanical properties. Surface modification is less often considered a paramount key for the bone healing performance of implants for bone regeneration. The 4D process, which is a new concept, is also discussed below (Figure 13).

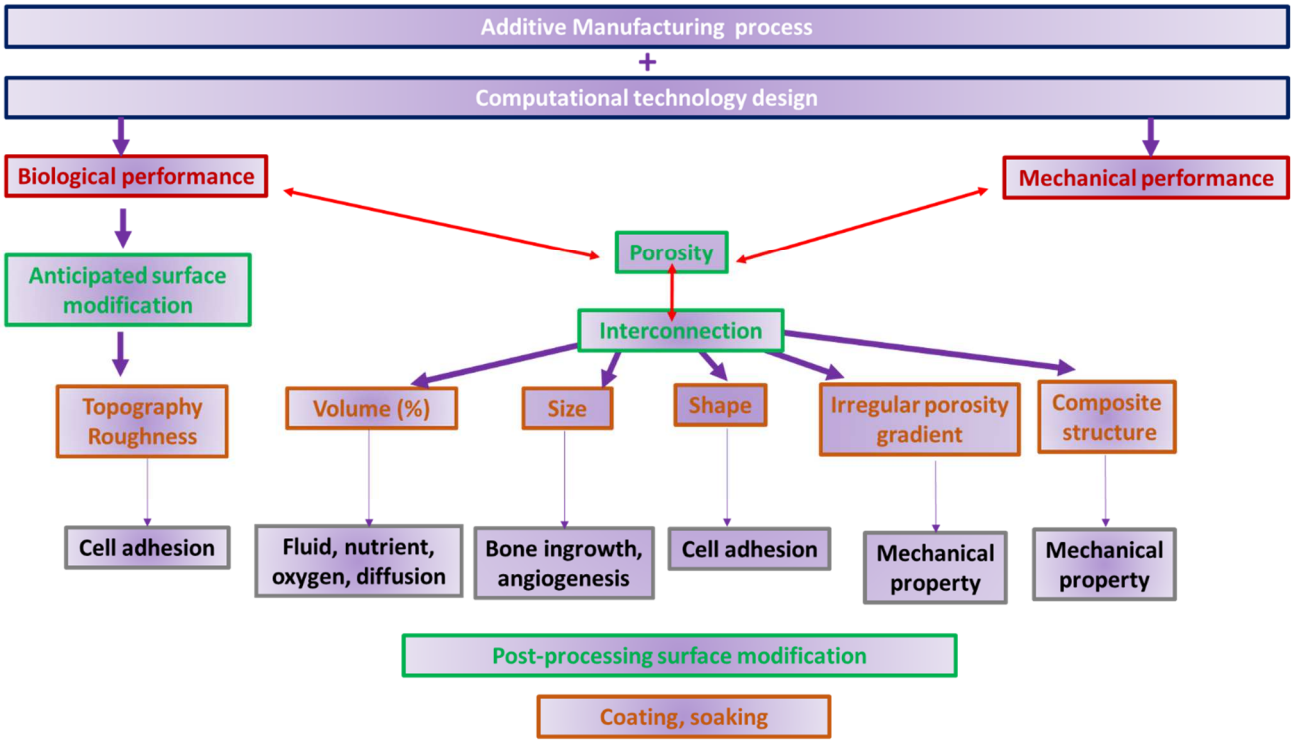

Figure 13: Summary of possible enhancements of the regenerative performance of 3D-printed implants

11.1 AM for optimized porosity structures

The AM process allows for control of the structure of the implant, namely, the pore size, shape of pores, location of pores, and percentage of interconnected porosity. The inherent advantages of using direct rapid prototyping when compared to traditional methods to obtain porosity, such as the leaching method and gas foaming, are the accurate control of the architecture of the construct and its high reproducibility. Porosity, especially if it is interconnected, was found to be more important than the composition of the scaffold as a property of growth factor carrier and the entrapment of circulating growth factors to induce bone repair [49].

Several dimensions of porosity must be considered including the volume, size, shape and organization.

Several studies have shown that concave pores stimulate bone ingrowth. This has been attributed to their ability to retain circulating biological molecules. Ripamonti demonstrated that BMPs were concentrated on the concavities of hydroxyapatite-based HA scaffolds [49], [31]. This finding has also been published by Barba et al., who noted that the spherical, concave macropores of foamed scaffolds significantly promoted both material resorption and bone regeneration compared to 3D-printed scaffolds with orthogonal-patterned struts and therefore prismatic, convex macropores [112], [169]. Chang et al. also found that porous HA with cylindrical pores could be a useful graft material due to its strength and osteoconductivity when compared to a cross shape [73]. Bidan et al. found that in cross-shaped pores (nonconvex), the initial overall tissue deposition is twice as fast as in square-shaped pores (convex) [71]. Square and star geometries are the least favored [145].

In addition to the shape, the size of pores is paramount. Cells are able to sense and react to curvature radii much larger than them [203].

The mean pore size of the scaffold is a critical determinant of blood vessel ingrowth. The scaffold design has a profound effect on the rate of vascularization after implantation. Bone

tissue engineering studies suggest that pore sizes greater than 300 µm are required for vascular ingrowth whereas 100 µm is enough to promote cell migration [72]. New bone and bone marrow formation within porous HA was found in the larger cylindrical types (300, 500 micrometers in diameter) when compared with those that were 50–100 micrometers [73]. Implants with a 565-micron pore size provided more abundant newly formed bone in both peripheral and deep pores than those with a 300-micrometer pore size. No significant differences were found between implants with 40 and 50% macroporosity, suggesting that the influence of the macropore size on bone ingrowth was greater than that of macroporosity percentage [74]. This is interesting, as there is an inverse proportion between the volume of porosity and the mechanical properties. Hollister described a new paradigm that requires the balance of temporary mechanical function of scaffolds with mass transport ensured by porosity to aid biological delivery and tissue regeneration [204]. The critical issue for design is to compute the precise value of mechanical and mass-transport properties at a given scale based on more microscopic properties and structure. One way to achieve hierarchical design is to create libraries of unit cells (a mathematical entity not to be confused with a biological cell) at different physical scales that can be assembled to form scaffold architectures. Such libraries may be created using image-based design approaches or approaches based on computer-aided design (CAD). Homogenization theory, which uses asymptotic expansion of relevant physical variables to generate multiscale equilibrium equations, can be used to compute effective properties based on these unit-cell designs. By solving unit-cell deformation under six local strain states, the effective stiffness at a macroscopic level is computed from the stiffness at a microscopic level and the 3D spatial arrangement of the microscopic level as given by the strain localization tensor and volume of the unit cell [204]. For mass transport purposes, the macroscopic permeability is computed based on the average Stokes flow velocity vectors calculated in response to three separately applied unit pressure gradients [204]. Recent research into the incorporation of physical and chemical gradients

within scaffolds indicates that integrating these features improves the mechanical and biological function of a tissue-engineered construct [205]. Native tissue often exists as a series of connected and graded transitional zones to build distinct functional regions. This is the case of the osteoarticular zone [206]. The lack of heterogeneity within previous scaffolds does not support the diverse populations of cells and surrounding environment of the native tissue. Thus, it is critical that engineers incorporate graded properties within scaffolds to properly guide the development of new tissue. Extrusion-based materials are best used for structural gradients within scaffolds. For example, the pore size, morphology, and interconnectivity can be controlled through parameters such as the raster thickness and angle, space between rasters, height of the layer, and extrusion pressure, making it possible to create multidirectional physical gradients within scaffolds. Moreover, multiple extrusion heads can be added to the system to generate compositional gradients within the scaffolds in the X, Y and/or Z directions. In SLS, powder beds and SLA, compositional gradients in the vertical direction can be easily achieved by rolling out different powders or resin between layers; however, material gradients in the horizontal direction are more difficult [152]. The powder bed technique has already been used to make chemical gradients with well-controlled spatial biological molecules [118]. To achieve spatial control of more than one bioactive molecule by SLA, multiple resins that have been loaded with different bioactive molecules must be used. Incorporating two different resins requires a sequential photopolymerization step in addition to multiple washings to remove uncrosslinked monomers [152]. The assessment of the AM processes, with their ability to perform physical and chemical gradients is summarized in Table 14.

AM process	Physical gradient	Chemical gradient	Horizontal gradient	Vertical gradient
SLA	+ +	+ +	+	+ +
SLS	+ +	+ +	- +	+ +
Material-based extrusion	+ + +	+ + +	+++	+ + +

Powder bed	+ +	+ +	- - +	+ +

Table 14: AM processes for the fabrication of gradients
+ + +: satisfactory
+ +: intermediate
+: insufficient

11.2 AM to optimize the mechanical properties of implants: stress shielding and ductility

The factors that influence the mechanical properties of porous scaffolds include the porosity, pore diameter, strut diameter, and shape of the strut section. Porosity is thought to be the most influential factor.

Multimaterial composite structures exhibit highly enhanced mechanical properties by mimicking natural hierarchical materials such as nacre, crocodiles, armadillos, and turtles [207]. The design and fabrication of 3D-printed scaffolds can make it possible to reach mechanical strength comparable to that of cortical bone [208]. Voronoi tessellation is a method of space partitioning based on the seed point. This method was successful in obtaining porous structures with specified and functionally graded porosities with enhanced mechanical performance. This method generates irregular but controllable porous scaffolds [205].

The orientation of the stacked layers has a substantial influence on the mechanical behavior of the 3D sample. Samples with layers stacked parallel to the mechanical compressive load are stronger than those with layers stacked perpendicular to the load [209]. Finite element (FE) models allow for the prediction of mechanical evolution over time and are an accurate tool to compare different parameter effects. FE was used to investigate how porous PEEK and porous Ti mechanical properties affect load sharing with bone within the porous architectures over time [48].

11.3 Surface modification

The material surface plays a crucial role in biological interactions. Modification of the surface topography, surface roughness or surface chemistry can lead to the best osseointegration, biocompatibility, and mechanical resistance performance.

Creating nanotopography at the surface of materials stimulates cell adhesion, which can influence cell differentiation [115]. AM allows for the modification of surface topography and can be implemented in the design of the implant. Nanotopography can easily be performed on metal materials. Electron beam lithography [210] and femtolaser [211], [212] have been used to pattern a well organism surface and nanogroove on metal. An indirect method consists of soft lithography, which is utilized to create micro- and nanosized features on the substrates of interest. It is a general term that encompasses a wide range of lithography techniques, including replica molding (RM), microcontact printing (μCP), micromolding in microcapillaries (MIMIC), microtransfer molding (μTM), and solvent-assisted micromolding (SAMIM). These techniques usually employ a patterned elastomer of polydimethylsiloxane (PDMS) as the mold or stamp to create a transfer pattern [213]. These techniques have an issue, which is the postprocessing step that requires extra time to finish the part.

A more deliberate approach to implement surface porosity is to create a functionally graded implant with a porous structure on the outermost layer and a partially or fully dense body (Table 13). This makes it possible to improve the efficiency of postprocessing treatments such as soaking.

Postprocessing of coatings by soaking 3D implants in a biological solution is a fast and efficient method to improve surface properties that enhance cell adhesion.

Polydopamine coatings have attracted keen interest to improve the properties of materials in various fields, including energy, environmental studies and medicine [214].

Lee et al. reported a method to form multifunctional polymer coatings through simple dip-coating of objects in an aqueous solution of dopamine. Inspired by the composition of

adhesive proteins in mussels, they used dopamine self-polymerization to form thin, surface-adherent polydopamine films on a wide range of inorganic and organic materials, including noble metals, oxides, polymers, semiconductors, and ceramics. Secondary reactions can be used to create a variety of ad-layers, including self-assembled monolayers through deposition of long-chain molecular building blocks, metal films by electroless metallization, and bioinert and bioactive surfaces by grafting of macromolecules [215]

Polycaprolactone scaffolds manufactured by selective laser sintering (SLS) were surface modified through immersion coating with gelatin or collagen. Three groups of scaffolds were created and compared to evaluate the mechanical and biological properties. Surface modification with collagen or gelatin improved the hydrophilicity, water uptake and mechanical strength of the pristine scaffold [105]. The biomimetic precipitation process is an efficient and safe process that consists of soaking material in acellular aqueous solution at various pH values and ion concentrations for alloy crystal apatite precipitation. This process can be used on calcium phosphate material and bioglass as well as metal [41], [216], [217]. Different solutions were investigated using the Kokubo simulated body fluid. When immersed in NaCl 0.9% aqueous solution, a calcium-deficient apatite crystal precipitated, close to the natural mineral part of bone [218], and formed on calcium phosphate cement. Regarding the nature of aqueous phosphate solutions, Yang et al. found that surface modification gives rise to a controllable nanotopography of nanoneedle or nanosheet apatite precipitation [116].

A fiber engraving technique was used to create a groove on the surface of a thermoplastic printed fiber containing poly(ε-caprolactone) (PCL) as the thermoplastic polymer using a commercial 3D printer. The advantage of this strategy is the possibility of creating a multimaterial scaffold. The scaffold is made with a fused deposition modeling (FDM) technique that requires a high temperature but allows for strong mechanical properties to be obtained and limits the lateral spread of the ink. Engraving created in the printed PCL yarn can be fulfilled with a cell-laden bioink through an extrusion process. The viscosity and the

gelation time point of the cell-laden bioink can be adapted to be compatible with cell viability instead of increasing the bioink viscosity to prevent lateral spreading or shear stress in the nozzle, which can damage cells during extrusion [219].

11.4 4D

Only the initial state of the printed scaffolds is considered, and AM 4DP adds a time dimension based on AM technologies similar to that found in nature in plants, leaves, organs, and tissue that respond to various external stimuli over time. 4DP technology, also referred to as 4D bioprinting, shape-morphing systems or active origami, takes this evolution into account.

Research that extends from an examination of fascinating natural phenomena can lead to the development of advanced materials. Functional materials are added to the raw materials used to build the scaffolds, which can respond to external stimuli. Functional materials, which are also known as smart materials, are used as raw materials in 4DP technology based on external stimuli. These materials have the inherent properties of reshaping themselves based on external stimuli, such as a mechanical signal, electrical stimulation, temperature or pH. Inspired by these botanical systems, Gladman et al. printed composite hydrogel architectures that are encoded with localized, anisotropic swelling behavior controlled by the alignment of cellulose fibrils along prescribed four-dimensional printing pathways. When combined with a minimal theoretical framework that allows for us to solve the inverse problem of designing the alignment patterns for prescribed target shapes, we can fabricate plant-inspired architectures that change shape upon immersion in water, yielding complex three-dimensional morphologies [220]. This application should be of great interest in musculoskeletal repair, which is subject to different morphological changes due to stimulation.

Acknowledgments

The figures were built with the help of medical image bank of servier and with the image bank of biorender.

References

[1] Bose S, ke D, Sahasrabudhe H, Bandyopadhyay A. Additive Manufacturing of Biomaterials. Prog Mater Sci 2017;93. https://doi.org/10.1016/j.pmatsci.2017.08.003.

[2] Murphy SV, Atala A. 3D bioprinting of tissues and organs. Nat Biotechnol 2014;32:773–85. https://doi.org/10.1038/nbt.2958.

[3] Chen Y, Li W, Zhang C, Wu Z, Liu J. Recent Developments of Biomaterials for Additive Manufacturing of Bone Scaffolds. Adv Healthc Mater 2020;9:2000724. https://doi.org/10.1002/adhm.202000724.

[4] Hull CW, Gabriel S. (54) APPARATUS FOR PRODUCTION OF THREE-DMENSONAL OBJECTS BY STEREO THOGRAPHY 1984:16.

[5] Fudim E. ing', Mechanical Engineering, Sep. 1985, pp. 54-59. Efrem Fudim, "Sculpting with Light', Machine Design, Mar. 6, 1986, pp. 102-106. Primary Examiner-Norman Morgenstern Assistant Examiner-Marianne L. Podgett n.d.:5.

[6] USPTO.report. Method and apparatus for production of three-dimensional objects by photosolidification. USPTOReport n.d. https://uspto.report/patent/grant/4,752,498 (accessed November 11, 2020).

[7] US4818562.pdf n.d.

[8] Office EP. European publication server n.d. https://data.epo.org/publication-server/rest/v1.0/publication-dates/20180328/patents/EP2914433NWB1/document.pdf (accessed November 11, 2020).

[9] Bagaria V, Bhansali R, Pawar P. 3D printing- creating a blueprint for the future of orthopedics: Current concept review and the road ahead! J Clin Orthop Trauma 2018;9:207–12. https://doi.org/10.1016/j.jcot.2018.07.007.

[10] Gramanzini M, Gargiulo S, Zarone F, Megna R, Apicella A, Aversa R, et al. Combined microcomputed tomography, biomechanical and histomorphometric analysis of the peri-implant bone: a pilot study in minipig model. Dent Mater Off Publ Acad Dent Mater 2016;32:794–806. https://doi.org/10.1016/j.dental.2016.03.025.

[11] Shahlaie M, Gantes B, Schulz E, Riggs M, Crigger M. Bone density assessments of dental implant sites: 1. Quantitative computed tomography. Int J Oral Maxillofac Implants 2003;18:224–31.

[12] Turkyilmaz I, Tumer C, Ozbek EN, Tözüm TF. Relations between the bone density values from computerized tomography, and implant stability parameters: a clinical study of 230 regular platform implants. J Clin Periodontol 2007;34:716–22. https://doi.org/10.1111/j.1600-051X.2007.01112.x.

[13] Reznikov N, Bilton M, Lari L, Stevens MM, Kröger R. Fractal-like hierarchical organization of bone begins at the nanoscale. Science 2018;360. https://doi.org/10.1126/science.aao2189.

[14] Wang J, Ye M, Liu Z, Wang C. Precision of cortical bone reconstruction based on 3D CT scans. Comput Med Imaging Graph Off J Comput Med Imaging Soc 2009;33:235–41. https://doi.org/10.1016/j.compmedimag.2009.01.001.

[15] Lalone EA, Willing RT, Shannon HL, King GJW, Johnson JA. Accuracy assessment of 3D bone reconstructions using CT: an intro comparison. Med Eng Phys 2015;37:729–38. https://doi.org/10.1016/j.medengphy.2015.04.010.

[16] Qu H, Fu H, Han Z, Sun Y. Biomaterials for bone tissue engineering scaffolds: a review. RSC Adv 2019;9:26252–62. https://doi.org/10.1039/C9RA05214C.

[17] Bahraminasab M. Challenges on optimization of 3D-printed bone scaffolds. Biomed Eng Online 2020;19:69. https://doi.org/10.1186/s12938-020-00810-2.
[18] Wang C, Huang W, Zhou Y, He L, He Z, Chen Z, et al. 3D printing of bone tissue engineering scaffolds. Bioact Mater 2020;5:82–91. https://doi.org/10.1016/j.bioactmat.2020.01.004.
[19] Placone JK, Mahadik B, Fisher JP. Addressing present pitfalls in 3D printing for tissue engineering to enhance future potential. APL Bioeng 2020;4:010901. https://doi.org/10.1063/1.5127860.
[20] Donate R, Monzón M, Alemán-Domínguez ME. Additive manufacturing of PLA-based scaffolds intended for bone regeneration and strategies to improve their biological properties. E-Polym 2020;20:571–99. https://doi.org/10.1515/epoly-2020-0046.
[21] Belhabib S, Guessasma S. Compression performance of hollow structures: From topology optimisation to design 3D printing. Int J Mech Sci 2017;133:728–39. https://doi.org/10.1016/j.ijmecsci.2017.09.033.
[22] Guessasma S, Belhabib S, Nouri H. Significance of pore percolation to drive anisotropic effects of 3D printed polymers revealed with X-ray μ-tomography and finite element computation. Polymer 2015;C:29–36. https://doi.org/10.1016/j.polymer.2015.10.041.
[23] Nouri H, Guessasma S, Belhabib S. Structural imperfections in additive manufacturing perceived from the X-ray micro-tomography perspective. J Mater Process Technol 2016;234:113–24. https://doi.org/10.1016/j.jmatprotec.2016.03.019.
[24] Boyle WJ, Simonet WS, Lacey DL. Osteoclast differentiation and activation. Nature 2003;423:337–42. https://doi.org/10.1038/nature01658.
[25] Matsuo K, Irie N. Osteoclast-osteoblast communication. Arch Biochem Biophys 2008;473:201–9. https://doi.org/10.1016/j.abb.2008.03.027.
[26] Manolagas SC. Birth and death of bone cells: basic regulatory mechanisms and implications for the pathogenesis and treatment of osteoporosis. Endocr Rev 2000;21:115–37. https://doi.org/10.1210/edrv.21.2.0395.
[27] Couret I. Biology of bone remodeling. Med Nucleaire 2004;28:57–65.
[28] Weiner S, Price PA. Disaggregation of bone into crystals. Calcif Tissue Int 1986;39:365–75. https://doi.org/10.1007/BF02555173.
[29] Bigi A, Cojazzi G, Panzavolta S, Ripamonti A, Roveri N, Romanello M, et al. Chemical and structural characterization of the mineral phase from cortical and trabecular bone. J Inorg Biochem 1997;68:45–51. https://doi.org/10.1016/s0162-0134(97)00007-x.
[30] Anselme K. Osteoblast adhesion on biomaterials. Biomaterials 2000;21:667–81. https://doi.org/10.1016/s0142-9612(99)00242-2.
[31] LeGeros RZ. Calcium Phosphate-Based Osteoinductive Materials. Chem Rev 2008;108:4742–53. https://doi.org/10.1021/cr800427g.
[32] Olszta MJ, Cheng X, Jee SS, Kumar R, Kim Y-Y, Kaufman MJ, et al. Bone structure and formation: A new perspective. Mater Sci Eng R Rep 2007;58:77–116. https://doi.org/10.1016/j.mser.2007.05.001.
[33] Carlisle EM. Silicon: a possible factor in bone calcification. Science 1970;167:279–80. https://doi.org/10.1126/science.167.3916.279.
[34] Olsen BR, Reginato AM, Wang W. Bone development. Annu Rev Cell Dev Biol 2000;16:191–220. https://doi.org/10.1146/annurev.cellbio.16.1.191.
[35] Raisz LG. Physiology and pathophysiology of bone remodeling. Clin Chem 1999;45:1353–8.
[36] Cappariello A, Maurizi A, Veeriah V, Teti A. The Great Beauty of the osteoclast. Arch Biochem Biophys 2014;558:70–8. https://doi.org/10.1016/j.abb.2014.06.017.

[37] Detsch R, Boccaccini AR. The role of osteoclasts in bone tissue engineering. J Tissue Eng Regen Med 2015;9:1133–49. https://doi.org/10.1002/term.1851.
[38] Kokubo T, Yamaguchi S. Simulated body fluid and the novel bioactive materials derived from it. J Biomed Mater Res A 2019;107:968–77. https://doi.org/10.1002/jbm.a.36620.
[39] Kokubo T. Bioactive glass ceramics: properties and applications. Biomaterials 1991;12:155–63. https://doi.org/10.1016/0142-9612(91)90194-f.
[40] Rousselle A-V, Heymann D. Osteoclastic acidification pathways during bone resorption. Bone 2002;30:533–40. https://doi.org/10.1016/s8756-3282(02)00672-5.
[41] Kokubo T, Kushitani H, Sakka S, Kitsugi T, Yamamuro T. Solutions able to reproduce in vivo surface-structure changes in bioactive glass-ceramic A-W. J Biomed Mater Res 1990;24:721–34. https://doi.org/10.1002/jbm.820240607.
[42] Barrère F, van Blitterswijk CA, de Groot K. Bone regeneration: molecular and cellular interactions with calcium phosphate ceramics. Int J Nanomedicine 2006;1:317–32.
[43] Hench LL, Polak JM. Third-generation biomedical materials. Science 2002;295:1014+1016-1017. https://doi.org/10.1126/science.1067404.
[44] Dorri M, Oliver R. WITHDRAWN: Resorbable versus titanium plates for facial fractures. Cochrane Database Syst Rev 2018;5:CD007158. https://doi.org/10.1002/14651858.CD007158.pub3.
[45] Bugler KE, Watson CD, Hardie AR, Appleton P, McQueen MM, Court-Brown CM, et al. The treatment of unstable fractures of the ankle using the Acumed fibular nail: development of a technique. J Bone Joint Surg Br 2012;94:1107–12. https://doi.org/10.1302/0301-620X.94B8.28620.
[46] Jastifer JR. Topical review: locking plate technology in foot and ankle surgery. Foot Ankle Int 2014;35:512–8. https://doi.org/10.1177/1071100714523274.
[47] Panchbhavi VK, Vallurupalli S, Morris R. Comparison of augmentation methods for internal fixation of osteoporotic ankle fractures. Foot Ankle Int 2009;30:696–703. https://doi.org/10.3113/FAI.2009.0696.
[48] Carpenter RD, Klosterhoff BS, Torstrick FB, Foley KT, Burkus JK, Lee CSD, et al. Effect of porous orthopaedic implant material and structure on load sharing with simulated bone ingrowth: A finite element analysis comparing titanium and PEEK. J Mech Behav Biomed Mater 2018;80:68–76. https://doi.org/10.1016/j.jmbbm.2018.01.017.
[49] Ripamonti U, Roden LC, Renton LF. Osteoinductive hydroxyapatite-coated titanium implants. Biomaterials 2012;33:3813–23. https://doi.org/10.1016/j.biomaterials.2012.01.050.
[50] Bosshardt DD, Chappuis V, Buser D. Osseointegration of titanium, titanium alloy and zirconia dental implants: current knowledge and open questions. Periodontol 2000 2017;73:22–40. https://doi.org/10.1111/prd.12179.
[51] Winder J, Cooke RS, Gray J, Fannin T, Fegan T. Medical rapid prototyping and 3D CT in the manufacture of custom made cranial titanium plates. J Med Eng Technol 1999;23:26–8. https://doi.org/10.1080/030919099294401.
[52] Scolozzi P, Martinez A, Jaques B. Complex orbito-fronto-temporal reconstruction using computer-designed PEEK implant. J Craniofac Surg 2007;18:224–8. https://doi.org/10.1097/01.scs.0000249359.56417.7e.
[53] Chen C-C, Ho C-C, David Chen C-H, Wang W-C, Ding S-J. In vitro bioactivity and biocompatibility of dicalcium silicate cements for endodontic use. J Endod 2009;35:1554–7. https://doi.org/10.1016/j.joen.2009.08.006.
[54] Prati C, Gandolfi MG. Calcium silicate bioactive cements: Biological perspectives and clinical applications. Dent Mater Off Publ Acad Dent Mater 2015;31:351–70. https://doi.org/10.1016/j.dental.2015.01.004.

[55] Sinjab YH, Sinjab KH, Navarette-Bedoya C, Gutmann JL. Calcium sulfate applications in dentistry: A literature review Sinjab YH, Sinjab KH, Navarrete-Bedoya C, Gutmann JL - Endodontology 2020. https://www.endodontologyonweb.org/article.asp?issn=0970-7212;year=2020;volume=32;issue=4;spage=167;epage=174;aulast=Sinjab (accessed January 31, 2021).
[56] Thomas MV, Puleo DA, Al-Sabbagh M. Calcium sulfate: a review. J Long Term Eff Med Implants 2005;15:599–607. https://doi.org/10.1615/jlongtermeffmedimplants.v15.i6.30.
[57] Thomas M, Puleo D. Calcium sulfate: Properties and clinical applications. J Biomed Mater Res B Appl Biomater 2009;88:597–610. https://doi.org/10.1002/jbm.b.31269.
[58] Chichiricco PM, Riva R, Thomassin J-M, Lesoeur J, Struillou X, Le Visage C, et al. In situ photochemical crosslinking of hydrogel membrane for Guided Tissue Regeneration. Dent Mater Off Publ Acad Dent Mater 2018;34:1769–82. https://doi.org/10.1016/j.dental.2018.09.017.
[59] Maini L, Mishra A, Agarwal G, Verma T, Sharma A, Tyagi A. 3D printing in designing of anatomical posterior column plate. J Clin Orthop Trauma 2018;9:236–40. https://doi.org/10.1016/j.jcot.2018.07.009.
[60] Lin H-H, Chang H-W, Lo L-J. Development of customized positioning guides using computer-aided design and manufacturing technology for orthognathic surgery. Int J Comput Assist Radiol Surg 2015;10:2021–33. https://doi.org/10.1007/s11548-015-1223-0.
[61] Deng T, Jiang M, Lei Q, Cai L, Chen L. The accuracy and the safety of individualized 3D printing screws insertion templates for cervical screw insertion. Comput Assist Surg 2016;21:143–9. https://doi.org/10.1080/24699322.2016.1236146.
[62] Anderson JM, Rodriguez A, Chang DT. Foreign body reaction to biomaterials. Semin Immunol 2008;20:86–100. https://doi.org/10.1016/j.smim.2007.11.004.
[63] Williams JM, Adewunmi A, Schek RM, Flanagan CL, Krebsbach PH, Feinberg SE, et al. Bone tissue engineering using polycaprolactone scaffolds fabricated via selective laser sintering. Biomaterials 2005;26:4817–27. https://doi.org/10.1016/j.biomaterials.2004.11.057.
[64] Brown BN, Badylak SF. Expanded applications, shifting paradigms and an improved understanding of host-biomaterial interactions. Acta Biomater 2013;9:4948–55. https://doi.org/10.1016/j.actbio.2012.10.025.
[65] Naahidi S, Jafari M, Logan M, Wang Y, Yuan Y, Bae H, et al. Biocompatibility of hydrogel-based scaffolds for tissue engineering applications. Biotechnol Adv 2017;35:530–44. https://doi.org/10.1016/j.biotechadv.2017.05.006.
[66] Blair HC, Kahn AJ, Crouch EC, Jeffrey JJ, Teitelbaum SL. Isolated osteoclasts resorb the organic and inorganic components of bone. J Cell Biol 1986;102:1164–72. https://doi.org/10.1083/jcb.102.4.1164.
[67] Barrère F, van Blitterswijk CA, de Groot K. Bone regeneration: molecular and cellular interactions with calcium phosphate ceramics. Int J Nanomedicine n.d.:16.
[68] Discher DE, Mooney DJ, Zandstra PW. Growth factors, matrices, and forces combine and control stem cells. Science 2009;324:1673–7. https://doi.org/10.1126/science.1171643.
[69] Wagoner Johnson AJ, Herschler BA. A review of the mechanical behavior of CaP and CaP/polymer composites for applications in bone replacement and repair. Acta Biomater 2011;7:16–30. https://doi.org/10.1016/j.actbio.2010.07.012.
[70] Misch CE, Qu Z, Bidez MW. Mechanical properties of trabecular bone in the human mandible: Implications for dental implant treatment planning and surgical placement. J Oral Maxillofac Surg 1999;57:700–6. https://doi.org/10.1016/S0278-2391(99)90437-8.

[71] Bidan CM, Kommareddy KP, Rumpler M, Kollmannsberger P, Fratzl P, Dunlop JWC. Geometry as a Factor for Tissue Growth: Towards Shape Optimization of Tissue Engineering Scaffolds. Adv Healthc Mater 2013;2:186–94. https://doi.org/10.1002/adhm.201200159.
[72] Karageorgiou V, Kaplan D. Porosity of 3D biomaterial scaffolds and osteogenesis. Biomaterials 2005;26:5474–91. https://doi.org/10.1016/j.biomaterials.2005.02.002.
[73] Chang B-S, Lee >>>inits>C. K. >>>fnm>Choon-Ki, Hong K-S, Youn H-J, Ryu H-S, Chung S-S, et al. Osteoconduction at porous hydroxyapatite with various pore configurations. Biomaterials 2000;21:1291–8. https://doi.org/10.1016/S0142-9612(00)00030-2.
[74] Gauthier O, Bouler JM, Aguado E, Pilet P, Daculsi G. Macroporous biphasic calcium phosphate ceramics: influence of macropore diameter and macroporosity percentage on bone ingrowth. Biomaterials 1998;19:133–9.
[75] Ghayor C, Chen T-H, Bhattacharya I, Özcan M, Weber FE. Microporosities in 3D-Printed Tricalcium-Phosphate-Based Bone Substitutes Enhance Osteoconduction and Affect Osteoclastic Resorption. Int J Mol Sci 2020;21:9270. https://doi.org/10.3390/ijms21239270.
[76] Ghayor C, Weber FE. Osteoconductive Microarchitecture of Bone Substitutes for Bone Regeneration Revisited. Front Physiol 2018;9:960. https://doi.org/10.3389/fphys.2018.00960.
[77] Hench LL. Biomaterials: a forecast for the future. Biomaterials 1998;19:1419–23. https://doi.org/10.1016/S0142-9612(98)00133-1.
[78] Hench LL, Splinter RJ, Allen WC, Greenlee TK. Bonding mechanisms at the interface of ceramic prosthetic materials. J Biomed Mater Res 1971;5:117–41. https://doi.org/10.1002/jbm.820050611.
[79] Dorozhkin SV. Calcium orthophosphates as bioceramics: state of the art. J Funct Biomater 2010;1:22–107. https://doi.org/10.3390/jfb1010022.
[80] 14:00-17:00. ISO 23317:2014. ISO n.d. https://www.iso.org/cms/render/live/fr/sites/isoorg/contents/data/standard/06/50/65054.html (accessed December 5, 2021).
[81] Ducheyne P, Qiu Q. Bioactive ceramics: the effect of surface reactivity on bone formation and bone cell function. Biomaterials 1999;20:2287–303. https://doi.org/10.1016/s0142-9612(99)00181-7.
[82] Redey SA, Razzouk S, Rey C, Bernache-Assollant D, Leroy G, Nardin M, et al. Osteoclast adhesion and activity on synthetic hydroxyapatite, carbonated hydroxyapatite, and natural calcium carbonate: relationship to surface energies. J Biomed Mater Res 1999;45:140–7. https://doi.org/10.1002/(sici)1097-4636(199905)45:2<140::aid-jbm9>3.0.co;2-i.
[83] Detsch R, Mayr H, Ziegler G. Formation of osteoclast-like cells on HA and TCP ceramics. Acta Biomater 2008;4:139–48. https://doi.org/10.1016/j.actbio.2007.03.014.
[84] Detsch R, Hagmeyer D, Neumann M, Schaefer S, Vortkamp A, Wuelling M, et al. The resorption of nanocrystalline calcium phosphates by osteoclast-like cells. Acta Biomater 2010;6:3223–33. https://doi.org/10.1016/j.actbio.2010.03.003.
[85] Giannoudis PV, Einhorn TA, Marsh D. Fracture healing: the diamond concept. Injury 2007;38 Suppl 4:S3-6. https://doi.org/10.1016/s0020-1383(08)70003-2.
[86] Giannoudis PV, Einhorn TA, Schmidmaier G, Marsh D. The diamond concept – open questions. Injury 2008;39:S5–8. https://doi.org/10.1016/S0020-1383(08)70010-X.
[87] Janicki P, Schmidmaier G. What should be the characteristics of the ideal bone graft substitute? Combining scaffolds with growth factors and/or stem cells. Injury 2011;42 Suppl 2:S77-81. https://doi.org/10.1016/j.injury.2011.06.014.

[88] Giannoudis PV, Chris Arts JJ, Schmidmaier G, Larsson S. What should be the characteristics of the ideal bone graft substitute? Injury 2011;42:S1–2. https://doi.org/10.1016/j.injury.2011.06.001.
[89] Corre P, Merceron C, Longis J, Khonsari RH, Pilet P, Thi TN, et al. Direct comparison of current cell-based and cell-free approaches towards the repair of craniofacial bone defects - A preclinical study. Acta Biomater 2015;26:306–17. https://doi.org/10.1016/j.actbio.2015.08.013.
[90] Corre P, Merceron C, Vignes C, Sourice S, Masson M, Durand N, et al. Determining a Clinically Relevant Strategy for Bone Tissue Engineering: An "All-in-One" Study in Nude Mice. PLoS ONE 2013;8. https://doi.org/10.1371/journal.pone.0081599.
[91] Niel G van, D'Angelo G, Raposo G. Shedding light on the cell biology of extracellular vesicles. Nat Rev Mol Cell Biol 2018;19:213–28. https://doi.org/10.1038/nrm.2017.125.
[92] Brennan MÁ, Layrolle P, Mooney DJ. Biomaterials Functionalized with MSC Secreted Extracellular Vesicles and Soluble Factors for Tissue Regeneration. Adv Funct Mater 2020;30:1909125. https://doi.org/10.1002/adfm.201909125.
[93] Wiklander OPB, Brennan MÁ, Lötvall J, Breakefield XO, EL Andaloussi S. Advances in therapeutic applications of extracellular vesicles. Sci Transl Med 2019;11:N.PAG.
[94] Sanz M, Dahlin C, Apatzidou D, Artzi Z, Bozic D, Calciolari E, et al. Biomaterials and regenerative technologies used in bone regeneration in the craniomaxillofacial region: Consensus report of group 2 of the 15th European Workshop on Periodontology on Bone Regeneration. J Clin Periodontol 2019;46:82–91. https://doi.org/10.1111/jcpe.13123.
[95] Parent M, Baradari H, Champion E, Damia C, Viana-Trecant M. Design of calcium phosphate ceramics for drug delivery applications in bone diseases: A review of the parameters affecting the loading and release of the therapeutic substance. J Controlled Release 2017;252:1–17. https://doi.org/10.1016/j.jconrel.2017.02.012.
[96] ISO / ASTM52900 - 15 Standard Terminology for Additive Manufacturing – General Principles – Terminology n.d. https://www.astm.org/Standards/ISOASTM52900.htm (accessed December 5, 2020).
[97] Melchels FPW, Feijen J, Grijpma DW. A review on stereolithography and its applications in biomedical engineering. Biomaterials 2010;31:6121–30. https://doi.org/10.1016/j.biomaterials.2010.04.050.
[98] Crump SS. Apparatus and method for creating three-dimensional objects. US5121329A, 1992.
[99] Sheinman Y. System and Method for Direct Inkjet Printing of 3d Objects, 2014.
[100] Levy RA, Chu TM, Halloran JW, Feinberg SE, Hollister S. CT-generated porous hydroxyapatite orbital floor prosthesis as a prototype bioimplant. Am J Neuroradiol 1997;18:1522–5.
[101] Lee K-W, Wang S, Fox BC, Ritman EL, Yaszemski MJ, Lu L. Poly(propylene fumarate) Bone Tissue Engineering Scaffold Fabrication Using Stereolithography: Effects of Resin Formulations and Laser Parameters. Biomacromolecules 2007;8:1077–84. https://doi.org/10.1021/bm060834v.
[102] Melchels FPW, Feijen J, Grijpma DW. A poly(d,l-lactide) resin for the preparation of tissue engineering scaffolds by stereolithography. Biomaterials 2009;30:3801–9. https://doi.org/10.1016/j.biomaterials.2009.03.055.
[103] Elomaa L, Teixeira S, Hakala R, Korhonen H, Grijpma DW, Seppälä JV. Preparation of poly(ε-caprolactone)-based tissue engineering scaffolds by stereolithography. Acta Biomater 2011;7:3850–6. https://doi.org/10.1016/j.actbio.2011.06.039.

[104] Arcaute K, Mann BK, Wicker RB. Stereolithography of Three-Dimensional Bioactive Poly(Ethylene Glycol) Constructs with Encapsulated Cells. Ann Biomed Eng 2006;34:1429–41. https://doi.org/10.1007/s10439-006-9156-y.
[105] Chen C-H, Lee M-Y, Shyu VB-H, Chen Y-C, Chen C-T, Chen J-P. Surface modification of polycaprolactone scaffolds fabricated via selective laser sintering for cartilage tissue engineering. Mater Sci Eng C Mater Biol Appl 2014;40:389–97. https://doi.org/10.1016/j.msec.2014.04.029.
[106] Xia Y, Zhou P, Cheng X, Xie Y, Liang C, Li C, et al. Selective laser sintering fabrication of nano-hydroxyapatite/poly-ε-caprolactone scaffolds for bone tissue engineering applications. Int J Nanomedicine 2013;8:4197–213. https://doi.org/10.2147/IJN.S50685.
[107] Wiria FE, Leong KF, Chua CK, Liu Y. Poly-epsilon-caprolactone/hydroxyapatite for tissue engineering scaffold fabrication via selective laser sintering. Acta Biomater 2007;3:1–12. https://doi.org/10.1016/j.actbio.2006.07.008.
[108] Tsai K-Y, Lin H-Y, Chen Y-W, Lin C-Y, Hsu T-T, Kao C-T. Laser Sintered Magnesium-Calcium Silicate/Poly-ε-Caprolactone Scaffold for Bone Tissue Engineering. Materials 2017;10:65. https://doi.org/10.3390/ma10010065.
[109] Das S, Wohlert M, Beaman JJ, Bourell DL. Direct Selective Laser Sintering and Containerless Hot Isostatic Pressing for High Performance Metal Components, 1997. https://doi.org/10.15781/T2PZ52629.
[110] Zein I, Hutmacher DW, Tan KC, Teoh SH. Fused deposition modeling of novel scaffold architectures for tissue engineering applications. Biomaterials 2002;23:1169–85. https://doi.org/10.1016/s0142-9612(01)00232-0.
[111] Ramirez Caballero SS, Saiz E, Montembault A, Tadier S, Maire E, David L, et al. 3-D printing of chitosan-calcium phosphate inks: rheology, interactions and characterization. J Mater Sci Mater Med 2018;30:6. https://doi.org/10.1007/s10856-018-6201-y.
[112] Barba A, Maazouz Y, Diez-Escudero A, Rappe K, Espanol M, Montufar EB, et al. Osteogenesis by foamed and 3D-printed nanostructured calcium phosphate scaffolds: Effect of pore architecture. Acta Biomater 2018;79:135–47. https://doi.org/10.1016/j.actbio.2018.09.003.
[113] Chen M, Guo X, Zheng Y, Li L, Yan Z, Zhao P, et al. Effect of Tartaric Acid on the Printable, Rheological and Mechanical Properties of 3D Printing Sulphoaluminate Cement Paste. Materials 2018;11:2417. https://doi.org/10.3390/ma11122417.
[114] al AL et. Fabrication of porous scaffolds by three-dimensional plotting of a pasty calcium phosphate bone cement under mild conditions | EndNote Click n.d. https://kopernio.com/viewer?doi=10.1002%2Fterm.1563&token=WzI5MDY5MjgsIjEwLjEwMDIvdGVybS4xNTYzIl0.iSDbaCFybDmcMbl_4cLVupdLuGk (accessed December 2, 2020).
[115] Korn P, Ahlfeld T, Lahmeyer F, Kilian D, Sembdner P, Stelzer R, et al. 3D Printing of Bone Grafts for Cleft Alveolar Osteoplasty – In vivo Evaluation in a Preclinical Model. Front Bioeng Biotechnol 2020;8. https://doi.org/10.3389/fbioe.2020.00217.
[116] Yang C, Wang X, Ma B, Zhu H, Huan Z, Ma N, et al. 3D-Printed Bioactive Ca3SiO5 Bone Cement Scaffolds with Nano Surface Structure for Bone Regeneration. ACS Appl Mater Interfaces 2017;9:5757–67. https://doi.org/10.1021/acsami.6b14297.
[117] Zhang Y, Yu W, Ba Z, Cui S, Wei J, Li H. 3D-printed scaffolds of mesoporous bioglass/gliadin/polycaprolactone ternary composite for enhancement of compressive strength, degradability, cell responses and new bone tissue ingrowth. Int J Nanomedicine 2018;13:5433–47. https://doi.org/10.2147/IJN.S164869.

[118] Gbureck U, Hoelzel T, Doillon C, Müller F, Barralet J. Direct Printing of Bioceramic Implants with Spatially Localized Angiogenic Factors. Adv Mater 2007;19:795–800. https://doi.org/10.1002/adma.200601370.
[119] Gbureck U, Vorndran E, Müller FA, Barralet JE. Low temperature direct 3D printed bioceramics and biocomposites as drug release matrices. J Control Release Off J Control Release Soc 2007;122:173–80. https://doi.org/10.1016/j.jconrel.2007.06.022.
[120] Bertol LS, Schabbach R, Dos Santos LAL. Dimensional evaluation of patient-specific 3D printing using calcium phosphate cement for craniofacial bone reconstruction. J Biomater Appl 2017;31:799–806. https://doi.org/10.1177/0885328216682672.
[121] Seidenstuecker M, Kerr L, Bernstein A, Mayr HO, Suedkamp NP, Gadow R, et al. 3D Powder Printed Bioglass and β-Tricalcium Phosphate Bone Scaffolds. Materials 2018;11. https://doi.org/10.3390/ma11010013.
[122] Williams DF. On the mechanisms of biocompatibility. Biomaterials 2008;29:2941–53. https://doi.org/10.1016/j.biomaterials.2008.04.023.
[123] Liu C, Gai W, Pan S, Liu Z. The exothermal behavior in the hydration process of calcium phosphate cement. Biomaterials 2003;24:2995–3003. https://doi.org/10.1016/S0142-9612(03)00125-X.
[124] Ostrowski N, Roy A, Kumta P. Magnesium Phosphate Cement Systems for Hard Tissue Applications – A Review. ACS Biomater Sci Eng 2016;2. https://doi.org/10.1021/acsbiomaterials.6b00056.
[125] 14:00-17:00. ISO 11737-1:2018/Amd 1:2021. ISO n.d. https://www.iso.org/cms/render/live/fr/sites/isoorg/contents/data/standard/07/67/76751.html (accessed December 5, 2021).
[126] NF EN 556-1. Afnor Ed n.d. https://www.boutique.afnor.org/fr-fr/norme/nf-en-5561/sterilisation-des-dispositifs-medicaux-exigences-relatives-aux-dispositifs-/fa104541/19498 (accessed December 5, 2021).
[127] NF EN 556-2. Afnor Ed n.d. https://www.boutique.afnor.org/fr-fr/norme/nf-en-5562/sterilisation-des-dispositifs-medicaux-exigences-relatives-aux-dispositifs-/fa180533/46067 (accessed December 5, 2021).
[128] Guessasma S, Belhabib S, Altin A. On the Tensile Behaviour of Bio-Sourced 3D-Printed Structures from a Microstructural Perspective. Polymers 2020;12:1060. https://doi.org/10.3390/polym12051060.
[129] Vedadghavami A, Minooei F, Mohammadi MH, Khetani S, Rezaei Kolahchi A, Mashayekhan S, et al. Manufacturing of hydrogel biomaterials with controlled mechanical properties for tissue engineering applications. Acta Biomater 2017;62:42–63. https://doi.org/10.1016/j.actbio.2017.07.028.
[130] Davison NL, Barrère-de Groot F, Grijpma DW. Chapter 6 - Degradation of Biomaterials. In: Blitterswijk CAV, De Boer J, editors. Tissue Eng. Second Ed., Oxford: Academic Press; 2014, p. 177–215. https://doi.org/10.1016/B978-0-12-420145-3.00006-7.
[131] Lu J, Descamps M, Dejou J, Koubi G, Hardouin P, Lemaitre J, et al. The biodegradation mechanism of calcium phosphate biomaterials in bone. J Biomed Mater Res 2002;63:408–12. https://doi.org/10.1002/jbm.10259.
[132] Dorozhkin SV. Dissolution mechanism of calcium apatites in acids: A review of literature. World J Methodol 2012;2:1–17. https://doi.org/10.5662/wjm.v2.i1.1.
[133] Ludwig A, Dave SC, Higuchi WI, Fox JL, Katdare A. Dissolution rate of apatite powders in acidic fluoride solutions and the relationship to hydroxyapatite disk and bovine enamel behavior. Int J Pharm 1983;16:1–10. https://doi.org/10.1016/0378-5173(83)90122-9.

[134] Valdré G, Gandolfi M, Mongiorgi R, Monti S, Prati C. Dissolution behaviour of characterized hydroxyapatites in biological simulating solutions. GeoActa 2001;1:183–96.
[135] Doi Y, Iwanaga H, Shibutani T, Moriwaki Y, Iwayama Y. Osteoclastic responses to various calcium phosphates in cell cultures. J Biomed Mater Res 1999;47:424–33. https://doi.org/10.1002/(sici)1097-4636(19991205)47:3<424::aid-jbm19>3.0.co;2-0.
[136] Guillemin G, Hunter S, Gay C. Resorption of Natural Calcium Carbonate by Avian Osteoclasts In Vitro. Cells Mater 1995;5.
[137] Lai W, Garino J, Flaitz C, Ducheyne P. Excretion of resorption products from bioactive glass implanted in rabbit muscle. J Biomed Mater Res A 2005;75:398–407. https://doi.org/10.1002/jbm.a.30425.
[138] Ashby MF, Cebon D. Materials selection in mechanical design. J Phys IV 1993;03:C7-1-C7-9. https://doi.org/10.1051/jp4:1993701.
[139] Ngo TD, Kashani A, Imbalzano G, Nguyen KTQ, Hui D. Additive manufacturing (3D printing): A review of materials, methods, applications and challenges. Compos Part B Eng 2018;143:172–96. https://doi.org/10.1016/j.compositesb.2018.02.012.
[140] Wang X, Jiang M, Zhou Z, Gou J, Hui D. 3D printing of polymer matrix composites: A review and prospective. Compos Part B Eng 2017;110:442–58. https://doi.org/10.1016/j.compositesb.2016.11.034.
[141] Brie J, Chartier T, Chaput C, Delage C, Pradeau B, Caire F, et al. A new custom made bioceramic implant for the repair of large and complex craniofacial bone defects. J Cranio-Maxillo-Fac Surg Off Publ Eur Assoc Cranio-Maxillo-Fac Surg 2013;41:403–7. https://doi.org/10.1016/j.jcms.2012.11.005.
[142] Dhariwala B, Hunt E, Boland T. Rapid Prototyping of Tissue-Engineering Constructs, Using Photopolymerizable Hydrogels and Stereolithography. Tissue Eng 2004;10:1316–22. https://doi.org/10.1089/ten.2004.10.1316.
[143] Mapili G, Lu Y, Chen S, Roy K. Laser-layered microfabrication of spatially patterned functionalized tissue-engineering scaffolds. J Biomed Mater Res B Appl Biomater 2005;75B:414–24. https://doi.org/10.1002/jbm.b.30325.
[144] Pham DT, Gault RS. A comparison of rapid prototyping technologies. Int J Mach Tools Manuf 1998;38:1257–87. https://doi.org/10.1016/S0890-6955(97)00137-5.
[145] Bian W, Li D, Lian Q, Zhang W, Zhu L, Li X, et al. Design and fabrication of a novel porous implant with pre-set channels based on ceramic stereolithography for vascular implantation. Biofabrication 2011;3:034103. https://doi.org/10.1088/1758-5082/3/3/034103.
[146] Lasgorceix M, Champion E, Chartier T. Shaping by microstereolithography and sintering of macro–micro-porous silicon substituted hydroxyapatite. J Eur Ceram Soc 2016;36:1091–101. https://doi.org/10.1016/j.jeurceramsoc.2015.11.020.
[147] Porter AE, Patel N, Skepper JN, Best SM, Bonfield W. Comparison of in vivo dissolution processes in hydroxyapatite and silicon-substituted hydroxyapatite bioceramics. Biomaterials 2003;24:4609–20. https://doi.org/10.1016/S0142-9612(03)00355-7.
[148] Champion E. Sintering of calcium phosphate bioceramics. Acta Biomater 2013;9:5855–75. https://doi.org/10.1016/j.actbio.2012.11.029.
[149] Porter NL, Pilliar RM, Grynpas MD. Fabrication of porous calcium polyphosphate implants by solid freeform fabrication: a study of processing parameters and in vitro degradation characteristics. J Biomed Mater Res 2001;56:504–15. https://doi.org/10.1002/1097-4636(20010915)56:4<504::aid-jbm1122>3.0.co;2-j.
[150] Gunatillake PA, Adhikari R. Biodegradable synthetic polymers for tissue engineering. Eur Cell Mater 2003;5:1–16; discussion 16. https://doi.org/10.22203/ecm.v005a01.

[151] Hutmacher DW, Schantz T, Zein I, Ng KW, Teoh SH, Tan KC. Mechanical properties and cell cultural response of polycaprolactone scaffolds designed and fabricated via fused deposition modeling. J Biomed Mater Res 2001;55:203–16. https://doi.org/10.1002/1097-4636(200105)55:2<203::aid-jbm1007>3.0.co;2-7.
[152] Bracaglia LG, Smith BT, Watson E, Arumugasaamy N, Mikos AG, Fisher JP. 3D printing for the design and fabrication of polymer-based gradient scaffolds. Acta Biomater 2017;56:3–13. https://doi.org/10.1016/j.actbio.2017.03.030.
[153] Jahani Babak, Wang Xinnan, Brooks Amanda. Additive Manufacturing Techniques for Fabrication of Bone Scaffolds for Tissue Engineering Applications. Recent Prog Mater Addit Manuf Tech Fabr Bone Scaffolds Tissue Eng Appl n.d.
[154] Hutmacher DW, Schantz T, Zein I, Ng KW, Teoh SH, Tan KC. Mechanical properties and cell cultural response of polycaprolactone scaffolds designed and fabricated via fused deposition modeling. J Biomed Mater Res 2001;55:203–16. https://doi.org/10.1002/1097-4636(200105)55:2<203::aid-jbm1007>3.0.co;2-7.
[155] Rohner D, Hutmacher DW, Cheng TK, Oberholzer M, Hammer B. In vivo efficacy of bone-marrow-coated polycaprolactone scaffolds for the reconstruction of orbital defects in the pig. J Biomed Mater Res B Appl Biomater 2003;66:574–80. https://doi.org/10.1002/jbm.b.10037.
[156] Probst FA, Hutmacher DW, Müller DF, Machens H-G, Schantz J-T. [Calvarial reconstruction by customized bioactive implant]. Handchir Mikrochir Plast Chir Organ Deutschsprachigen Arbeitsgemeinschaft Handchir Organ Deutschsprachigen Arbeitsgemeinschaft Mikrochir Peripher Nerven Gefasse Organ V 2010;42:369–73. https://doi.org/10.1055/s-0030-1248310.
[157] Chen MH, Wang LL, Chung JJ, Kim Y-H, Atluri P, Burdick JA. Methods To Assess Shear-Thinning Hydrogels for Application As Injectable Biomaterials. ACS Biomater Sci Eng 2017;3:3146–60. https://doi.org/10.1021/acsbiomaterials.7b00734.
[158] Ketel S, Falzone G, Wang B, Washburn N, Sant G. A printability index for linking slurry rheology to the geometrical attributes of 3D-printed components. Cem Concr Compos 2019;101:32–43. https://doi.org/10.1016/j.cemconcomp.2018.03.022.
[159] Townsend JM, Beck EC, Gehrke SH, Berkland CJ, Detamore MS. Flow Behavior Prior to Crosslinking: The Need for Precursor Rheology for Placement of Hydrogels in Medical Applications and for 3D Bioprinting. Prog Polym Sci 2019;91:126–40. https://doi.org/10.1016/j.progpolymsci.2019.01.003.
[160] Chimene D, Kaunas R, Gaharwar AK. Hydrogel Bioink Reinforcement for Additive Manufacturing: A Focused Review of Emerging Strategies. Adv Mater 2020;32:1902026. https://doi.org/10.1002/adma.201902026.
[161] Chimene D, Miller L, Cross LM, Jaiswal MK, Singh I, Gaharwar AK. Nanoengineered Osteoinductive Bioink for 3D Bioprinting Bone Tissue. ACS Appl Mater Interfaces 2020. https://doi.org/10.1021/acsami.9b19037.
[162] De Godoy RF, Hutchens S, Campion C, Blunn G. Silicate-substituted calcium phosphate with enhanced strut porosity stimulates osteogenic differentiation of human mesenchymal stem cells. J Mater Sci Mater Med 2015;26:54. https://doi.org/10.1007/s10856-015-5387-5.
[163] Fatimi A, Tassin JF, Quillard S, Axelos MAV, Weiss P. The rheological properties of silated hydroxypropylmethylcellulose tissue engineering matrices. Biomaterials 2008;29:533–43. https://doi.org/10.1016/j.biomaterials.2007.10.032.
[164] Fatimi A, Axelos MAV, Tassin JF, Weiss P. Rheological Characterization of Self-Hardening Hydrogel for Tissue Engineering Applications: Gel Point Determination and Viscoelastic Properties. Macromol Symp 2008;266:12–6. https://doi.org/10.1002/masy.200850603.

[165] Fatimi A, Tassin J-F, Axelos MAV, Weiss P. The stability mechanisms of an injectable calcium phosphate ceramic suspension. J Mater Sci Mater Med 2010;21:1799–809. https://doi.org/10.1007/s10856-010-4047-z.
[166] Fatimi A, Tassin J-F, Turczyn R, Axelos MAV, Weiss P. Gelation studies of a cellulose-based biohydrogel: the influence of pH, temperature and sterilization. Acta Biomater 2009;5:3423–32. https://doi.org/10.1016/j.actbio.2009.05.030.
[167] Ginebra MP, Espanol M, Montufar EB, Perez RA, Mestres G. New processing approaches in calcium phosphate cements and their applications in regenerative medicine. Acta Biomater 2010;6:2863–73. https://doi.org/10.1016/j.actbio.2010.01.036.
[168] Zhang J, Zhao S, Zhu Y, Huang Y, Zhu M, Tao C, et al. Three-dimensional printing of strontium-containing mesoporous bioactive glass scaffolds for bone regeneration. Acta Biomater 2014;10:2269–81. https://doi.org/10.1016/j.actbio.2014.01.001.
[169] Barba A, Diez-Escudero A, Maazouz Y, Rappe K, Espanol M, Montufar EB, et al. Osteoinduction by Foamed and 3D-Printed Calcium Phosphate Scaffolds: Effect of Nanostructure and Pore Architecture. ACS Appl Mater Interfaces 2017;9:41722–36. https://doi.org/10.1021/acsami.7b14175.
[170] Lode A, Meissner K, Luo Y, Sonntag F, Glorius S, Nies B, et al. Fabrication of porous scaffolds by three-dimensional plotting of a pasty calcium phosphate bone cement under mild conditions. J Tissue Eng Regen Med 2014;8:682–93. https://doi.org/10.1002/term.1563.
[171] Zein I, Hutmacher DW, Tan KC, Teoh SH. Fused deposition modeling of novel scaffold architectures for tissue engineering applications. Biomaterials 2002;23:1169–85. https://doi.org/10.1016/s0142-9612(01)00232-0.
[172] Engel B, Bourell DL. Titanium alloy powder preparation for selective laser sintering. Rapid Prototyp J 2000;6:97–106. https://doi.org/10.1108/13552540010323574.
[173] Goodridge RD, Dalgarno KW, Wood DJ. Indirect selective laser sintering of an apatite-mullite glass-ceramic for potential use in bone replacement applications. Proc Inst Mech Eng [H] 2006;220:57–68. https://doi.org/10.1243/095441105X69051.
[174] Rimell JT, Marquis PM. Selective laser sintering of ultra high molecular weight polyethylene for clinical applications. J Biomed Mater Res 2000;53:414–20. https://doi.org/10.1002/1097-4636(2000)53:4<414::aid-jbm16>3.0.co;2-m.
[175] Williams JM, Adewunmi A, Schek RM, Flanagan CL, Krebsbach PH, Feinberg SE, et al. Bone tissue engineering using polycaprolactone scaffolds fabricated via selective laser sintering. Biomaterials 2005;26:4817–27. https://doi.org/10.1016/j.biomaterials.2004.11.057.
[176] Stoodley MA, Abbott JR, Simpson DA. Titanium cranioplasty using 3-D computer modelling of skull defects. J Clin Neurosci 1996;3:149–55. https://doi.org/10.1016/S0967-5868(96)90009-0.
[177] Sun S, Takeo K, Nakano T. Direct selective laser melting of Hydroxyapatite without using binder. Front Bioeng Biotechnol 2016;4. https://doi.org/10.3389/conf.FBIOE.2016.01.02366.
[178] Tan KH, Chua CK, Leong KF, Cheah CM, Cheang P, Abu Bakar MS, et al. Scaffold development using selective laser sintering of polyetheretherketone–hydroxyapatite biocomposite blends. Biomaterials 2003;24:3115–23. https://doi.org/10.1016/S0142-9612(03)00131-5.
[179] Sachs E, Cima M, Williams P, Brancazio D, Cornie J. Three Dimensional Printing: Rapid Tooling and Prototypes Directly from a CAD Model. J Eng Ind 1992;114:481–8. https://doi.org/10.1115/1.2900701.
[180] Habibovic P, Gbureck U, Doillon CJ, Bassett DC, van Blitterswijk CA, Barralet JE. Osteoconduction and osteoinduction of low-temperature 3D printed bioceramic

implants. Biomaterials 2008;29:944–53. https://doi.org/10.1016/j.biomaterials.2007.10.023.
[181] Gbureck U, Hölzel T, Klammert U, Würzler K, Müller FA, Barralet JE. Resorbable Dicalcium Phosphate Bone Substitutes Prepared by 3D Powder Printing. Adv Funct Mater 2007;17:3940–5. https://doi.org/10.1002/adfm.200700019.
[182] Klammert U, Gbureck U, Vorndran E, Rödiger J, Meyer-Marcotty P, Kübler AC. 3D powder printed calcium phosphate implants for reconstruction of cranial and maxillofacial defects. J Cranio-Maxillofac Surg 2010;38:565–70. https://doi.org/10.1016/j.jcms.2010.01.009.
[183] Fukase Y, Eanes ED, Takagp S, Chow LC, Brown WE. Setting Reactions and Compressive Strengths of Calcium Phosphate Cements. J Dent Res 1990;69:1852–6. https://doi.org/10.1177/00220345900690121201.
[184] Gbureck U, Barralet JE, Spatz K, Grover LM, Thull R. Ionic modification of calcium phosphate cement viscosity. Part I: hypodermic injection and strength improvement of apatite cement. Biomaterials 2004;25:2187–95. https://doi.org/10.1016/j.biomaterials.2003.08.066.
[185] Liu W, Zhang J, Rethore G, Khairoun K, Pilet P, Tancret F, et al. A novel injectable, cohesive and toughened Si-HPMC (silanized-hydroxypropyl methylcellulose) composite calcium phosphate cement for bone substitution. Acta Biomater 2014;10:3335–45. https://doi.org/10.1016/j.actbio.2014.03.009.
[186] Liu W, Zhang J, Weiss P, Tancret F, Bouler J-M. The influence of different cellulose ethers on both the handling and mechanical properties of calcium phosphate cements for bone substitution. Acta Biomater 2013;9:5740–50. https://doi.org/10.1016/j.actbio.2012.11.020.
[187] Bohner M, Galea L, Doebelin N. Calcium phosphate bone graft substitutes: Failures and hopes. J Eur Ceram Soc 2012;32:2663–71. https://doi.org/10.1016/j.jeurceramsoc.2012.02.028.
[188] Prati C, Gandolfi MG. Calcium silicate bioactive cements: Biological perspectives and clinical applications. Dent Mater Off Publ Acad Dent Mater 2015;31:351–70. https://doi.org/10.1016/j.dental.2015.01.004.
[189] Chow LC, Takagi S. A Natural Bone Cement-A Laboratory Novelty Led to the Development of Revolutionary New Biomaterials. J Res Natl Inst Stand Technol 2001;106:1029–33. https://doi.org/10.6028/jres.106.053.
[190] Ginebra MP, Driessens FCM, Planell JA. Effect of the particle size on the micro and nanostructural features of a calcium phosphate cement: a kinetic analysis. Biomaterials 2004;25:3453–62. https://doi.org/10.1016/j.biomaterials.2003.10.049.
[191] Taddei P, Di Foggia M, Causa F, Ambrosio L, Fagnano C. In vitro bioactivity of poly(epsilon-caprolactone)-apatite (PCL-AP) scaffolds for bone tissue engineering: the influence of the PCL/AP ratio. Int J Artif Organs 2006;29:719–25. https://doi.org/10.1177/039139880602900712.
[192] Paxton NC, Ren J, Ainsworth MJ, Solanki AK, Jones JR, Allenby MC, et al. Rheological Characterization of Biomaterials Directs Additive Manufacturing of Strontium-Substituted Bioactive Glass/Polycaprolactone Microfibers. Macromol Rapid Commun 2019;40:1900019. https://doi.org/10.1002/marc.201900019.
[193] Chaunier L, Guessasma S, Belhabib S, Della Valle G, Lourdin D, Leroy E. Material extrusion of plant biopolymers: Opportunities & challenges for 3D printing. Addit Manuf 2018;21:220–33. https://doi.org/10.1016/j.addma.2018.03.016.
[194] Maazouz Y, Montufar EB, Guillem-Marti J, Fleps I, Öhman C, Persson C, et al. Robocasting of biomimetic hydroxyapatite scaffolds using self-setting inks. J Mater Chem B 2014;2:5378–86. https://doi.org/10.1039/C4TB00438H.

[195] Buck ME, Lynn DM. Layer-by-Layer Fabrication of Covalently Crosslinked and Reactive Polymer Multilayers Using Azlactone-Functionalized Copolymers: A Platform for the Design of Functional Biointerfaces. Adv Eng Mater 2011;13:B343–52. https://doi.org/10.1002/adem.201080085.
[196] Ebrahimi M, Botelho MG, Dorozhkin SV. Biphasic calcium phosphates bioceramics (HA/TCP): Concept, physicochemical properties and the impact of standardization of study protocols in biomaterials research. Mater Sci Eng C Mater Biol Appl 2017;71:1293–312. https://doi.org/10.1016/j.msec.2016.11.039.
[197] Dorozhkin SV. Medical Application of Calcium Orthophosphate Bioceramics 2011:51.
[198] de Andrade LM, Paternoster C, Chevallier P, Gambaro S, Mengucci P, Mantovani D. Surface processing for iron-based degradable alloys: A preliminary study on the importance of acid pickling. Bioact Mater 2022;11:166–80. https://doi.org/10.1016/j.bioactmat.2021.09.026.
[199] Mantovani MM and D. Biodegradable Metals for Cardiovascular Stent Application: Interests and New Opportunities | EndNote Click n.d. https://click.endnote.com/viewer?doi=10.3390%2Fijms12074250&token=WzI5MDY5MjgsIjEwLjMzOTAvaWptczEyMDc0MjUwIl0.YLOQRpl8XaThL0T_lchNNiP_f8I (accessed February 8, 2022).
[200] Purnama A, Hermawan H, Couet J, Mantovani D. Assessing the biocompatibility of degradable metallic materials: state-of-the-art and focus on the potential of genetic regulation. Acta Biomater 2010;6:1800–7. https://doi.org/10.1016/j.actbio.2010.02.027.
[201] Han H-S, Jun I, Seok H-K, Lee K-S, Lee K, Witte F, et al. Biodegradable Magnesium Alloys Promote Angio-Osteogenesis to Enhance Bone Repair. Adv Sci Weinh Baden-Wurtt Ger 2020;7:2000800. https://doi.org/10.1002/advs.202000800.
[202] Linde F, Hvid I, Madsen F. The effect of specimen geometry on the mechanical behaviour of trabecular bone specimens. J Biomech 1992;25:359–68. https://doi.org/10.1016/0021-9290(92)90255-Y.
[203] Rumpler M, Woesz A, Dunlop JWC, van Dongen JT, Fratzl P. The effect of geometry on three-dimensional tissue growth. J R Soc Interface 2008;5:1173–80. https://doi.org/10.1098/rsif.2008.0064.
[204] Hollister SJ. Porous scaffold design for tissue engineering. Nat Mater 2005;4:518–24. https://doi.org/10.1038/nmat1421.
[205] Wang G, Shen L, Zhao J, Liang H, Xie D, Tian Z, et al. Design and Compressive Behavior of Controllable Irregular Porous Scaffolds: Based on Voronoi-Tessellation and for Additive Manufacturing. ACS Biomater Sci Eng 2018;4:719–27. https://doi.org/10.1021/acsbiomaterials.7b00916.
[206] Sherwood JK, Riley SL, Palazzolo R, Brown SC, Monkhouse DC, Coates M, et al. A three-dimensional osteochondral composite scaffold for articular cartilage repair. Biomaterials 2002;23:4739–51.
[207] Ko K, Jin S, Lee SE, Lee I, Hong J-W. Bio-inspired bimaterial composites patterned using three-dimensional printing. Compos Part B Eng 2019;165:594–603. https://doi.org/10.1016/j.compositesb.2019.02.008.
[208] Roohani-Esfahani S-I, Newman P, Zreiqat H. Design and Fabrication of 3D printed Scaffolds with a Mechanical Strength Comparable to Cortical Bone to Repair Large Bone Defects. Sci Rep 2016;6:19468. https://doi.org/10.1038/srep19468.
[209] Y S, Y H, Rm P, E T. Mechanical characteristics of solid-freeform-fabricated porous calcium polyphosphate structures with oriented stacked layers. Acta Biomater 2010;7:1788–96. https://doi.org/10.1016/j.actbio.2010.12.017.
[210] Loesberg WA, te Riet J, van Delft FCMJM, Schön P, Figdor CG, Speller S, et al. The threshold at which substrate nanogroove dimensions may influence fibroblast

alignment and adhesion. Biomaterials 2007;28:3944–51. https://doi.org/10.1016/j.biomaterials.2007.05.030.
[211] Dumas V, Guignandon A, Vico L, Mauclair C, Zapata X, Linossier MT, et al. Femtosecond laser nano/micro patterning of titanium influences mesenchymal stem cell adhesion and commitment. Biomed Mater Bristol Engl 2015;10:055002. https://doi.org/10.1088/1748-6041/10/5/055002.
[212] Raimbault O, Benayoun S, Anselme K, Mauclair C, Bourgade T, Kietzig A-M, et al. The effects of femtosecond laser-textured Ti-6Al-4V on wettability and cell response. Mater Sci Eng C 2016;69:311–20. https://doi.org/10.1016/j.msec.2016.06.072.
[213] Zhang J, Yang B. Patterning Colloidal Crystals and Nanostructure Arrays by Soft Lithography. Adv Funct Mater 2010;20:3411–24. https://doi.org/10.1002/adfm.201000795.
[214] Liu Y, Ai K, Lu L. Polydopamine and Its Derivative Materials: Synthesis and Promising Applications in Energy, Environmental, and Biomedical Fields. Chem Rev 2014;114:5057–115. https://doi.org/10.1021/cr400407a.
[215] Lee H, Dellatore SM, Miller WM, Messersmith PB. Mussel-Inspired Surface Chemistry for Multifunctional Coatings. Science 2007;318:426–30. https://doi.org/10.1126/science.1147241.
[216] Barrère F, Layrolle P, Van Blitterswijk CA, De Groot K. Biomimetic coatings on titanium: a crystal growth study of octacalcium phosphate. J Mater Sci Mater Med 2001;12:529–34. https://doi.org/10.1023/a:1011271713758.
[217] Liu Y, Layrolle P, de Bruijn J, van Blitterswijk C, de Groot K. Biomimetic coprecipitation of calcium phosphate and bovine serum albumin on titanium alloy. J Biomed Mater Res 2001;57:327–35. https://doi.org/10.1002/1097-4636(20011205)57:3<327::aid-jbm1175>3.0.co;2-j.
[218] Ginebra MP, Rilliard A, Fernández E, Elvira C, San Román J, Planell JA. Mechanical and rheological improvement of a calcium phosphate cement by the addition of a polymeric drug. J Biomed Mater Res 2001;57:113–8.
[219] Diaz-Gomez L, Elizondo ME, Koons GL, Diba M, Chim LK, Cosgriff-Hernandez E, et al. Fiber engraving for bioink bioprinting within 3D printed tissue engineering scaffolds. Bioprinting 2020;18:e00076. https://doi.org/10.1016/j.bprint.2020.e00076.
[220] Sydney Gladman A, Matsumoto EA, Nuzzo RG, Mahadevan L, Lewis JA. Biomimetic 4D printing. Nat Mater 2016;15:413–8. https://doi.org/10.1038/nmat4544.